DEVELOPMENT OF A CHEMICAL KINETIC MODEL FOR HYDROPROCESSED RENWABLE JET FUEL FOR TURBINE ENGINES
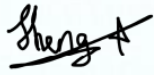
KUAH JIE SHENG

A project report submitted in partial fulfilment of the requirements for the award of Bachelor of Engineering (Honours) Mechanical Engineering

**Lee Kong Chian Faculty of Engineering and Science
Universiti Tunku Abdul Rahman**

April 2022

DECLARATION

I hereby declare that this project report is based on my original work except for citations and quotations which have been duly acknowledged. I also declare that it has not been previously and concurrently submitted for any other degree or award at UTAR or other institutions.

Signature   :

Name   :   Kuah Jie Sheng

ID No.   :   17UEB01463
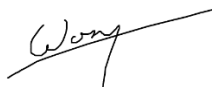
Date   :   25/4/2022

APPROVAL FOR SUBMISSION

I certify that this project report entitled **"DEVELOPMENT OF A CHEMICAL KINETIC MODEL FOR HYDROPROCESSED RENEWABLE JET FUEL FOR TURBINE ENGINES"** was prepared by **Kuah Jie Sheng** has met the required standard for submission in partial fulfilment of the requirements for the award of Bachelor of Engineering (Honours) Mechanical Engineering at Universiti Tunku Abdul Rahman.

Approved by,

Signature   :

Supervisor   :   Dr. Wong Hong Mun

Date   :   25/4/2022

The copyright of this report belongs to the author under the terms of the copyright Act 1987 as qualified by Intellectual Property Policy of Universiti Tunku Abdul Rahman. Due acknowledgement shall always be made of the use of any material contained in, or derived from, this report.

ACKNOWLEDGEMENTS

ABSTRACT

Hydroprocessed Renewable Jet (HRJ) fuels were approved recently for use in the aviation industry to minimize the aircraft pollution. The conventional jet fuels can be directly replaced by HRJ fuels without any modification in the existing infrastructure. Camelina-based Hydroprocessed Renewable Jet-6152 (CHRJ-6152) fuels are chosen as the target fuel in this project. The detailed chemical kinetic models of fuel are developed to investigate the combustion characteristics of the turbine engines in Computational Fluid Dynamics (CFD) simulations. Nevertheless, it is not feasible to use them in complex CFD simulations due to large mechanism size. The main goal of this work was to formulate a reduced chemical kinetic model for HRJ fuel for turbine engine applications. This study reports the development of two reduced chemical kinetic models, namely the reduced n-hexadecane (HXN) model and the reduced 2,2,4,4,6,8,8-heptamethylnonane (HMN) model. The detailed HXN model with 2115 species and the detailed HMN model with 1114 species served as the parent mechanism for kinetic model reduction in this study. A combination technique of DRGEP with Dijkstra's Algorithm, isomer lumping, reaction path analysis, DRG reduction approach and adjustment of A-factor constant was applied to reduce the size of the chosen detailed models. Consequently, a reduced HXN model with 108 species and a reduced HMN model with 132 species were successfully derived. Meanwhile, the computational time of the simulation had been shortened by approximately 99 % and 97 % for the reduced HXN and HMN models respectively with the use of Intel core i5 laptop with 8 GB RAM and 2.5 GHz processing speed. Both reduced models were comprehensively validated under a broad range of auto-ignition conditions. Upon extensive validation works in zero-dimensional simulations, both reduced models were then combined with the formerly developed models for methyl-cyclohexane (MCH) to produce a multi-component HRJ surrogate fuel model with 246 species, namely, J3_246. J3_246 was also validated against the detailed counterpart in terms of ID timings in 0-D chemical kinetic simulation. J3_246 was able to replicate the ignition behaviour of the detailed models and hence J3_246 can be used to represent the HRJ surrogate fuel model in CFD simulations.

TABLE OF CONTENTS

LIST OF TABLES

LIST OF FIGURES

LIST OF SYMBOLS / ABBREVIATIONS

A	Pre-Exponential Factor, mole·cm·sec·K
β	Temperature Exponent
C_c	Consumption Rate for Species c, mol/(m³·s)
C_p	Specific Heat, J/(kg · K)
$\frac{dNr}{dt}$	Build Up Rate of Species r within the Reactor, *mol/s*
E_a	Activation Energy, cal/mol
$F_{in,r}$	Inflow Rate of Species *r, mol/s*
$F_{out,r}$	Outflow Rate of Species *r, mol/s*
G_r	Production Rate of Species r within the Reactor, *mol/s*
H	Enthalpy, J/mol
k_c	Equilibrium Constant
k_n	Leading Coefficient
$k_{f,x}$	Forward Reaction Rate Constant of Species i^{th}
$k_{r,x}$	Reverse Reaction Rate Constant of Species i^{th}
N_{rec}	Number of Reactions
N_{sp}	Number of Species
$N_{s,x}$	Total Number of Species in Path x
P	Pressure, bar
P_c	Production Rate for Species c, mol/(m³·s)
q_x	Progress Rate for x^{th} Reaction, mol/(m^3·s).
r	Coefficient of Direct Interaction
R	Gas Constant, J/(mol·K)
r_{cd}	Normalised Involvement
R_{cd}	Overall Path-Dependent Coefficient
S	Entropy, J/mol
$Sen_{normalised}$	Normalised Temperature A-factor Sensitivity Coefficient
s_j	j^{th} Species
T	Temperature, K
t_D	ID Timing Computed by Detailed Model, s
t_R	ID Timing Computed by Reduced Model, s
V	Volume of the Reactor, m³

v_{ix}	Overall Stoichiometric Coefficient of Species i^{th} in x^{th}
v_r	Stoichiometric Coefficient of Species r
$\dot{w}_i$	Rate of Production of Species i^{th}, mol/($m^3 \cdot$s)
X_i	Mole Concentration of Species i^{th}, mol/($m^3 \cdot$s)

$\delta_{d,k}$	Participation of Species d in k^{th} Reaction
ω	Rate of Reaction, $m^3 \cdot$s
ω_k	Rate of Reactions for k^{th} Reaction, $m^3 \cdot$s
ϕ	Equivalence Ratio

0-D	Zero-Dimensional
2-D	Two-Dimensional
3-D	Three-Dimensional
ASTM	American Society for Testing and Material
CAAFI	Commercial Aviation Alternative Fuels Initiative
CFD	Computational Fluid Dynamics
CHRJ	Camelina-based Hydroprocessed Renewable Jet
C_2H_2	Acetylene
$C_3H_8O_3$	Glycerol
CO	Carbon Monoxide
CO_2	Carbon Dioxide
DIC	Direct Interdependency Coefficient
DRG	Directed Relation Graph
DRGEP	DRG with Error Propagation
DRGEPSA	DRG with Error Propagation and Sensitivity Analysis
EIA	Energy Information Administration
FYP	Final Year Project
GHG	Greenhouse Gases
H_2	Hydrogen
H_2O_2	Hydrogen Peroxide
HCO	Formyl
HEFA	Hydroprocessed Esters and Fatty Acids
HMN	2,2,4,4,6,8,8-Heptamethylnonane

HO$_2$	Hydroperoxyl
HRJ	Hydroprocessed Renewable Jet
HXN	N-Hexadecane
ID	Ignition Delay
IPCC	Intergovernmental Panel Climate Changes
J2_201	Two Components Reduced HRJ Surrogate Fuel Model
J3_246	Multi-Component Reduced HRJ Surrogate Fuel Model
JAL	Japan Airline
JP-8	Jet-Propellant 8
JSR	Jet-Stirred Reactor
MCH	Methyl-Cyclohexane
N$_2$	Nitrogen
N$_2$O	Nitrous Oxide
NTC	Negative Temperature Coefficient
O$_2$	Oxygen
OH	Hydroxyl
PSR	Perfectly Stirred Reactor
RCM	Rapid Compression Machine
SPK	Synthetic Paraffinic Kerosene
U.S.	United States

LIST OF APPENDICES

CHAPTER 1

INTRODUCTION

1.1 General Introduction

The first aviation gas turbine engines were patented by an Englishman, John Barber in 1791 (Escobar, 2006). To date, almost all commercial aircraft are powered by the gas turbine engines. The current aircraft gas turbine engines are optimized for conventional jet fuel. Kerosene which is derived from petroleum was chosen as a base conventional aviation fuel due to its high flash point and high rate of vaporization particularly since the 1950s (Engineering and Technology History Wiki, 2019; Karanikas et al., 2021). However, the alternative jet fuels have recently been approved to replace the use of conventional jet fuel (National Academies of Sciences, 2016).

Jet fuel is recognised as one of the most valuable inventions because it is traded internationally in the world market until the present moment (Chu et al., 2017). Additionally, jet fuel is one of the aviation fuels which has stricter requirements of quality than fuels used in ground transportation (Wang et al., 2016). The use of petroleum in aviation over the past decades has driven few research on the effects of air pollution on human health. Humans may suffer from coughs, breathing difficulties, convulsions and abdominal pain due to exposure to kerosene-based aviation fuels (Karanikas et al., 2021).

US Energy Information Administration (EIA) claimed that four gallons out of every forty-two-gallon barrels of petroleum were consumed in the production of jet fuel in 2013. Besides, it is estimated that 1500 to 1700 million barrels of traditional jet fuel are consumed by the worldwide aviation industry per year (Stratton, Wong and Hileman, 2010). The combustion of the conventional jet fuel also produces greenhouse gases (GHG) such as nitrous oxide (N_2O) and carbon dioxide (CO_2) that contribute to global warming and climate change. It is noted that 2 % of the total carbon dioxide (CO_2) emissions are caused by the commercial aviation industry (Hileman and Stratton, 2014). In addition, the combustion of petroleum leads to high levels of pollution as it is a non-renewable energy source. Due to the rapid growth in the aviation sector,

the global demand for jet fuels is expected to be increased in the coming decades (Zhang et al., 2016).

A strong interest in the development of the alternative fuel has been driven due to increasingly stringent pollutant regulations and the unstable prices of petroleum (Pan, Kokjohn and Huang, 2015; Wang et al., 2016). Commercial Aviation Alternative Fuels Initiative (CAAFI) has mentioned that all alternative fuels produced are a member of drop-in jet fuels. The definition of drop-in fuels will be further discussed in Section 2.3. Generally, the alternative (non-petroleum) jet fuels can be classified into two groups which are bio-jet fuels and synthetic fuels. Synthetic fuels are created from the sources of fossil feedstock such as natural gas, crude oil and coal. On the other hand, the potential renewable feedstocks for deriving bio-jet fuels can be divided into three types which are solid-based feedstocks, gas-based feedstocks and oil-based feedstocks (Wang et al., 2016). This paper will focus on the bio-jet fuels that are produced from oil-based feedstocks such as vegetable oils.

Bio-jet fuels are also called as renewable jet fuels which play a vital role in green aviation. The government and the aviation industry around the world have invested a lot of efforts into investigating all kinds of alternative jet fuels that can be used to replace the conventional jet fuel over the past 10 years (Zhang et al., 2016). For example, a 50 % blend of Hydroprocessed Renewable Jet (HRJ) fuels produced from camelina feedstocks were flight-tested successfully by KLM Royal Dutch Airlines and Japan Airline (JAL) in 2009. Camelina is recognised as a famous energy crop and it is widely used for advanced bio-jet fuel production. In Northern Plains of the United States (U.S.), camelina feedstocks are either planted on fallow land as a rotation crop or on marginal lands. Thus, the conflict with food cultivation can be prevented by using camelina as a renewable energy source (Shonnard, Williams and Kalnes, 2010).

The aviation industry has recently begun using HRJ fuel. In July 2011, HRJ fuels are certified by ASTM International for aviation use (Ajam and Viljoen, 2011). HRJ fuels are preferred to be used because they have a great potential to reduce the energy reliance on the non-renewable energy source and produce lower GHG as compared to conventional jet fuel. For instance, the life cycle GHG emissions level of HRJ fuels is 37.3 % to 93.4 % lower than that of

conventional jet fuel (Zhang et al., 2016). The detailed chemical kinetic mechanism is a necessary tool to examine the combustion reaction of HRJ fuel and carry out the computational fluid dynamics (CFD) research on engine combustion. However, the detailed models are not suitable to be used in CFD simulation due to high computational costs and expenses. Thus, the goal of this research is to derive a reduced chemical kinetic model of HRJ fuel for turbine engine applications.

1.2 Importance of the Study

In the past decade, only a few of kinetic studies of HRJ fuel combustion have been conducted, either using computational modeling or experimentally. There are some rationales for this lack of attention.

First, HRJ fuels have just recently been developed and approved by ASTM International in 2011. Consequently, HRJ fuels have gained increasing attention from researchers in recent years because they have several advantages over the conventional jet fuel. They have the potential to mitigate GHG emissions and reduce aviation pollution. HRJ fuel is also considered as one of the alternative fuels which produced from sources other than petroleum. This helps to displace the imports of fossil fuels in some countries such as the U.S.

HRJ fuels usually contain a large amount of fuel molecules that make the development of the detailed mechanism for HRJ fuel become extremely difficult. Therefore, this study is paramount to provide a simplified version of the detailed model for HRJ fuel which is also known as the reduced chemical kinetic mechanism. This reduced mechanism is significant to be used in multi-dimensional CFD simulations. Additionally, the computational time and cost can be greatly reduced by using the reduced model instead of the detailed model.

1.3 Problem Statement

In the past few years, the development of detailed chemical kinetic mechanisms has gained increasing attention from the researchers as these models are capable to describe the chemical kinetics of the processes of combustion accurately. CFD modelling method is more preferable than the experimental approach as the operating cost of CFD modelling approach is much lower than that of the experimental approach. However, it is impractical to use the detailed model in

computational combustion analysis and CFD simulations due to high computational cost and time (Niemeyer, Sung and Raju, 2010). Herbinet, Pitz and Westbrook (2008) mentioned that the simulations with detailed models are very time-consuming. It took 169 hours to completely simulate a detailed chemical kinetic mechanism of methyl decanoate with 8820 reactions and 3012 species.

The detailed chemical kinetic models usually consist of hundreds or thousands of reactions and species. For instance, the detailed n-hexadecane (HXN) model and the detailed 2,2,4,4,6,8,8-heptamethylnonane (HMN) model that served as the parent mechanisms for this project contain 2115 species and 1114 species respectively. The sizes of these two detailed models are typically large for application in multi-dimensional CFD simulation (Zheng et al., 2002). This causes the cost-effective benefit of CFD simulation is eliminated.

1.4   Aim and Objectives

The general purpose of this project is to formulate a reduced chemical kinetic mechanism for Hydroprocessed Renewable Jet (HRJ) fuel for turbine engine applications. A valid reduced model of HRJ fuel is capable of providing reasonable simulation results as compared to the corresponding detailed chemical kinetic mechanism. The size of the detailed model can be reduced drastically by using the mechanism reduction techniques. Nevertheless, only the unimportant reactions and species that have a minor effect on simulation results can be eliminated. Otherwise, the simulation results would be not accurate as compared to the experimental results. In order to accomplish the aim, the specific objectives of this research are listed as below:

1. To identify the essential elementary reaction and species in the detailed chemical kinetic mechanism.

2. To simplify the detailed mechanism by eliminating the unimportant elementary reaction and species through integrated reduction techniques.

3. To develop a reduced HRJ surrogate fuel model by using integrated reduction techniques.

4. To validate the accuracy of the reduced surrogate model for HRJ fuels by comparing the difference of ignition delays (ID) timings and species

profiles between the detailed chemical kinetic model and the reduced chemical kinetic model in 0-D simulations.

1.5   Scope and Limitation of the Study

The working scope of this project is to develop a reduced chemical kinetic model for Camelina-based Hydroprocessed Renewable Jet-6152 (CHRJ-6152) fuel with the use of ANSYS CHEMKIN-PRO and Microsoft Excel software. The reduced model for CHRJ fuel is derived from the corresponding detailed model by using integrated reduction techniques proposed by Poon et al. (2013). The reductions of the detailed HXN model and the detailed HMN model are performed in this project. The reduced methyl-cyclohexane (MCH) model derived by Tan et al. (2021) is directly used to merge with the reduced models developed in this work to form the surrogate model for CHRJ-6152 fuel. The limitations of this research are listed as follows:

1. The detailed chemical kinetic models that used as the base models for reduction in this paper are chosen from the existing model developed by other researchers. The development of the detailed model for HRJ fuel is not involved in this work.

2. The chosen detailed chemical models are not specified for HRJ fuel but a surrogate of HRJ fuel and thus this study is limited by the availability of the detailed chemical kinetic mechanism in the literature.

3. The reduced models are only validated by using simulation results since there is no experimental study will be done in this work.

4. The reliabilities of the reduced models developed in this paper are only measured in 0-D simulation under a broad range of conditions of auto-ignition.

1.6   Contribution of the Study

At the end of this research, a reduced HRJ fuel surrogate model was developed through integrated reduction scheme. This study showed the use of integrated reduction scheme as an effective approach for large-scale model reduction. This valid reduced model can replicate the actual ignition behaviour of HRJ fuel when applied in the multi-dimensional CFD simulation of complex combustion of the turbine engines. With this newly developed reduced HRJ fuel surrogate

model, the computational time and cost will be reduced significantly. As such, engineers can simulate the combustion reaction of HRJ fuel and develop better turbine engines in lesser time.

1.7   Outline of the Report

This paper is organised into five chapters. The first chapter of this paper begins with a general introduction to the background of this study. This is followed by the importance of the study and the problem statement for this article. The objectives, scope and limitations and the contribution of the project can be reviewed in Chapter 1 as well.

A review of the related literature is presented in Chapter 2. This chapter discusses the published information in the areas of the conventional jet fuels and Hydroprocessed Renewable Jet (HRJ) fuel. Also, the reduction techniques of the detailed chemical kinetic model are discussed in this chapter. Furthermore, the work plan and research methodology of this study are described in Chapter 3.

Chapter 4 reports the main findings of this work. It consists of the discussion of the simulation results, the development processes and the validation exercises of the reduced models. On top of that, this chapter also covers the details of the reduction techniques that had been conducted in this paper. In Chapter 5, the conclusion of this study is drawn and this paper ends with the recommendations for future works.

CHAPTER 2

LITERATURE REVIEW

2.1   Introduction

The focus of this study is Hydroprocessed Renewable Jet (HRJ) fuel. The related research findings will be reviewed in this chapter. The introduction and the composition of the conventional jet fuel will be discussed in Section 2.2. Moreover, the definition of drop-in jet fuels is described in Section 2.3. Subsequently, the details and the conversion process of HRJ fuels are presented in Section 2.4. Additionally, the comparisons between HRJ fuel and traditional jet fuel are presented in Section 2.5. Furthermore, the kinetic modeling for HRJ fuel surrogates is described in Section 2.6 while the reduction techniques of detailed chemical kinetic mechanisms will be reviewed in Section 2.7. Lastly, the main findings will be summarized in Section 2.8.

2.2   Conventional Jet Fuel

Conventional jet fuels also known as kerosene-type aviation fuels are comprised of cyclo-paraffins and aromatics but mostly normal paraffins (n-paraffins) and isoparaffins (Karanikas et al., 2021). Jet-Propellant 8 (JP-8), Jet A and Jet A-1 fuels are the most-studied kerosene-based jet fuel derived from petroleum (Mangus, Mattson and Depcik, 2015; Karanikas et al., 2021). The range of their carbon numbers is dependent on the requirements for the products such as smoke point and freeze point (SGS Spain, 2013). Most of the conventional jet fuels have a carbon range of C9 to C16 and their compositions are very similar (Agency for Toxic Substances and Disease Registry, 2017; National Academies of Sciences, 2016). However, the exact compositions of the jet fuels are fully restricted by the types of refinery processes used for production. Another factor that affects the composition of the jet fuel is the crude oil from which it was extracted. For instance, distinct supplies of crude oils show variation in colour due to the changes in chemical compositions (National Geographic Society, 2021). Regardless of the refinery process and the source of crude oil, the conventional jet fuels consist of roughly 70 % of n-paraffins, isoparaffins and cyclo-paraffins and less than 25 % of aromatic compounds. Besides, the

conventional jet fuels are comprised of typically 1 % of olefins (Agency for Toxic Substances and Disease Registry, 2017).

Jet A fuel predominates in the U.S. while Jet A-1 fuel is widely used by the rest of the countries (National Academies of Sciences, 2016; SGS Spain, 2013; Zhang et al., 2016). The main difference between them is the essential condition for the addition of anti-static additive to Jet A-1 fuel. Moreover, JP-8 fuels are kerosene-based military fuels which comprised of anti-icing additives. This kind of fuel must satisfy the stringent requirements of MIL-DTL-83133 specification (Repsol, 2018). In this study, JP-8 fuel is selected to compare with HRJ fuel. The comparison between JP-8 fuel and HRJ fuel will be discussed in Section 2.5. Table 2.1 displays the fuel properties of JP-8 fuel while Figure 2.1 shows the distribution of chemical compositions of JP-8 fuel.

Table 2.1: The Fuel Properties of JP-8 Fuel (Zhang et al., 2016).

Fuel Properties	Values
Cetane Number	47.3
Density at 15 °C (kg/m³)	790
Kinematic Viscosity at -20 °C (mm^2/s)	4.1
Net Heat of Combustion (MJ/kg)	43
Flash Point (°C)	48
Smoke Point (mm)	25
Freezing Point (°C)	-49
Total Sulphur (wt%)	0.0064
H/C ratio by mole	1.937
Molecular Weight (g/mol)	153
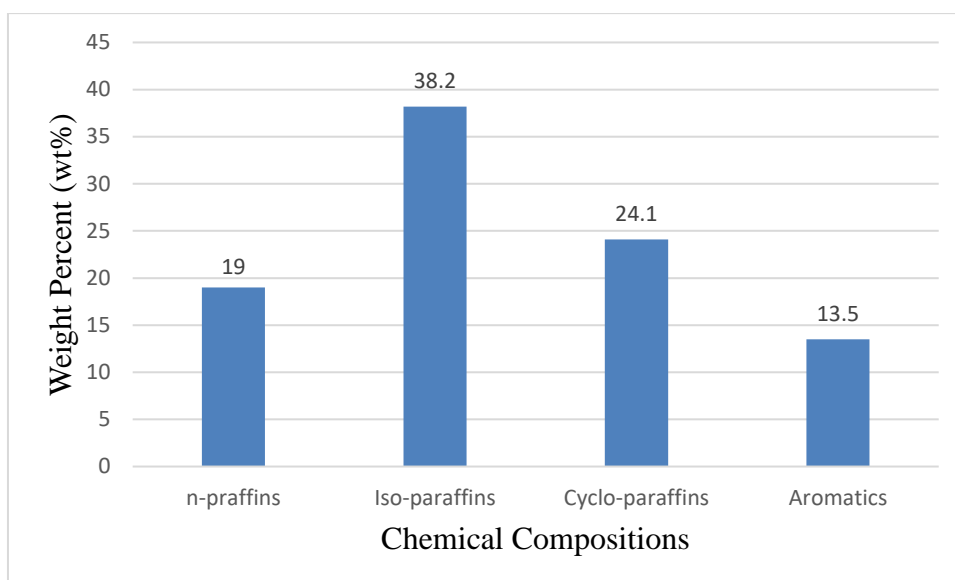
Figure 2.1: Distribution of Chemical Compositions of JP-8 Fuel (Zhang et al., 2016).

To date, the traditional jet fuels such as and JP-8, Jet A and Jet A-1 fuels are the primary jet fuels powering global aviation. The total demand for the conventional jet fuels estimates 294 million tons per annum. Besides, the conventional jet fuels consist of approximately 200 toxic hydrocarbon compounds in total such as toluene, n-hexane and benzene. Several health issues for humans are generated due to the exposure to toxic hydrocarbon compounds (Karanikas et al., 2021). In addition, the conventional jet fuels are extracted from crude oil which is a non-renewable source (Adewuyi, 2016). Consequently, the combustion of petroleum-based fuels emits greenhouse gases at high level (Pearlson, Wollersheim and Hileman, 2013). As such, it is paramount to seek a way to lower the net emission of greenhouse gases and reduce the health risks (Wang and Tao, 2016). The alternative jet fuels which are extracted from renewable energy sources have become a viral strategy for attaining a green and sustainable aviation (Zhang et al., 2016).

2.3   Drop-in Jet Fuel

Drop-in jet fuels are referred to as a replacement for conventional fuel (International Civil Aviation Organization, 2021). It has aggregate properties which are essentially close to the properties of conventional jet fuels (National Academies of Sciences, 2016). Due to this reason, drop-in jet fuels are

completely interchangeable, miscible, and compatible with conventional jet fuel. As such, it does not need any adjustment of the existing fuel infrastructure and aircraft (Zhang et al., 2016). Furthermore, drop-in jet fuels can be used without any new system certification (International Civil Aviation Organization, 2021).

Drop-in jet fuels play a key role in saving unnecessary costs and preventing the risks of mishandling because a "non-drop-in" jet fuel must be handled individually from conventional jet fuel. This may cause some safety issues and require a lot of costs to build up a parallel infrastructure at all airports (International Civil Aviation Organization, 2021). HRJ fuels have been approved for blending with conventional jet fuel such as Jet A-1 up to 50 % by volume and hence they can be used as drop-in fuels (Shila, 2017; International Civil Aviation, 2021).

Nevertheless, a reasonable level of difference in particular physical and chemical properties of jet fuel is acceptable to tolerate the difference in refining and sources of petroleum throughout the globe. The capacity to accommodate this variability allows the development of fuel components generated from renewable feedstocks such as camelina while still fulfilling the requirements and providing the final physical of jet fuel (National Academies of Sciences, 2016). This explains why HRJ fuel is able to substitute the traditional jet fuel even if their properties are not exactly the same.

2.4 Hydroprocessed Renewable Jet (HRJ) Fuel

HRJ fuel can be named as bio-synthetic paraffinic kerosene (bio-SPK) and Hydroprocessed Esters and Fatty Acids (HEFA) fuel. It is a kind of bio-jet fuel derived from HEFA technology (Ajam, Viljoen and Viljoen, 2011; Zhang et al., 2016; Allen et al., 2012; Alhikami and Wang, 2021). Nowadays, most of the bio-jet fuels are derived from animal fats and plant oils through hydroprocessing (Zhang et al., 2016). This kind of alternative fuel is converted from biomass through a chemical process of refining animal-based or plant-based oils and turning the lipids of these oils into hydrocarbons through addition reaction with hydrogen (Oldani et al., 2015). Beef tallow (animal fats) and camelina (plant oil) are the most common biological feedstock that used to produce HRJ fuel (Allen et al., 2012).

HEFA technology is a chemical process used to produce aviation fuel from renewable feedstocks through a series of reactions. For instance, the glyceride-based fats or oils are turning into n-paraffins through decarboxylation, deoxygenation and decarboxylation. Then, the paraffins undergo hydrocracking and hydro-isomerization reaction to produce medium-chain isomers and n-alkanes (in the range of C8 to C16) to conform the requirements of the aviation fuel (Chen, Lin and Wang, 2020). In HEFA process, the chemically-bound oxygen is removed to create appropriate molecular weight components for HRJ fuels (Hui et al., 2012). More detailed information on the conversion process of HRJ fuel can be found in Section 2.4.1. The fuels produced from the HEFA process can be made from renewable feedstocks such as camelina and algae which do not compete with food crops at all (Corporan et al., 2012).

As aforementioned, HRJ fuels can be used to replace conventional jet fuel as they are a member of drop-in jet fuels. In 2011, ASTM International approved the use of HRJ fuels in the aviation industry as sustainable alternative fuels due to their chemical properties are very similar to the conventional jet fuels (Alhikami and Wang, 2021). Moreover, HRJ fuels comply with the current needs for jet fuel due to their proper ratio of hydrocarbons such as n-paraffins (n-alkanes), isoparaffins (branched-alkanes), cyclo-paraffins (cyclo-alkanes) and aromatics (National Academies of Sciences, 2016). Therefore, HRJ fuels are able to replace the use of conventional jet fuel since they are "drop-in" quality (Pearlson, Wollersheim and Hileman, 2013). Additionally, HRJ fuels are designed to have limited cyclo-paraffins and high ratio of branched to normal paraffins (Allen et al., 2012). The purpose of this action will be discussed in Section 2.5.

In order to maintain the quality and performance of jet fuel, fuel specifications are essential to control the properties of fuel within the satisfactory range. A non-profit organization, American Society for Testing and Material (ASTM) plays an important role in setting the specifications for jet fuels (Zhang et al., 2016). HRJ fuels have been certified by ASTM standard specification D7566 for use in blends of up to 50 % with traditional jet fuel while the conventional jet fuel such as Jet A fuel was approved under ASTM D1655 (Mawhood et al., 2016; National Academies of Sciences, 2016). All the new aviation fuels approved by ASTM D7566 can be treated as D1655 turbine

fuels as they meet the requirements of ASTM D1655 as well (Zhang et al., 2016). In other words, HRJ fuels can be used for the existing infrastructures that are certificated for conventional jet fuels.

Of late, HRJ fuels have become increasingly important in the aviation industry. The main purpose of introducing bio-jet fuel is to mitigate greenhouse gas (GHG) emissions of aviation. Based on the Intergovernmental Panel Climate Changes (IPCC), the aviation only accounts for 2 to 2.5 % of total carbon emissions (Larsson et al., 2018; Ajam and Viljoen, 2011). Nevertheless, the GHG emissions from aviation are anticipated to rise with non-stop air traffic growth. By increasing the efficiency of fuel alone does not bring substantial effect on carbon emissions ascribable to technological effects. Hence, it is essential to introduce a sustainable low carbons jet fuel such as HRJ fuels due to their large potentials for mitigating aviation carbon emissions.

Furthermore, one of the main benefits of HRJ fuels is that they are made from renewable feedstock. This helps to minimize the energy reliance on the petroleum resources. Theoretically, carbon neutrality can be achieved by using HRJ fuels. The carbon dioxide released from the combustion of HRJ fuels can be offset by absorbing the carbon dioxide from the atmosphere when the feedstock grew (Zhang et al., 2016; National Academies of Sciences, 2016). As such, HRJ fuels are commonly considered by the aviation industry to be an alternative to petroleum-based fuels as they have the potential to immediately reduce the aviation emissions of carbon dioxide (Ajam and Viljoen, 2011).

For HRJ fuels to be effective and sustainable over a long period of time, a few factors are considered such as the economic, environmental and the potentiality for reduction in the total carbon emissions (National Academies of Sciences, 2016). Figure 2.2 has proved that all the HRJ fuels have better carbon emissions benefits relative to conventional jet fuels. The economical sustainability of HRJ fuels mainly focuses on the expenses of the fuels while the environmental sustainability requires to examine the land use. One of the most frequently used HRJ fuels is known as Camelina-based Hydroprocessed Renewable Jet (CHRJ) fuel. As the name implies, CHRJ fuel is an isoparaffin-rich bio-jet fuel extracted from a short-season and non-food crop which is known as camelina (Shonnard, Williams and Kalnes, 2010; Zhang et al., 2016). As illustrated in Figure 2.3, CHRJ-6152 fuel is comprised almost entirely of

isoparaffins and its aromatic contents are only 0.2 % which is much lower than the traditional jet fuel.
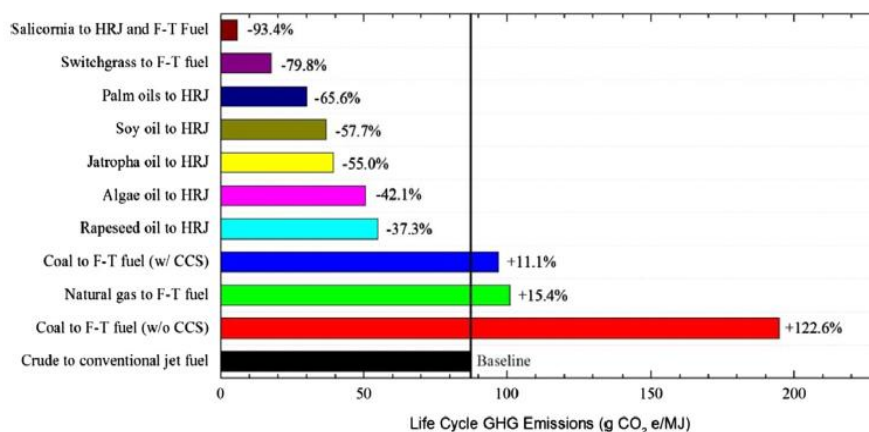
Figure 2.2: Life Cycle GHG Emissions for Conventional and HRJ Fuels (Zhang et al., 2016).
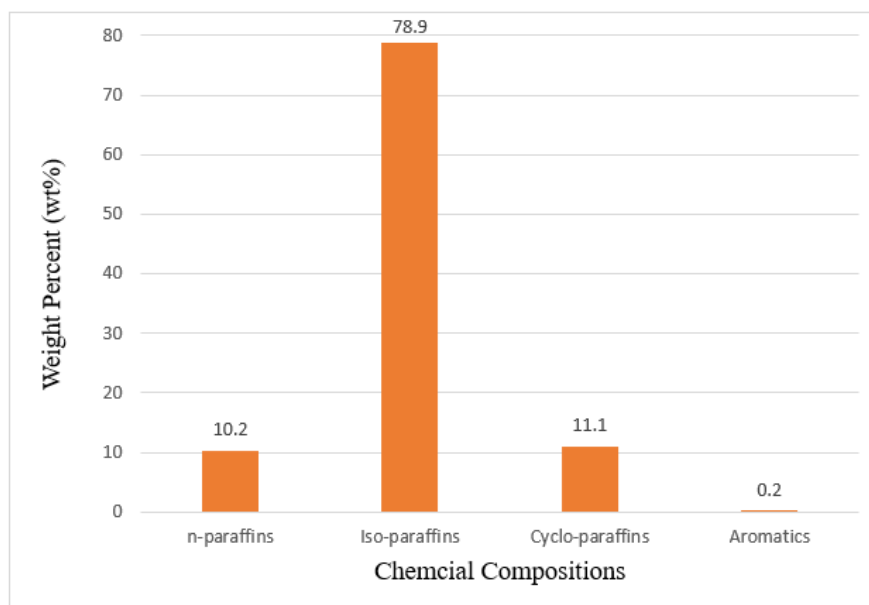
Figure 2.3: Distribution of Chemical Compositions of CHRJ-6152 Fuel (Zhang et al., 2016; Edwards, Shafer and Klein, 2012).

Camelina is the best suited as a sustainable renewable fuel crop because it is naturally comprised of high oil content about 35 % oil by weight (Farm Energy, 2019; Renewable Carbon News, 2009). Furthermore, camelina does not replace other food crops as it can grow in marginal land. Additionally, in the Northern Plains of the United States, it can be planted on existing agricultural

lands as a rotation crop with wheat during the fallow season. Therefore, the conflict with food cultivation and the food shortage can be prevented by using camelina as a renewable source (Shonnard, Williams and Kalnes, 2010). Moreover, camelina needs lesser fertilizer than most other crops which means the input cost of camelina is low (Renewable Carbon News, 2009; Shonnard, Williams and Kalnes, 2010). Thus, it can be concluded that CHRJ fuels are sustainable in terms of both environmental and economic factors.

The data collected by David Shonnard Robbins demonstrates that the performance of CHRJ fuels is as good as the conventional jet fuel and they produce 75 % lower GHG emissions as compared to conventional jet fuel (Renewable Carbon News, 2009). The general manager of Sustainable Oils, Scott Johnson stated that the fastest way to lower the net life cycle carbon emissions from aviation is to start using sustainable and renewable oil instead of petroleum fuel. As mentioned in Section 2.2, the compositions of the jet fuels may vary based on the different sources and refined in distinct ways. Thus, there are two types of CHRJ fuels available in the market which are HRJ-5 and HRJ-8 fuels. In this research, CHRJ-6152 (HRJ-8) fuel is chosen to be further studied. The fuel properties of CHRJ-6152 fuel are presented in Table 2.2.

Table 2.2:   The Fuel Properties of CHRJ-6152 Fuel (Zhang et al., 2016; Allen et al., 2012; Edwards, Shafer and Klein, 2012; Hui et al., 2012).

Fuel Properties	Values
Cetane Number	53.9
Density at 15 °C (kg/m³)	751
Kinematic Viscosity at -20 °C (mm^2/s)	3.3
Net Heat of Combustion (MJ/kg)	44.3
Flash Point (°C)	43
Smoke Point (mm)	50
Freezing Point (°C)	< - 77
Total Sulphur (wt%)	< 0.0018
H/C ratio by mole	2.169
Molecular Weight (g/mol)	160

2.4.1   HRJ Fuel Conversion Process

In recent years, HEFA technology is widely used to convert renewable feedstock into HRJ fuel for aviation used through a series of reactions. It is the most-studied commercially accessible technology to manufacture renewable aviation fuel until now due to its high level of economic, environmental and maturity considerations (Chen, Lin and Wang, 2020). The renewable oils and fats are comprised of mostly triglycerides. The first step of the HRJ fuel conversion process is to saturate the double bond in triglyceride through catalytic hydrogenation. This hydrogenation process enables the unsaturated double bonds in the triglyceride to react with hydrogen (H_2) gas in the existence of catalyst to form a saturated one. With the addition of hydrogen, the propane is produced from the glycerol portion of the triglyceride. Three moles of long fatty acid chains are produced when the propane backbone is cleaved (Pearlson, 2011).

The alternative way to produce three moles of free fatty acids is known as thermal hydrolysis. In this chemical process, three moles of water are added and processed with the feedstocks. The glycerol backbone reacts with the hydrogen ion from water molecule and produces one mole of glycerol ($C_3H_8O_3$). The remaining hydroxyl ion from the water molecule is then attached to the ester group and generates three moles of free fatty acids. On top of that, high pressure and high temperature are needed to keep the reactants in liquid phase and dissolve the water in oil phase respectively.

Next, hydrodeoxygenation or decarboxylation is carried out to remove the oxygen from the fatty acid molecules. The hydrodeoxygenation needs additional nine moles of hydrogen gas as compared to decarboxylation. The oxygen is removed in the form of water through hydrodeoxygenation while the decarboxylation reaction removes the oxygen in the form of carbon dioxide. At this stage, the renewable plant oils and animal fats have been transformed from unsaturated triglycerides into completely saturated hydrocarbons (Pearlson, 2011). However, the resulting n-paraffins have not met all the requirements of jet fuel yet and thus they require further processing (Ajam and Viljoen, 2011).

It is necessary to hydroisomerize and hydrocrack the n-paraffins generated from hydrodeoxygenation reaction to a synthetic paraffinic kerosene (SPK) product in order to fulfil the specifications and requirements of jet fuel.

For instance, the HRJ fuels must have good cold flow properties, high flash points and so on. Besides, the deoxygenated product's cloud point is increased by hydro-isomerization and hydrocracking reactions. A study conducted by Wang and Tao (2016) shows that hydro-isomerization of n-paraffins takes place first and followed by hydrocracking reaction. In general, branched molecules have a higher freezing point as compared to straight chain configuration. To conform the specification of the jet fuel, the hydro-isomerization reaction must be carried out to convert the straight-chain hydrocarbons into the branched structures to decrease the freezing point (Corporan et al., 2012).

Hydrocracking is a relatively slow reaction and hence most of the hydrocracking reaction only occurs in the last portion of the reaction. On top of that, it is an exothermic reaction and hence it produces lighter gas and liquids products. This reaction mainly includes saturation and cracking of paraffins. Cracking basically means the chain length is decreased and two molecules are formed (Pearlson, 2011). Bifunctional catalysts are usually used in hydro-isomerization reaction because they consist of acid sites for skeletal isomerization and metallic sites for dehydrogenation by way of carbenium ions (Ajam and Viljoen, 2011).

In hydro-isomerization, the n-paraffins undergo dehydrogenation on the metal sites of the bifunctional catalysts while the olefins protonate with development of the alkylcarbenium ion are produced when the n-paraffins react on the acid sites. The monobranched, dibranched and tribranched alkylcarbenium ions are formed on the acid sites through the rearrangement of alkylcarbenium ions. Then, the corresponding paraffins are formed when the branched alkylcarbenium ions are hydrogenated and deprotonated. The selectivity of bifunctional catalyst is important in modifying the yield of jet fuel range product as it will cause some differences of cracking at the end of molecule of paraffin. Lastly, the distillation of mixtures must be carried out to produce light gases, naphtha, paraffinic diesel and paraffinic kerosene (HRJ SPK) through a fractionation process (Wang and Tao, 2016).

In short, the HEFA conversion process is comprised of several stages such as catalytic hydrogenation and hydrodeoxygenation to form primarily n-paraffins. Then, the conventional refinery processes are carried out to hydroisomerise and hydrocrack the n-paraffins to conform the jet fuel

specifications (Corporan et al., 2012). The HRJ fuel is produced after the fractionation process. The overview of the HEFA conversion process is illustrated in Figure 2.4.
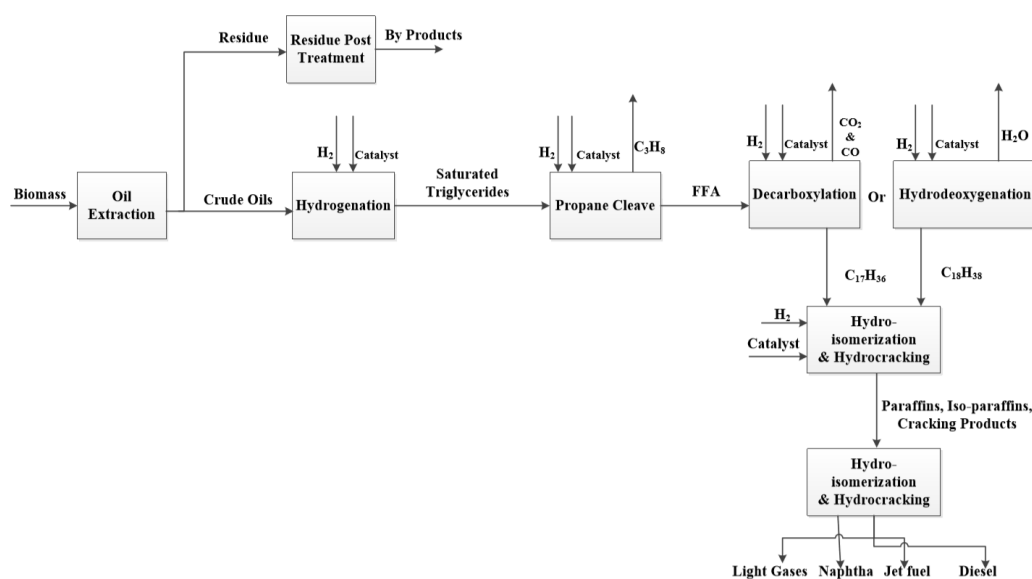
Figure 2.4: HEFA Conversion Process (Wang and Tao, 2016).

2.5 Comparison between HRJ Fuel and Conventional Jet Fuel

The major discrepancy between HRJ fuels (e.g., CHRJ) and conventional jet fuel (e.g., JP-8) is the raw material. Based on the aforementioned discussion, HRJ fuel has lower carbon production than conventional petroleum jet fuel as it is derived from renewable sources. Besides, CHRJ fuel contains more percentage of isoparaffins as compared to JP-8 fuel and thus it has the benefit of lesser exhaust emission of harmful gases (Johnson, 2017). Generally, HRJ fuels have advantages over the conventional fuel because they have higher cetane numbers, lower sulphur and aromatic contents, higher reactivity and shorter ignition delay (ID) time (Pearlson, Wollersheim and Hileman, 2013). It is notable that cetane number and the reactivity of jet fuel are mainly influenced by the molecular compositions of jet fuel (Alhikami and Wang, 2021).

According to Figure 2.1 and Figure 2.3, it can be found that JP-8 fuel has a higher percentage of n-paraffins than CHRJ fuel. Hui et al. (2012) stated that both isoparaffins and cyclo-paraffins are less reactive than n-paraffins. Theoretically, jet fuels with more n-paraffins should have a higher cetane number. However, the reactivity of cyclo-paraffins is much lower than n-

paraffins because of their olefin formation and isomerization pathways. In addition, the free hydrogen distribution in the isomerization of fuel peroxyl radicals might be diminished by the cyclic structures of aromatics compounds and cyclo-paraffins (Allen, Toulson and Lee, 2011). Due to these reasons, the cetane number of JP-8 fuels is lower than CHRJ fuels as JP-8 fuels contain more percentage of cyclo-paraffins.

As reviewed in Section 2.2 and Section 2.4, it was found that CHRJ fuel has a cetane number of 53.94 which is larger than that of JP-8 fuel. Hui et al. (2012) and Allen et al. (2013) stated that jet fuel with a larger cetane number has a shorter ID time. Allen, Toulson and Lee (2011) also concluded that CHRJ fuel ignites more rapidly than JP-8 fuel. Therefore, it can be concluded that the higher the cetane number, the higher the reactivity of jet fuel. On top of that, the ignition acceleration and the reactivity of JP-8 fuels are lower as compared to CHRJ fuel because the conventional jet fuel consists of a larger concentration of aromatics and cyclo-paraffin (Alhikami and Wang, 2021). Thus, the combustion of the CHRJ fuels charge in the combustion chamber is more complete and this can help to reduce the harmful emissions of aviation. Moreover, the turbine engine runs smoother and performs better with HRJ fuels (Hui et al., 2012).

It also can be seen in Figure 2.1 and Figure 2.3 that JP-8 fuel has higher aromatic content than CHRJ fuel. This is the reason why the conventional jet fuel will not burn as cleanly as HRJ fuels (Hemighaus et al., 2006). To reduce this effect, it is better to use the jet fuel with lower aromatics concentration. There are no jet fuel specifications to describe the minimum aromatics concentrations as the conventional jet fuels have a significant concentration of aromatics. For instance, the maximum aromatics concentration for JP-8 fuel is 25 %. Furthermore, the results of the experiment conducted by Walluk et al. (2015) are summarised in Figure 2.5. It showed that CHRJ fuels have higher reforming efficiency than JP-8 fuels due to lower concentration of sulphur in CHRJ fuel. Additionally, Walluk et al. (2015) also claimed that the use of CHRJ fuels is able to afford developers of fuel cells with higher efficiencies, lower operating expenses, longer system life and larger design flexibility as they do not consist of high contents of aromatic and sulphur.
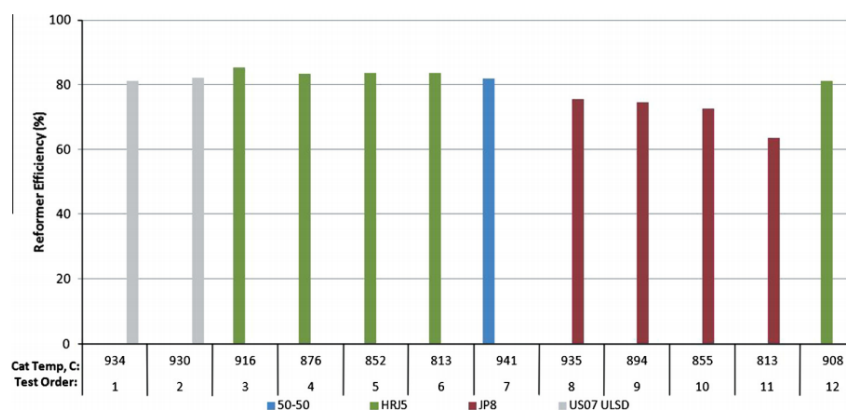
Figure 2.5: Reforming Efficiency for CHRJ and JP-8 Fuels (Walluk et al., 2015).

2.6 Detailed Chemical Kinetic Modeling for HRJ Fuel Surrogate

To date, there are many different detailed chemical kinetics models have been developed for various types of jet fuel and they are varying significantly in the total number of species and elementary reactions. For example, the detailed model proposed by Malewicki et al. which consists of 8310 reactions and 2080 species is used to study the oxidation of Jet-A fuel while the detailed model with 3556 reactions and 564 species proposed by Naik et al. is developed for alternative jet fuels surrogates (Acampora and Marra, 2017).

These detailed chemical kinetic models are developed to investigate the flame phenomena, the phenomenology of soot formation, the combustion of hydrocarbons of fuel and oxidation processes (Poon, 2016). On top of that, the detailed models are also a useful tool to improve the environmental performance of combustion technologies and the efficiency of jet fuels (Aasberg-Petersen et al., 2004; Xin et al., 2014). However, modeling every single jet fuel component would be very complex and expensive since the jet fuels derived from petroleum and biological feedstock usually consist of thousands of various kinds of hydrocarbon compounds that can be categorised into numerous structural classes including n-paraffins, isoparaffins, cyclo-paraffins and aromatic compounds (Stagni et al., 2016; Westbrook et al., 2008). Due to the sizes of the detailed models are too large, it is not viable to use them in complex computational fluid dynamics (CFD) simulations (Xin et al., 2014).

One approach to reduce the complexity is to develop a smaller model of surrogate fuel that defines both chemical and physical characteristics of the

actual fuel. Besides, the hydrocarbon compounds can be grouped together into basic structural classes (Westbrook et al., 2008). In such manner, the development of the chemical kinetic model becomes simpler and less computationally costly to perform the multi-dimensional simulations (Sarathy et al., 2011). Moreover, the reproducibility of experiments can be achieved by using the surrogate fuel model (Pepiot-Desjardins and Pitsch, 2008). This statement proved that the surrogate fuel models are helpful to formulate the chemical kinetic models. Additionally, the surrogate fuel models are also suitable for CFD simulations and emulate the combustion behaviours of real fuels as they exhibit comparable combustion characteristics and thermodynamics properties (Poon, 2016). Examples of surrogates for jet fuel include n-decane, n-butylbenzene, n-hexadecane and so on. In addition, several reduction techniques have been developed to overcome the complexity of the detailed mechanism. For further details of the reduction technique are discussed in Section 2.7.

In this study, the detailed chemical kinetic models of n-hexadecane (HXN) and 2,2,4,4,6,8,8-heptamethylnonane (HMN) developed by Westbrook et al. (2008) and Oehlschlaeger, et al. (2009) respectively are chosen as the base model for kinetic model reduction. The reduced models derived from these two detailed models will be combined together with the formerly developed methyl-cyclohexane (MCH) model to develop the reduced surrogate model of HRJ fuel. The chosen detailed kinetic model of HXN is comprised of 8157 reactions and 2115 species while the chosen detailed kinetic model of HMN contains 4469 reactions and 1114 species. In this paper, HMN is selected as the surrogate to be the representative of isoparaffins component in CHRJ fuel. On the other hand, n-hexadecane (n-HXN) is chosen to represent the n-paraffins of CHRJ fuel. Moreover, the reduced methyl-cyclohexane (MCH) model with 524 reactions and 86 species developed by Tan et al. (2021) will be used to represent the constituent of cyclo-paraffins of CHRJ fuel. The "reduced prior to combination approach" is applied here to combine the reduced cyclo-paraffins model with the other two reduced models developed in this research. The mechanism merging will be reported in Section 4.9.

2.7   Reduction Techniques of Detailed Chemical Kinetic Mechanisms

Hundreds or thousands of distinct chemical compounds and reactions are involved in the combustions of jet fuels. The detailed mechanisms for real fuels are tremendously difficult to be simulated and incorporated into multi-dimensional modelling attributed to large number of elementary reactions and species. For instance, the selected detailed chemical kinetic model of HXN in this paper is comprised of 8157 reactions and 2115 species whereas the detailed model of HMN consists of 4469 reactions and 1114 species. As such, the detailed chemical kinetic models are necessary to be simplified drastically in order to avoid the high computational expenses of mathematical simulation of combustion machines (Pepiot-Desjardins and Pitsch, 2008). The reduced chemical kinetic model must be able to regenerate the results of simulation consistent with the detailed chemical kinetic model (Patel, Kong and Reitz, 2004). For instance, the reduced chemical kinetic model for n-heptane developed by Patel, Kong and Reitz (2004) is comprised of 52 reactions and 29 species only. The simulation results indicated that this reduced chemical kinetic mechanism can provide the same predictions with those of the detailed mechanism with 1642 reactions and 179 species.

Generally, the main objective of the reduction of the detailed chemical kinetic models is to identify the redundant reactions and species which have an insignificant impact to the phenomena of interest in order to decrease the number of variables and the complexity of chemistry mechanisms (Patel, Kong and Reitz, 2004). The important features of full schemes are remained after the reduction of the chemical kinetic model and thus the simulation results of the reduced model should be similar to that of the detailed model. According to Xin et al. (2014), the original species of the detailed chemical kinetic model can be classified into three levels which are essential, marginal and unnecessary. Stageni et al (2016) pointed out that the simulation results are greatly influenced by the essential species while the unnecessary species have no effect on the simulation results. Besides, the unimportant species has no consuming any reactions and it does not change the concentration of other species when the concentration of the unimportant species is reduced. Thus, unnecessary species can be removed straightforwardly but the marginal species are selected according to their desired level of accuracy (Stagni et al., 2016). Similarly, the

reaction is considered as redundant if the impact of the reaction to the production rate of each important species is not significant.

Various reduction techniques have been developed to simplify the detailed chemical kinetic model until the model reaches a level that it can be employed in multi-dimensional CFD modeling studies such as skeletal mechanism reduction, isomer lumping, diffusive species bundling and time scale analysis (Lu and Law, 2008). The directed relation graphs with error propagation (DRGEP) and directed relation graphs reduction (DRG) methods are the most efficient ways to downsize the detailed model (An and Jiang, 2013). Nevertheless, Poon (2016) claimed that the detailed chemical kinetic model reduced by a single reduction technique is not sufficiently small to be applied in simulation as the extent of reduction is limited. Hence, several reduction techniques are integrated and arranged in an appropriate order to compensate the incompatibility of every single reduction technique and increase the efficiency of the overall reduction effort (Lu and Law, 2009). In this paper, the integrated reduction techniques established by Poon, et al. (2013) are chosen to eliminate the insignificant elementary reactions and species of the detailed chemical kinetic model. The chosen integrated reduction techniques are also known as the five-stage chemical kinetic mechanism reduction scheme. The corresponding reduction procedure is presented in the next subsection.

2.7.1   Five-Stage Chemical Kinetic Mechanism Reduction Scheme

The procedures of the five-stage chemical kinetic mechanism reduction scheme are presented in Figure 2.6. The first stage of the selected integrated reduction methods is DRGEP using Dijkstra's algorithm. It is used to sort out a subset of unimportant species from the detailed chemical kinetic model with a set of universally specifiable threshold value normalised between 0 and 1 (Poon, Ng and Gan, 2018). DRGEP is classified as one of the skeletal mechanism reduction approaches and it was developed by Pepiot et al. (2005) to solve the drawbacks of Directed Relation Graph (DRG). For instance, DRG assumes that each of the chosen species is equally important. However, some of the groups of strongly coupled species that must be entirely maintained during DRG reduction are not essential (Lu and Law, 2008; Poon et al., 2014b).

Based on the studies carried out by Poon et al. (2014), DRGEP using Dijkstra's algorithm is favourable to be applied on large-scale model reduction due to its superior performance in contrast to DRG with Error Propagation and Sensitivity Analysis (DRGEPSA) which consumes longer computational time. Moreover, Dijkstra's algorithm is capable of determining the shortest pathways from the desired species to the rest of the species. Based on the research conducted by Poon (2016), it was found that Dijkstra's algorithm can produce the most compact reduced model unlike other algorithms like Breadth First Search (BFS) algorithm and Depth First Search (DFS) algorithm. As compared to DRG method, DRGEP reduction technique analyses the species further from the target to be less important. As such, the selection of target species must be done carefully to optimize the reduced model. By doing so, a larger reduction in DRGEP can be achieved. In this paper, the selected target species are H_2, HCO, HO_2, H_2O_2, N_2, CO and CO_2 (Poon et al., 2013). The reasons of choosing these target species will be further discussed in Section 4.7.1.

After the DRGEP reduction, the isomer lumping method is applied to further decrease the size of the detailed mechanism. Isomers are important for low temperature ignition and they can be found in the huge hydrocarbon fuels. Hence, isomers with similar configurations, diffusion properties, thermal properties and functionalities are categorized together to reduce the number of species. The size of the chemical kinetic models can be significantly reduced as a result of grouping the isomers into a single representative lump. Additionally, isomers are eliminated on the condition that their concentration levels are less than 1×10^{-10} mole/cm³ (Poon et al., 2013). After that, the remaining isomers will be used in the next stage.

Reaction path analysis is introduced after the isomer lumping method. The Reaction Pathway Analyser of the simulation software ANSYS CHEMKIN-PRO is used to determine the corresponding contribution of every single pathway of reaction to the total production rate of the relative species. Furthermore, the representative isomer selection is depending on path widths that determine the production rate of the relative species. The pathways of reaction are carefully selected according to their representative species. Additionally, the Reaction Pathway Analyser presented the sensitivity analysis function at the side panel as well. With this feature, the first-order sensitivity

coefficients of species mole fractions and gas temperature about the reaction rate constants are taken into account. Therefore, the reactions with respective species with low normalized temperature sensitivity are excluded from the chemical kinetic model in the stage of reaction pathway selection (Poon et al., 2014b).

After reaction path analysis is employed, the DRG method is carried out to efficiently remove the unimportant species which had lost pathway connection by applying threshold value of 1 (Poon et al., 2013). In recent years, the method of direct relation graph (DRG) has received great attention from scholars and practitioners (Niemeyer, Sung and Raju, 2010). This method was first proposed by Lu and Low in 2005 (Lu and Law, 2006). A directed relation graph is used to map the coupling of species in DRG method. This graph-searching approach is applied to detect undesirable species for elimination depending on the pre-set allowable error threshold and chosen species (Niemeyer, Sung and Raju, 2010).

According to a study conducted by Poon (2016), the DRG method consumes shorter computational time as compared to Jacobian analysis even though they have a comparable approach in detecting major coupling between essential species. The iterative procedure and validation for each removed species are not involved in the DRG method. On top of that, the skeletal mechanism with the time directly proportional to the edges number in the plots can be identified by using DRG method in one run. Consequently, the time cost for the reduction process can be greatly reduced by using this method. In addition, Niemeyer, Sung and Raju (2010) also stated that DRG method is a reliable and famous method to reduce a large detailed chemical kinetic model with high efficiency. For example, the reduction of large mechanisms such as iso-octane and n-heptane was successfully carried out by using DRG method (Lu and Law, 2006).

Last but not least, the reaction rate constant is adjusted in the last stage of the chosen integrated reduction techniques. Due to the deviation in the ignition delay timing prediction, the reaction rate constants must be adjusted appropriately. This deviation is caused by the elimination of species from the chemical kinetic models (Poon et al., 2014b). Consequently, a minor modification of the Arrhenius parameter's A-factor value is necessary to be

performed. In such circumstances, the A-factor values of the reactions with high normalised temperature sensitivity coefficient are preferred to be adjusted (Poon, Ng and Gan, 2018). The accuracy of the model is maintained since the effects of the removed reactions are integrated in the rate constants of Arrhenius equation of the preserved reactions (Wang et al., 2015). The adjustment of the A-factor constant is carried out continuously until the maximum deviation of the reduced model in ignition delay timing is less than the maximum allowable induced error of 50 %. In short, this five-stage chemical kinetic reduction scheme is suitable for large-scale model reduction (Poon et al., 2014a). The development of the reduced HXN and HMN models by using this integrated reduction techniques will be further discussed in Chapter 4.
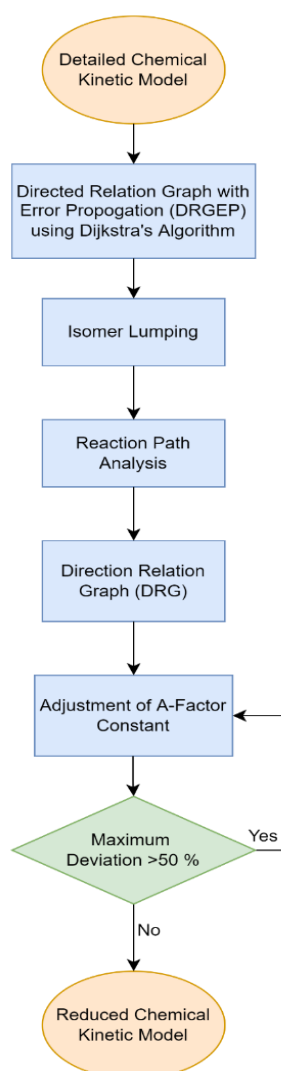
Figure 2.6: The Procedures of the Integrated Reduction Techniques (Poon et al., 2014a).

2.8   Summary

High emissions of GHG have increased the interest in the development of HRJ fuel in recent years. Based on the literature review conducted, HRJ fuels not only fulfil the stringent specifications for jet fuel but also play significant roles in limiting increases in net global GHG emissions from aviation. On top of that, HRJ fuels are classified as one of the drop-in jet fuels and thus the conventional jet fuel can be directly replaced by HRJ fuels. CHRJ-6152 fuels derived from camelina feedstock are selected to be further studied in this paper.

As illustrated in Section 2.4, CHRJ-6152 fuel is an isoparaffin-rich bio-jet fuel. Hence, the chosen detailed chemical kinetic model must be able to accommodate high molecular weight isoparaffins. In addition, the introduction of the detailed model into complicated multi-dimensional modeling is not practical at the moment as the model consists of a huge number of reactions and species. For example, the chosen detailed HXN model in this study contains 8157 elementary reactions and 2115 species whereas the detailed HMN model comprised 4469 reactions and 1114 species. Therefore, the integrated reduction techniques that incorporate five reduction techniques are selected to derive the reduced chemical kinetic models so that the restriction of the extent of reduction can be avoided.

CHAPTER 3

METHODOLOGY AND WORK PLAN

3.1   Introduction

In this chapter, the methodology and the work plan of this study will be discussed. In Section 3.2, the workflows of the research process are described. Next, Section 3.3 reports the schedule of the project. The contents of Chapter 3 are summarised in the last section of this chapter.

3.2   Workflow of Research Process

Figure 3.1 displays the flow chart of the entire research process. This flow chart is designed to visualise the sequence of stages to be followed throughout the research process. According to Figure 3.1, it can be observed that this study was carried out in two separate phases. First and foremost, Final Year Project (FYP) was started with project planning. Following that, the research articles that related to the topic of this paper were studied to understand the topic clearer. The data required for the tasks in the next few stages were also collected. After the data gathering stage, the literature review was conducted. The selections of the detailed chemical kinetic model for HRJ fuel surrogates and the reduction techniques to be performed in this study were executed in this stage as well. The next stage was the methodology formulation. The preparation of the presentation for FYP part 1 was carried out after the progress report was completed.

At the commencement of FYP part 2, the integrated reduction techniques proposed by Poon, et al. (2013) were used to downsize the selected detailed chemical kinetic models into a simplified version so the simulation can be performed smoothly. Then, the results obtained from the simulation were analysed. The reduction of the detailed chemical kinetic model was planned to be carried out again if the results are not satisfying. Once the results obtained established the objectives of this study, the final report was finalized. In the last stage of FYP part 2, all the findings and the results of this study were presented to related personnel.
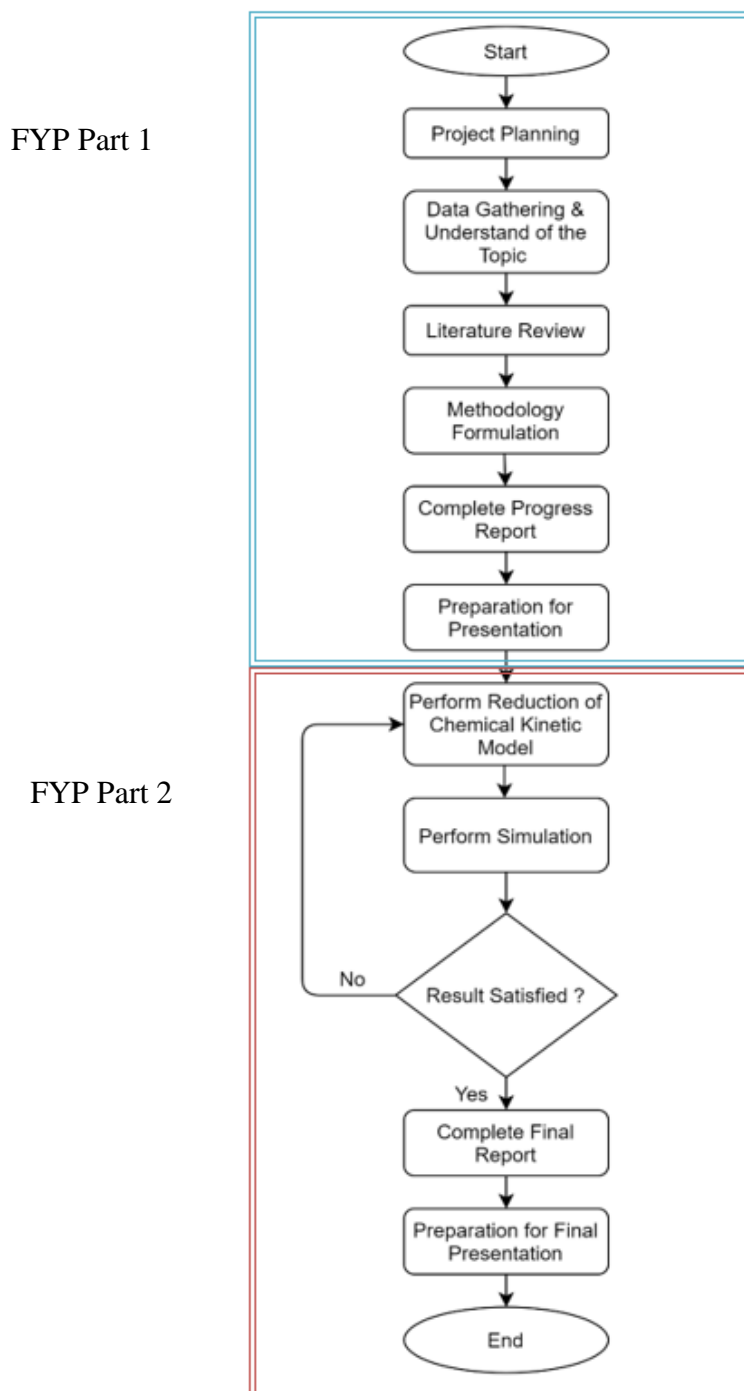
Figure 3.1: Flow Chart of Research Process.

A more detailed flow of the development of the reduced model for HRJ fuel is presented in Figure 3.2. Firstly, the selection of the existing detailed models for each fuel constituent was performed. In this study, the detailed chemical kinetic model of HXN and HMN established by Westbrook et al. (2008) and Oehlschlaeger et al. (2009) respectively were chosen for the model reduction since the main constituents of CHRJ fuel are n-alkanes (e.g., HXN)

and branched-alkanes (e.g., HMN). After that, the sizes of the chosen detailed models were reduced by using the integrated reduction techniques proposed by Poon et al. (2013). Consequently, a reduced model for HXN with 108 species and a reduced model for HMN with 132 species were derived. Intel core i5 laptop with 8 GB RAM and 2.5 GHz processing speed was applied to perform the simulation. Reaction Workbench in ANSYS CHEMKIN-PRO software was applied to perform DRGEP and DRG reduction methods whereas the isomer lumping and reaction analysis were conducted by using Reaction Pathway Analyser in ANSYS CHEMKIN-PRO. The reduced models developed were then validated against their corresponding detailed models in species profiles predictions and ID timing prediction. Both predictions were completed by executing 0-D chemical kinetic simulations in ANSYS CHEMKIN-PRO. The data collected from the simulation were extracted to Microsoft Excel to construct the graphs of ID timing and species profiles for each detailed and reduced model. After the model validations were performed, both optimized reduced models were then combined together to produce two components reduced surrogate of HRJ fuel model with 201 species, namely J2_201. Them, J2_201 is combined with the reduced MCH model developed by Tan et al. (2021) to form the multi-component reduced surrogate model for HRJ fuels with 246 species. If the maximum deviation of ID timings of the reduced model for HRJ fuels is larger than 50 %, the five-stage chemical kinetic reduction scheme is required to be performed again to obtain the optimized reduced model.
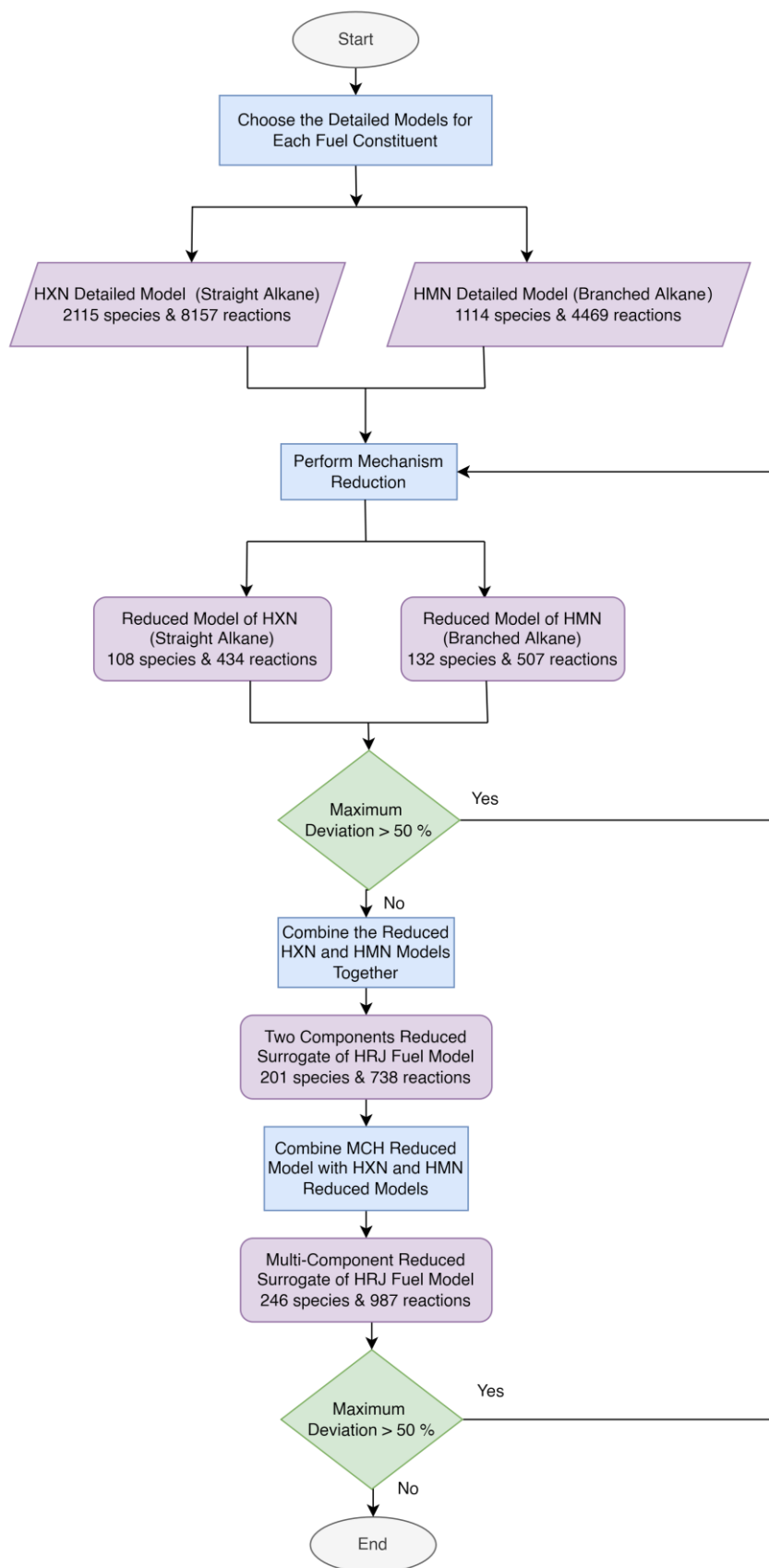
Figure 3.2: The Overall Flow of the Development of the Reduced Model for
HRJ Fuel.

3.3   Project Schedule

As aforementioned, this project is divided into two parts. Project Planning of this study is done by using the Gantt chart. The Gantt chart is vital to ensure the project can be completed within a specified period. The Gantt charts display the task description, the task duration, the planned and actual date of Final Year Project (FYP). As illustrated in Figure A-1, the first task was to register FYP title in week 1 of May trimester 2021. Next, the project planning was carried out from week 1 to week 2 to decide the tasks for the next 14 weeks. The next task was to collect the useful data consistently for the literature review. This task was conducted since week 2 to have a better understanding of the background of this research.

After that, a comprehensive literature review was performed from week 3 to week 8. This task was originally planned to complete within five weeks. However, an in-depth study of the reduction techniques of the detailed chemical kinetic model was carried out and thus it took an additional one week to complete the task. On top of that, the methodology was formulated from week 8 to week 9 which was completed in time. Then, the correction and adjustment of the progress report were completed within three weeks. Lastly, the preparation for the presentation was conducted two weeks before the end of the trimester. In summary, all the aforementioned tasks were completed as planned except the literature review.

The main task of FYP phase 2 was to develop the reduced model for HRJ fuel. In order to accomplish the goal, five steps of integrated reduction techniques were carried out. As displayed Figure A-2, the DRGEP reduction technique was first performed to reduce the size of the detailed models from week 1 to week 4 of Jan trimester 2022. It is followed by isomer lumping technique and reaction path analysis. These two tasks were conducted concurrently from week 4 to week 8. The next reduction technique that used to further downsize the chemical kinetic model is known as DRG. This task took approximately 2 weeks to be done.

The adjustment of A-factor values of Arrhenius parameter was performed to make sure the maximum tolerable error in all ID timing is less than 50 %. When both reduced models of HXN and HMN were derived, the model validations were carried out by comparing their species profiles trends and ID

timing with those of the detailed models. These two tasks were carried out continuously until the satisfactory results were obtained. Next, the reduced HRJ surrogate fuel model was finalized within one week through mechanism merging. After all the simulation works and validations of the reduced models were accomplished, the report was finished within three weeks. The last task of FYP phase 2 was to prepare the presentation slide. The presentation slide was prepared as planned. Based on and Figure A-2, it is noticed that the overall project timelines for phase 2 were in accordance with the planned schedules except for the first two tasks which are DRGEP reduction, isomer lumping and reaction path analysis. These two tasks took longer than anticipated due to the unfamiliarity of CHEMKIN-PRO software.

3.4 Summary

A series of works has been done in order to achieve the objective of this study. Based on the work plan discussed in Chapter 3, the general introduction, literature review and methodology formulation were completed at the end of FYP phase 1. The development of the reduced model for HRJ fuel and the simulation works were done at the closing stage of FYP phase 2. The integrated reduction techniques established by Poon et al. (2013) were chosen to eliminate the undesirable species from the detailed chemical kinetic model of HXN and HMN. The validations of the model were completed by comparing the ID timing and species profiles of the reduced models with their respective detailed models.

CHAPTER 4

DEVELOPMENT OF A REDUCED MODEL FOR CHRJ FUEL

4.1   Introduction

In this chapter, the constituents of HRJ fuel and the reactor models used in the simulation will be discussed in Section 4.2 and Section 4.3 respectively. In addition, the theory of the chemical kinetic will be described in the following section. Next, the testing conditions adopted in 0-D simulation to evaluate the performance of each model reduction approach are summarised in Section 4.5. The importance of ignition delay timing is depicted in Section 4.6. The 0-D simulation approach is employed here to assess and describe the surrogate mechanism of fuels because it can take into consideration many various elementary reactions and species with lower computational cost. The procedures of the mechanism reduction as well as the results of the model validation with respect to the detailed chemical kinetic model under auto-ignition condition are described in Section 4.7 and Section 4.8 respectively. DRGEP and DRG reduction approaches are performed by using Reaction Workbench in CHEMKIN-PRO software which is a profitable software package designed for kinetic modelling. Besides, Reaction Pathway Analyzer in CHEMKIN-PRO is applied to carry out the isomer lumping approach as well as the reaction path analysis. All the simulation, reduction and validation works are conducted by using Intel core i5 laptop with 8 GB RAM and 2.5 GHz processing speed. Moreover, the development of the reduced HRJ surrogate fuel model is discussed in Section 4.9. Lastly, the main findings of this study are highlighted in Section 4.10.

4.2   Fuel Constituents

The reduced HRJ surrogate fuel model is derived based on the constituents of HRJ fuel. As mentioned earlier, CHRJ-6152 fuel is selected as the target fuel in this study. Based on Figure 2.3, the compositions of CHRJ-6152 fuel comprised 78.9 % of isoparaffins (branched-alkanes), 11.1 % of cyclo-paraffins (cyclo-alkanes), 10.2 % of n-alkanes (straight alkanes) and 0.2 % of aromatic compound. Since the CHRJ-6152 fuel only contains a small amount of aromatic

compound, it is excluded from the development of the HRJ surrogate fuel model. On top of that, the major species in CHRJ-6152 fuel is branched-alkanes. Therefore, the reduced surrogate model of HRJ fuel must be derived from the detailed model of branched-alkanes. Also, it can be observed that CHRJ-6152 fuel is comprised of similar amount of cyclo-alkanes and n-alkanes. According to Westbrook et al. (2008), the n-alkanes or straight alkanes species are more crucial than cyclo-alkanes in all types of jet fuel. Hence, only the developmental works of the reduced model for straight alkanes and branched-alkanes are presented in this study. Both reduced models are derived by using the five-stage chemical kinetic reduction techniques.

HXN is the longest straight alkanes available and most works have been focused on the detailed model of HXN to study the characteristics of auto-ignition (Lee et al., 2022). Moreover, the reported work of Lee et al. (2022) also stated that the ignition properties of hydroprocessed fuel can be replicated when the detailed models of HXN and HMN are used to develop the reduced surrogate model. Due to these reasons, HXN and HMN are chosen to be the representatives of the straight alkanes and branched-alkanes of HRJ fuel respectively. The development of the reduced chemical kinetic model for HXN and HMN will be discussed in the next few sections. It is noteworthy that the development of the reduced MCH model is not involved in this study. Nevertheless, the formerly reduced MCH model developed by Tan et al. (2021) will be directly used in mechanism merging to form the reduced HRJ surrogate fuel model. This reduced MCH model was developed using the five-stage chemical kinetic mechanism reduction scheme as well. Cyclo-alkanes (e.g., MCH) is able to produce the aromatic compounds through the process of dehydrogenation because it plays a significant role in the formation of soot. Consequently, the aromatic compounds act as a soot precursor when it is converted into polycyclic aromatic hydrocarbons. MCH has a methyl group connected to 6 carbons cyclo-alkanes and hence it is recognised as one of the simplest alkylated cyclo-alkanes. Based on the research of Yang and Boehman (2009), the methyl group on the cyclo-alkanes ring improves the fuel reactivity. Thus, the HRJ surrogate fuel model has higher accuracy in the predictions of soot formation with the involvement of MCH as the fuel constituent of cyclo-alkanes.

4.3 Closed Homogeneous Batch Reactor

The closed homogeneous batch reactor of CHEMKIN-PRO software as shown in Figure 4.1 is utilised in order to validate the reduced kinetic mechanism in 0-D chemical kinetic simulations. The ID timings and mole fraction of the target species are determined as a function of time as the governing variables are time dependent variables. This reactor model is also known as a constant volume closed system in which there is no mass transfer occurs. Hence, the constrain volume and solve energy equation is set as the problem type of the simulation. The closed system only allows energy transfer across the boundary of the system as indicated in Figure 4.2. Moreover, the closed homogeneous batch reactor can be treated as an adiabatic system whereby no heat transfer from the surrounding to the system and no heat transfer from the system to the surrounding. The system is also assumed to be a transient system. In other words, the state changes of chemicals are depending on the species destruction and production when the reactions occur.
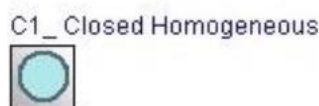
Figure 4.1: Closed Homogeneous Batch Reactor.
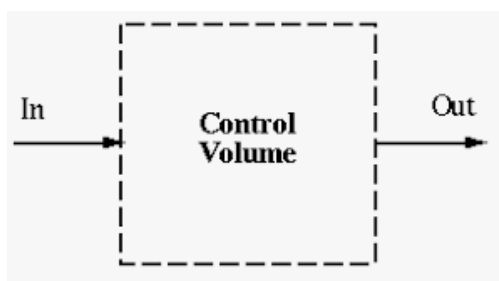
Figure 4.2: Control Volume.

The equation below is the common equation of mole balance on the reactor for species *r*.

$$\frac{dNr}{dt} = G_r + F_{in,r} - F_{out,r} \tag{4.1}$$

$\frac{dNr}{dt}$ is the build-up rate of species r within the reactor. Next, $F_{in,r}$ refers to the inflow rate of species r whereas $F_{out,r}$ is the outflow rate of species r. G_r is defined as the production rate of species r within the reactor. These parameters are measured in mole/sec. Besides, G_r can also be expressed as:

$$G_r = \nu_r \, \omega V \qquad\qquad (4.2)$$

where the stoichiometric coefficient of species r is denoted as ν_r and V refers to the volume of the reactor which is measured in m^3. Lastly, ω is defined as the rate of reaction and its unit is $m^3 \cdot$s. Since the closed homogeneous batch reactor model is used, there is no inflow and outflow of species r ($F_{in,r} = F_{out,r}$ = 0). Hence, Equation 4.1 can be rewritten as:

$$\frac{dNr}{dt} = \nu_r \, \omega V \qquad\qquad (4.3)$$

4.4 Chemical Kinetics

Chemical kinetics is one of the branches of physical chemistry that is focused on the rates of chemical reactions. The concepts of pyrolysis, oxidation and the reaction paths for fuel are crucial in the development of the reduced model. On top of that, the detailed descriptions of the chemical reactions and thermodynamic properties are satisfied with the reduced chemical kinetic models developed.

The gas-phase kinetic file of the chemical kinetic model is saved in INP format and it is comprised of every essential chemical species and elementary reaction involved in the gas-phase chemistry systems. In addition, the thermodynamic data files are saved in DAT format and the files contain the thermodynamic and the physical properties of all species. The thermodynamic files are used in 0-D simulation to obtain the ID timing predictions and species profiles predictions. The data saved inside the files can also be applied to determine the specific heat (C_p), entropy (S) and enthalpy (H). C_p is measured in the unit of J/(kg·K) whereas H and S have the same unit of J/mol. Their formulae are listed as below:

$$C_p = R \sum_{n=1}^{5} (k_n T^{n-1}) \tag{4.4}$$

$$S = R \left(k_1 \ln T + \sum_{n=2}^{5} \left(\frac{k_n T^{n-1}}{n-1} \right) + k_7 \right) \tag{4.5}$$

$$H = RT \left(\sum_{n=1}^{5} \left(\frac{k_n T^{n-1}}{n} \right) + \frac{k_6}{T} \right) \tag{4.6}$$

The gas constant R in the Equations 4.4, 4.5 and 4.6 has a unit of J/(mol·K). The parameter T refers to the temperature and it is measured in Kelvin whereas k_n is the leading coefficient. In addition, two different formulae can be applied to calculate the production rate of species i^{th} in x^{th} reaction. Both equations are affected by the forward reaction rate constant and reverse reaction rate constant and they are listed as below:

$$\dot{w}_i = \sum_{x=1}^{Nrec} v_{ix} \, q_x \tag{4.7}$$

$$\dot{w}_i = \sum_{x=1}^{Nrec} v_{ix} \left(k_{f,x} \prod_{i}^{N_{sp}} (X_i)^{v_{ix}} - k_{r,x} \prod_{i}^{N_{sp}} (X_i)^{v_{ix}} \right) \tag{4.8}$$

$\dot{w}_i$ is the production rate of species i^{th} and it is measured in the unit of mol/(m^3·s). Next, the number of reactions is represented by the abbreviation N_{rec} and v_{ix} is the overall stoichiometric coefficient of species i^{th} in x^{th} reaction. The parameter q_x represents the progress rate for x^{th} reaction and the capital letter X_i refers to the mole concentration of species i^{th}. These two parameters are measured in the unit of mol/(m^3·s). Moreover, N_{sp} is the number of species. Lastly, $k_{f,x}$ and $k_{r,x}$ represent the forward and reverse reaction rate constant of species i^{th} respectively.

Furthermore, the gas-phase kinetic files also provide the A-factor constants of Arrhenius parameters for all elementary reactions as shown in Figure 4.3. The Arrhenius parameters play a vital role in the consumption of each species and the computation of the production rates which consequently control the chemical pathways of the process of fuel combustion.

```
                                               (k = A T**b exp(-E/RT))
    REACTIONS CONSIDERED                           A        b         E

 1. hmn-r2+h=hmn                                 1.00E+14   0.0       0.0
 2. hmn-r4+h=hmn                                 1.00E+14   0.0       0.0
 3. hmn-r7+h=hmn                                 1.00E+14   0.0       0.0
 4. c12h25-1+pc4h9=nc16h34                       8.00E+12   0.0       0.0
 5. c10h21-1+pc4h9=nc14h30                       8.00E+12   0.0       0.0
 6. c6h13-1+pc4h9=nc10h22                        8.00E+12   0.0       0.0
 7. 2pc4h9=nc8h18                                8.00E+12   0.0       0.0
 8. ac15h31+ch3=hmn                              1.00E+13   0.0       0.0
 9. cc15h31+ch3=hmn                              1.00E+13   0.0       0.0
10. chx1*o2j=>c2h3+ch2co+c2h4                    8.11E+13   0.5   28517.0
11. chx1*o2j=>2c2h4+hcco                         4.24E+15   0.2   36287.0
```

Figure 4.3: Arrhenius Parameters in Gas-Phase Kinetic File.

According to Equation 4.9, three Arrhenius parameters are used to determine the forward reaction rate constant, k_f which are the pre-exponential factor, A (mole·cm·sec·K), the activation energy, E_a (cal/mol) and the temperature exponent, $ß$. The parameter R is the gas constant which is measured in J/(mol·K). Besides, $e^{(\frac{-E_a}{RT})}$ in Equation 4.9 is actually the fraction of collisions that required to overcome the activation barrier whereby the unit of the parameter T is Kelvin and it represents the temperature of the gas-phase combustible mixtures. On the other hand, the reverse reaction rate constant, k_r can be obtained by dividing the forward reaction rate constant, k_f with the equilibrium constant, k_c as illustrated in Equation 4.10.

$$k_f = AT^{ß}e^{(\frac{-E_a}{RT})}$$
(4.9)

$$k_r = \frac{k_f}{k_c}$$
(4.10)

4.5 Operating Conditions for Auto-ignition

In this study, the reduced model will only be validated under the auto-ignition condition. In order to perform the validation of the reduced mechanism in 0-D kinetic simulation, the closed homogeneous batch reactor in CHEMKIN-PRO software is used. The validation exercise of the reduced models usually requires analysing ID timing. One of the famous validation methods for the reduced models is to compare the computational predictions of ID timing. Such comparisons are able to offer a good understanding of the fundamental

chemistry as 0-D simulation is free from the transport effects. The test conditions used in the simulations are described in Table 4.1.

Table 4.1: The Operating Conditions Applied for Validation of the Reduced Model (Poon, 2016; Allen et al., 2016).

Parameter	Operating Conditions for Auto-ignition
Initial Temperature, T (K)	650 – 1350 (with interval of 100 Kelvin)
Initial Pressure, P (bar)	5, 10, 20
Equivalence Ratio, ϕ (-)	0.5, 1.0, 2.0

The range of initial temperature and equivalence ratio, ϕ are decided based on the studies of Poon (2016) and the traditional in-cylinder pressure values of light-duty machines during the event of fuel injection (Le and Kook Sanghoon, 2015). According to Allen et al. (2016), the ignition delay times of CHRJ fuels are measured at 5, 10 and 20 bar. Since the target fuel of this study is CHRJ fuels and thus the values of initial pressure are chosen according to their properties.

4.6   Ignition Delay Timing

Ignition delay (ID) timing is a vital parameter in the aircraft engines combustor design. Therefore, the reduced models developed in this work are validated through comparison with the predictions of ID timing computed by the detailed models and reduced models. The ID time is known as the interval of time between the starting reference points. Rapid spontaneous ignition is needed to achieve efficient combustion as well as the following complete reaction in the engine combustion. There are many autoignition research have been conducted for homogeneous fuel mixture in a closed device such as shock tube and rapid compression machine (RCM). ID timing measured in these closed devices is only affected by the chemical kinetics that rely on the pressure histories and

temperature of the mixture of fuel. It is noted that the pressure and the temperature of the mixture of fuel can be different broadly for various types of fuels (Zhang et al., 2016). For instance, the ID timing of S-8, JP-8 and Jet A fuels are measured in the range of temperature of 615 K to 1100 K and the range of pressure of 7 bar to 30 bar (Kumar and Sung, 2010). Moreover, Vasu, Davidson and Hanson (2008) measured the ID timing of the JP-8 and Jet A fuels in the pressures of 17 atm to 51 atm and a temperature range of 715 K to 1229 K. In short, ID timing is a useful parameter to validate the reduced model under auto-ignition condition. However, it is lack of stringency when the validation of the reduced models is carried out by comparing the ID timing only. Therefore, the reduced chemical kinetic model is validated against the detailed chemical kinetic model in both species mole fraction predictions and ID timing predictions instead of ID timing predictions only. By doing so, the reduced models developed are more reliable.

4.7   The Procedures of Mechanism Reduction through Integrated Reduction Techniques

The detailed explanations of the mechanisms reduction flow will be described in this section. The integrated reduction techniques that applied to perform mechanism reduction in this study consist of five different stages. The details of each stage of mechanism reduction are depicted from Section 4.7.1 to Section 4.7.5. Additionally, the model validations are performed right after applying DRGEP and DRG reduction techniques. The validations are carried out by evaluating the ID timing predictions and species mole fraction predictions of the reduced model with the detailed model under a broad range of test conditions in zero-dimensional simulation as discussed in Section 4.5. There are two detailed models are selected to be studied in this paper. Both HXN and HMN detailed models undergo the same reduction procedures as their reduced models are developed through the five-stage reduction scheme.

4.7.1   Directed Relation Graph with Error Propagation (DRGEP)

The first reduction technique that used to reduce the size of the detailed chemical kinetic model is known as DRGEP reduction with Dijkstra's algorithm. Direct Interdependency Coefficient (DIC) is used in this reduction technique to

compute the coupling between two different species in reference to the rate of production and consumption. DIC can be determined by the following equation:

$$\text{DIC} = \frac{\sum_{k=1,Nrec} |v_{c,k} \omega_k \delta_{d,k}|}{max \ (P_c, C_c)} \qquad (4.11)$$

From the equation above, N_{rec} represents the total number of reactions while $v_{c,k}$ refers to the coefficient of stoichiometric for species k. Next, ω_k is defined as the rate of reactions for k^{th} reaction and it is measured in the unit of m³·s. For $\delta_{d,k}$, it is defined as the participation of species d in k^{th} reaction. The production rate for species c is denoted as P_c while the consumption rate for species c is denoted as C_c. Both parameters are measured in mol/(m³·s).

DRGEP reduction technique has the advantage over DRG method. For example, DRGEP approach considers the process of error propagation while DRG method assumes all the interrelated species are equally critical. For DRGEP approach, the species is said to be insignificant when the overall path-dependent coefficient, R_{cd} of species is smaller than the tolerable error threshold, E_t of 50 %. In order to calculate R_{cd}, the parameters such as the total number of species in path x, $N_{s,x}$, the coefficient of direct interaction, r and the jth species, s_j must be determined first. R_{cd} can be found by using the equation below:

$$R_{cd} = max_{all \ path \ x} (\prod_{j=1}^{N_{s,x}-1} r_{s_j s_{j+1}}) \qquad (4.12)$$

As aforementioned, the target species such as H_2, HCO, H_2O_2, HO_2, N_2, CO and CO_2 are selected for DRGEP reduction exercise. According to Poon et al. (2013), H_2 is selected as one of the target species because it permits a larger degree of reduction. In addition, HCO species, H_2O_2 species and HO_2 radical are chosen because they play a significant role in chain branching reactions. N_2 is selected as an inert species while CO and CO_2 are the major emission species.

This ensures a greater degree of reduction with better accuracy by choosing these species as the target species in DRGEP reduction (Poon et al., 2013). The application of DRGEP in the first stage of reduction also makes sure

the essential elementary reactions and species involving in the chain-branching and oxidation processes are preserved during the removal procedures. The Reaction Workbench in CHEMKIN-PRO is used to perform DRGEP reduction and Figure 4.4 displays the selected target species that mentioned earlier.
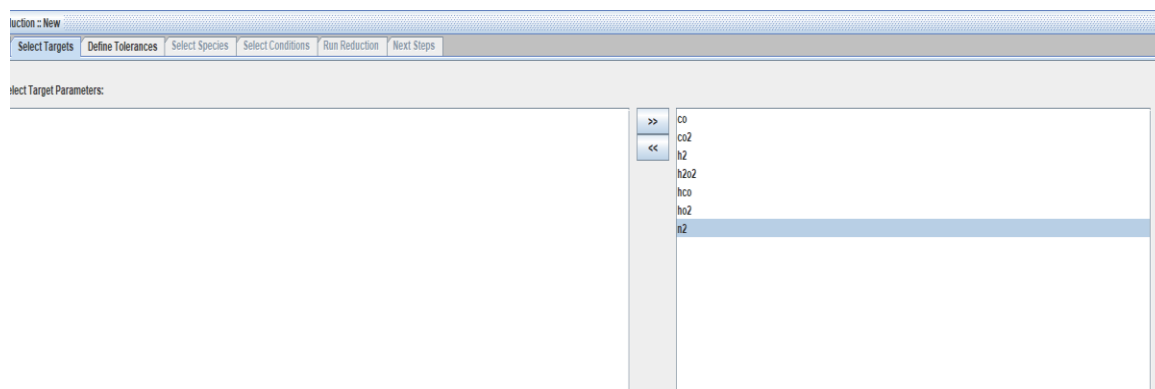
Figure 4.4: The Selected Target Species in DRGEP.

A reduced chemical kinetic model for HXN with 2296 reactions and 501 species and a reduced chemical kinetic model for HMN with 1617 reactions and 390 species are successfully produced upon application of DRGEP reduction method. Originally, the detailed model of HXN consists of 8157 elementary reactions and 2115 species while the detailed HMN model contains 4469 reactions and 1114 species. By using Equation 4.13, the reduction percentage in the number of species for the detailed HXN and HMN models are determined as 76.312 % and 64.991 % respectively. The equation below is used to calculate the percentage of reduction in number of species.

$$Percentage\ of\ reduction\ in\ species\ number = \frac{N_D - N_R}{N_D} \text{ x } 100\ \% \qquad (4.13)$$

Where

N_D = Number of species of detailed model

N_R = Number of species of reduced model

In order to ensure the reduced models developed in this stage are able to reproduce the combustion and thermodynamics properties of the detailed chemical kinetic mechanism, the validations of the reduced chemical kinetic

model against the detailed chemical kinetic model under a broad range of auto-ignition conditions are performed. Figure 4.5 and Figure 4.6 show the comparison between the ID timing of the detailed and the reduced mechanisms for HXN and HMN developed via DRGEP reduction respectively. According to the findings by Luo et al. (2012), Yang et al. (2012) and Poon (2016), the allowable error for large-scale model reduction is commonly varying from 30 % to 50 %. In this study, the maximum allowable induced error for ID timing comparisons against the detailed model is selected as 50 %. The maximum deviation can be determined by using Equation 4.14.

$$Maximum\ Deviation = |\frac{t_D - t_R}{t_D}| \times 100\ \% \qquad (4.14)$$

Where

t_D = ID timing computed by detailed model (s)

t_R = ID timing computed by reduced model (s)

Based on Figure 4.5 and Figure 4.6, it can be observed that both reduced models provide a similar trend of the ID timing prediction with their detailed counterparts for all equivalence ratios and the initial pressure. On top of that, the maximum deviations of ID timing of the reduced model for HXN and the reduced model for HMN developed by using DRGEP method are only 19.31 % and 10.23 % respectively as compared to their respective detailed model. The discrepancies of the ID timing are acceptable since the maximum deviations of both reduced models are within 50 %. As such, both reduced models developed through DRGEP reduction are said to be valid and ready to be used for the next stage of reduction.
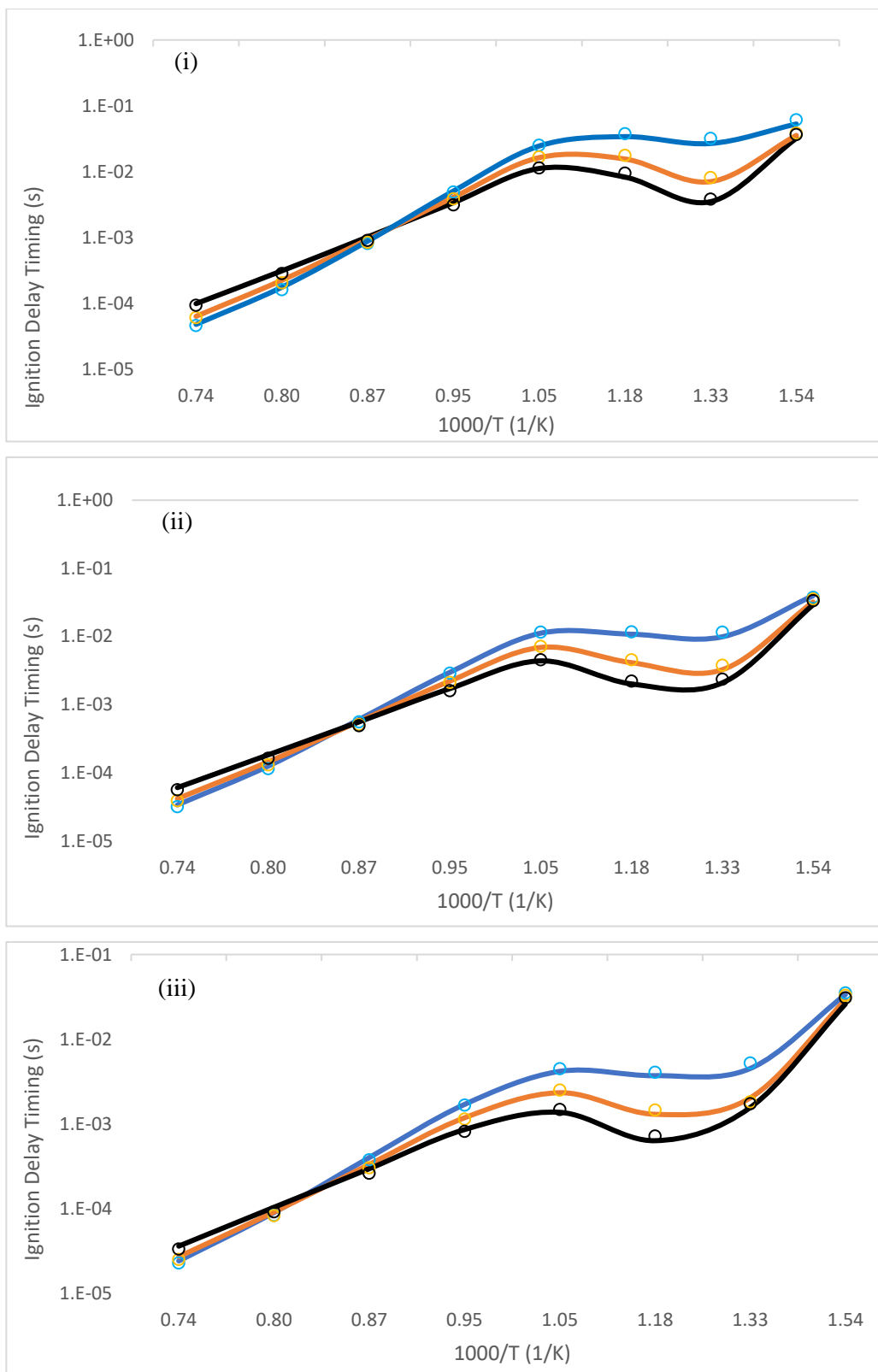
Figure 4.5: ID Timing predicted by the Detailed Model (solid lines) and the Reduced Model (symbols) of *N-Hexadecane* After Applying DRGEP Reduction at ϕ of 0.5 (Blue), 1.0 (Orange), 2.0 (Black) and Initial Pressure of (i) 5 bar, (ii) 10 bar, (iii) 20 bar.
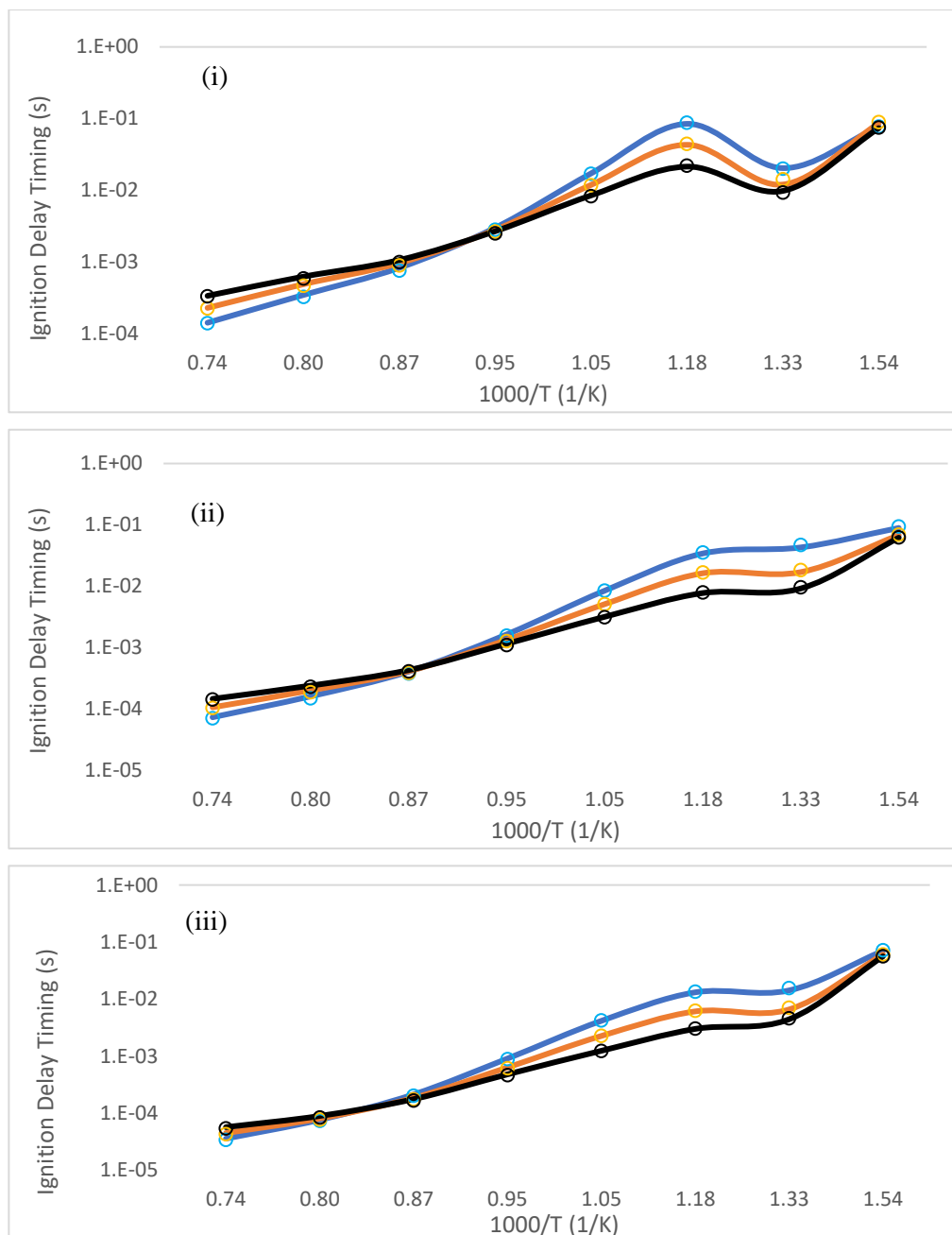
Figure 4.6: ID Timing predicted by the Detailed Model (solid lines) and the Reduced Model (symbols) of *HMN* After Applying DRGEP Reduction at ϕ of 0.5 (Blue), 1.0 (Orange), 2.0 (Black) and Initial Pressure of (i) 5 bar, (ii) 10 bar, (iii) 20 bar.

4.7.2 Isomer Lumping

Subsequently, the isomer lumping approach is performed to group the remaining isomer with similar thermodynamic properties and transport properties into a specific representative species. Besides, the isomers with low production rate ($< 1 \times 10^{-10}$ mole/(cm^{3}s)) are directly removed from the reduced

model. With the aid of the Reaction Pathway Analyzer, the unimportant isomers of the reduced model are able to be detected. Figure 4.7 shows the rate of production for each isomer in the Reaction Pathway Analyzer. Generally, the isomer with high rate of production is chosen as the representative isomer in each isomer group. For example, HMN-R2 has the highest production rate among its own isomer group as shown in Figure 4.7. On the other hand, the production rate of the species of $CC_{15}H_{31}$ is less than 1 x 10^{-10} mole/(cm^{3}s). Hence, HMN-R2 is selected as the representative isomer and the species $CC_{15}H_{31}$ is eliminated.
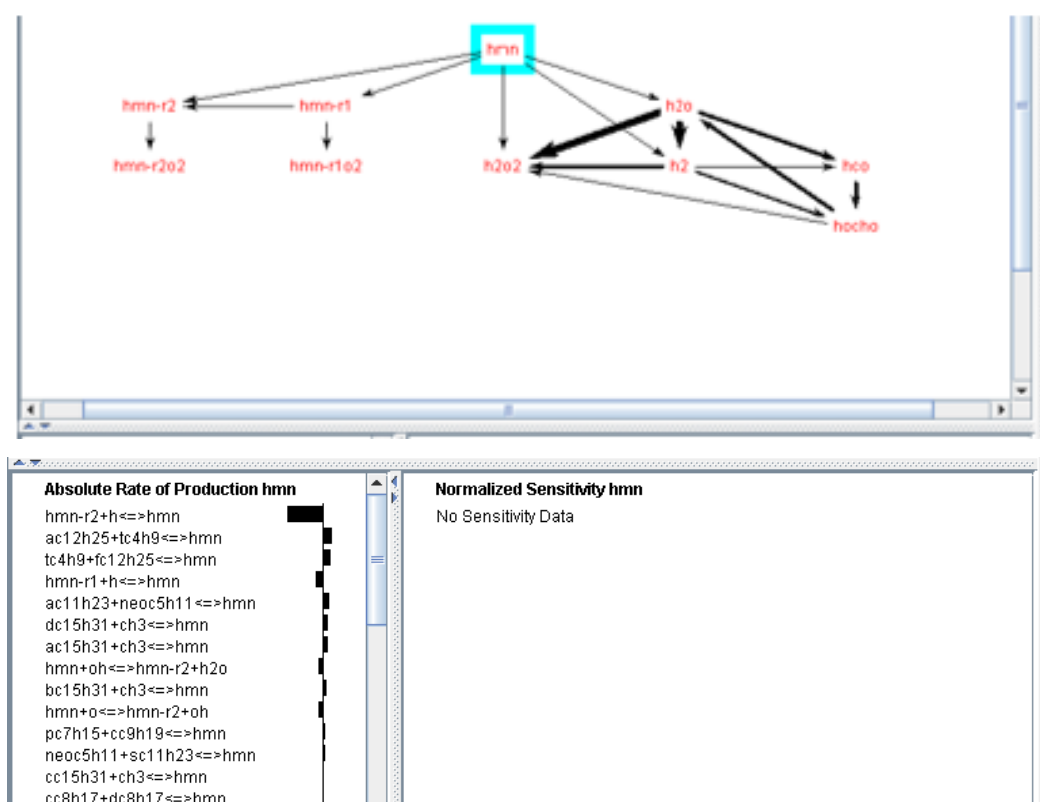
Figure 4.7: The Rates of Production for HMN.

Table 4.2 and Table 4.3 display several instances of the isomers that existed in the detailed HXN model and detailed HMN model respectively. There might be some repeated reactions present in the model due to the existence of the isomers in the chemical kinetic model. Therefore, isomer lumping is a useful technique to further downsize the chemical kinetic model with huge carbon number owing to the existence of large number of isomers.

Table 4.2: The Lumped Isomers and the Representative Lump for *n-Hexadecane* Mechanism.

Representative Lump	Lumped Isomers
$C_{16}H_{33}$-4	$C_{16}H_{33}$-1, $C_{16}H_{33}$-2, $C_{16}H_{33}$-3, $C_{16}H_{33}$-5, $C_{16}H_{33}$-6, $C_{16}H_{33}$-7, $C_{16}H_{33}$-8
$C_{16}H_{33}O_2$-4	$C_{16}H_{33}O_2$-1, $C_{16}H_{33}O_2$-2, $C_{16}H_{33}O_2$-3, $C_{16}H_{33}O_2$-5, $C_{16}H_{33}O_2$-6, $C_{16}H_{33}O_2$-7, $C_{16}H_{33}O_2$-8
$C_{16}KET_4$-3	$C_{16}KET_4$-2, $C_{16}KET_4$-5, $C_{16}KET_4$-6, $C_{16}KET_4$-7
$C_6H_{12}OOH_1$-2	$C_6H_{12}OOH_1$-3, $C_6H_{12}OOH_1$-4

Table 4.3: The Lumped Isomers and the Representative Lump for *HMN* Mechanism.

Representative Lump	Lumped Isomers
HMN-R2	HMN-R1, HMN-R3, HMN-R4 HMN-R5, HMN-R6, HMN-R7 HMN-R8
$HMNO_2$-4	$HMNO_2$-3 $HMNO_2$-5
$HMNOOH_4$-2	$HMNOOH_4$-3, $HMNOOH_4$-5 $HMNOOH_4$-7

4.7.3   Reaction Path Analysis

Upon completion of the isomer lumping approach, a reduced HXN model with 1538 reactions and 389 species and a reduced HMN model with 1220 reactions and 288 species are generated successfully. The next stage of the reduction is known as reaction path analysis. In this stage, Reaction Pathway Analyzer in

ANSYS CHEMKIN-PRO is utilized to identify the main pathways of reaction. Reaction path analysis is important because the parallel pathways of reaction are still present in the process of oxidation despite all the unimportant isomers were lumped into the particular representative species.

The reaction analysis process for both HXN and HMN models will proceed until the basic species such as CO_2 is obtained. The main reaction pathways for both mechanisms are displayed in Figure 4.8 and Figure 4.9. In this study, only the results of the main reaction pathways for ϕ of 1.0, initial pressure of 10 bar and temperature of 950 K are shown since comparable reaction pathways can be found for other test conditions. According to Figure 4.8, H-atom abstraction is first taking place to convert n-$C_{16}H_{34}$ to $C_{16}H_{33}$-4. Next, $C_{16}H_{33}O_2$-4 is formed through the addition of O_2 molecule to the alkyl radical, R which is $C_{16}H_{33}$-4. This is followed by RO_2 isomerization to produce $C_{16}OOH_4$-3 and O_2 addition to QOOH group to get $C_{16}OOH_4$-3O_2. After that, $C_{16}KET_4$-3 is produced due to the production of ketohydroperoxides occur. Ketohydroperoxides decomposition is taking place to generate $NC_{12}H_{25}CHO$. Then, this compound undergoes aldehyde decomposition to form $NC_{12}H_{25}CO$. This series of reactions will proceed to produce smaller alkyl radical until the basic species is found. It is noted that the reaction path of HMN is similar to that of HXN.

nC16H34

↓

C16H33-4

↓

C16H33O2-4

↓

C16OOH4-3

↓

C16OOH4-3O2

↓

C16KET4-3

↓

nC12H25CHO

↓

nC12H25CO

┆ Long reaction

nC4H9CO

↓

C2H4

↓

C2H3

↓

CH2O

↙   ↘

HCO   H2O

↓

CO

↓

CO2
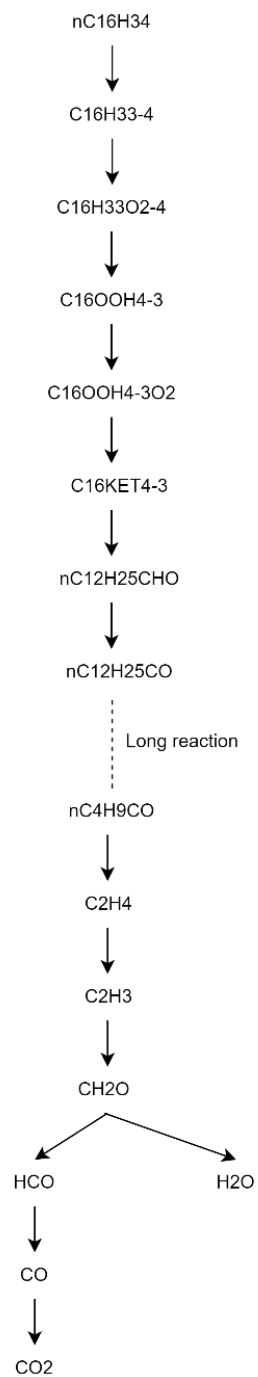
Figure 4.8: Main Reaction Pathway of *n-Hexadecane* for ϕ of 1.0, Pressure of 10 bar and Temperature of 950 K.

HMN

↓

HMN-R7

↓

HMN-R7O2

↓

HMNOOH7-8

↓

HMNOOH7-8O2

↓

HMNKET7-8

↓

SC11H23

⋮

Long Reaction

⋮

CO2
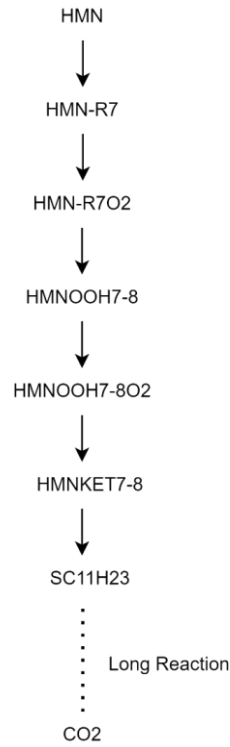
Figure 4.9: Main Reaction Pathway of *HMN* for ϕ of 1.0, Pressure of 10 bar and Temperature of 950 K.

Furthermore, the normalised temperature A-factor sensitivity, $Sen_{normalised}$ is also determined in this stage to further downsize the reduced model. The reactions with more than 0.2 of $Sen_{normalised}$ are maintained in the reduced model while the reactions with low $Sen_{normalised}$ are eliminated. There is only a slight impact on the predictions of ID timing after eliminating the species that involved in the reactions with low $Sen_{normalised}$. The temperature A-factor sensitivity for each reaction can be obtained by using CHEMKIN-PRO software. The formula of normalised temperature A-factor sensitivity, $Sen_{normalised}$ for i^{th} reaction is written as below:

$$\text{Normalised Temperature A-factor for } i^{th} \text{ reaction} = \frac{Temperature\ Sensitivity\ for\ i^{th}\ reaction}{Maximum\ Temperature\ Sensitivity\ Among\ All\ Reactions} \quad (4.15)$$

It is noted that the normalized temperature sensitivities of reactions are similar for all testing conditions. Therefore, only the normalized temperature sensitivities of reactions for HXN and HMN mechanism at ϕ of 1.0, pressure of

10 bar and temperature of 950 K are presented in Figure 4.10. Besides, Figure 4.10 only displays the normalized temperature sensitivity of some reactions. Based on the figure below, it can be observed that the normalized temperature sensitivities of the reactions $C_{16}H_{33}O_2$-2<=>$C_{16}OOH_2$-4 and $C_{12}OOH_1$-3<=>$C_{12}O_1$-3+OH of HXN are less than 0.2. Hence, both of these reactions can be removed. Similarly, the reactions $C_2H_3+O_2$<=>CH_2O+HCO and C_3H_6+OH<=>C_3H_5-a+H_2O of HMN are eliminated due to their low normalized temperature sensitivities. The problem of parallel reaction pathways is now significantly diminished as all the reactions with low normalized temperature sensitivity are excluded.

Figure 4.10: Normalised Temperature A-Factor Sensitivity of Reactions for (i) *n-Hexadecane* and (ii) *HMN* models at ϕ of 1.0, Pressure of 10 bar and Temperature of 950 K.

4.7.4   DRG

For DRG reduction method, the normalised involvement, r_{cd} is important in determining the importance of species d to the species c production. It can be determined by the equation:

$$r_{cd} = \frac{\sum_{k=1,Nres} |v_{c,k}\omega_k\delta_{d,k}|}{\sum_{k=1,Nrex} |v_{c,k}\omega_k|}$$

(4.16)

The parameters of $N_{rec}, v_{c,k}$, ω_k and $\delta_{d,k}$ are similar to those of DRGEP. When the species d is not involved in the kth reaction, the value of $\delta_{d,k}$ will be set to 0. On the other hand, $\delta_{d,k}$ is assigned to 1 when species d participates in kth reaction. In this study, DRG method is employed by using CHEMKIN-PRO software once the reduced HXN model with 846 reactions and 221 species and the reduced HMN model with 786 reactions and 189 species were generated. The purpose of conducting DRG reduction is to remove the unimportant species which have lost the pathway connection to the main species due to the application of isomer lumping and reaction pathway analysis.

After the reduced model of HXN with 108 species and the reduced model of HMN with 132 species are formed, the validations of the reduced mechanisms against the detailed mechanisms under auto-ignition conditions are carried out again. Figure 4.11 and Figure 4.12 presented the ignition delay time that computed by the reduced models and detailed models of HXN and HMN respectively. It is spotted that the difference in ID timing predictions between the detailed models and reduced models are huge in all temperature regions. This is due to the removal of the pathways of reaction that were specific for oxidation at overall temperature in isomer lumping and reaction path analysis stages. On top of that, the maximum deviations between the detailed model and reduced model of HXN and HMN are 338.91 % and 254.3 % which are greater than the maximum tolerable induced error. Therefore, the next phase of the reduction technique must be carried out to minimize the percentage error.
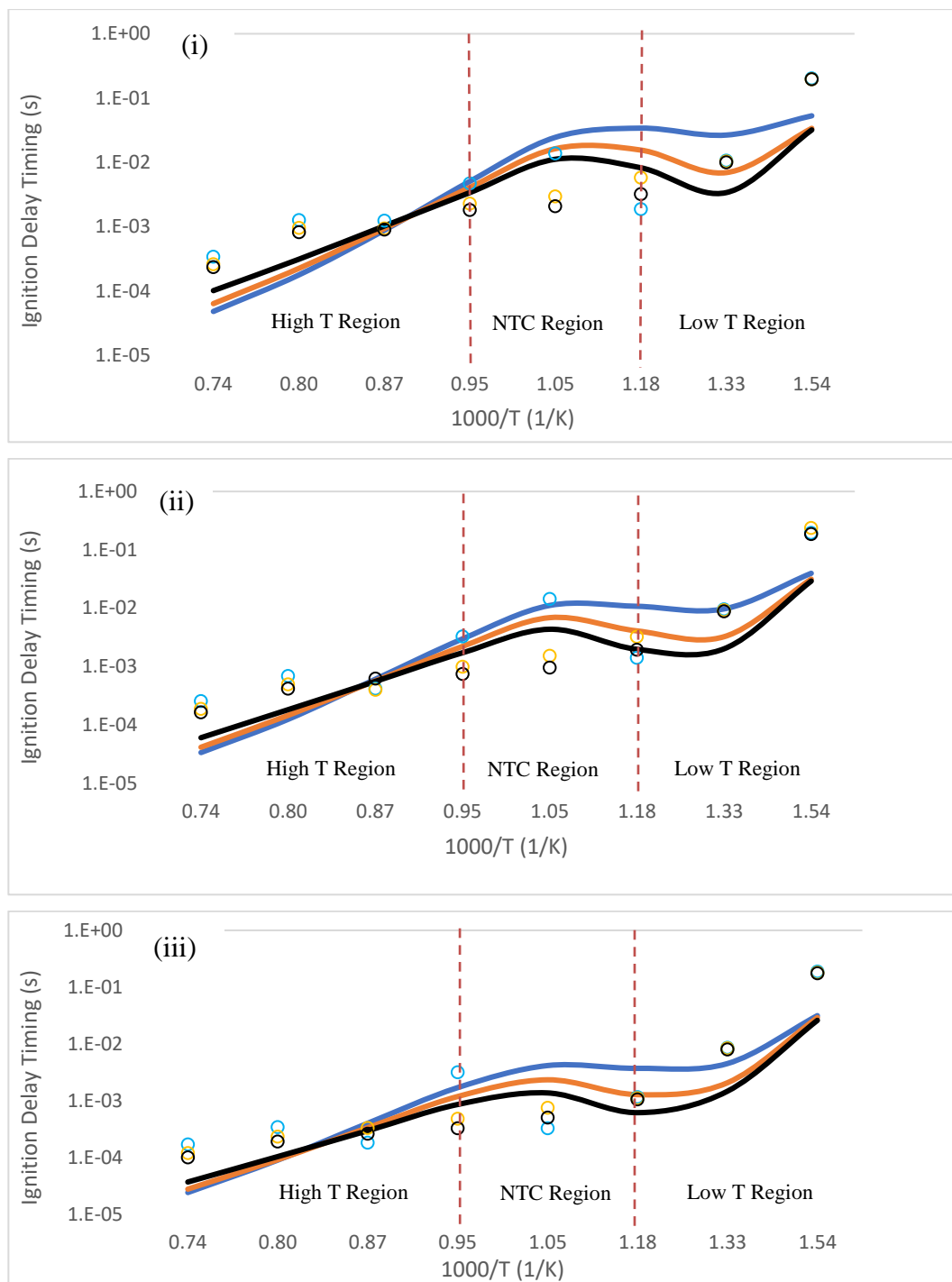
Figure 4.11: ID Timing predicted by the Detailed Model (solid lines) and the Reduced Model (symbols) of *N-Hexadecane* **Before** the Adjustment of A-Factor Constant at ϕ of 0.5 (Blue), 1.0 (Orange), 2.0 (Black) and Initial Pressure of (i) 5 bar, (ii) 10 bar, (iii) 20 bar.
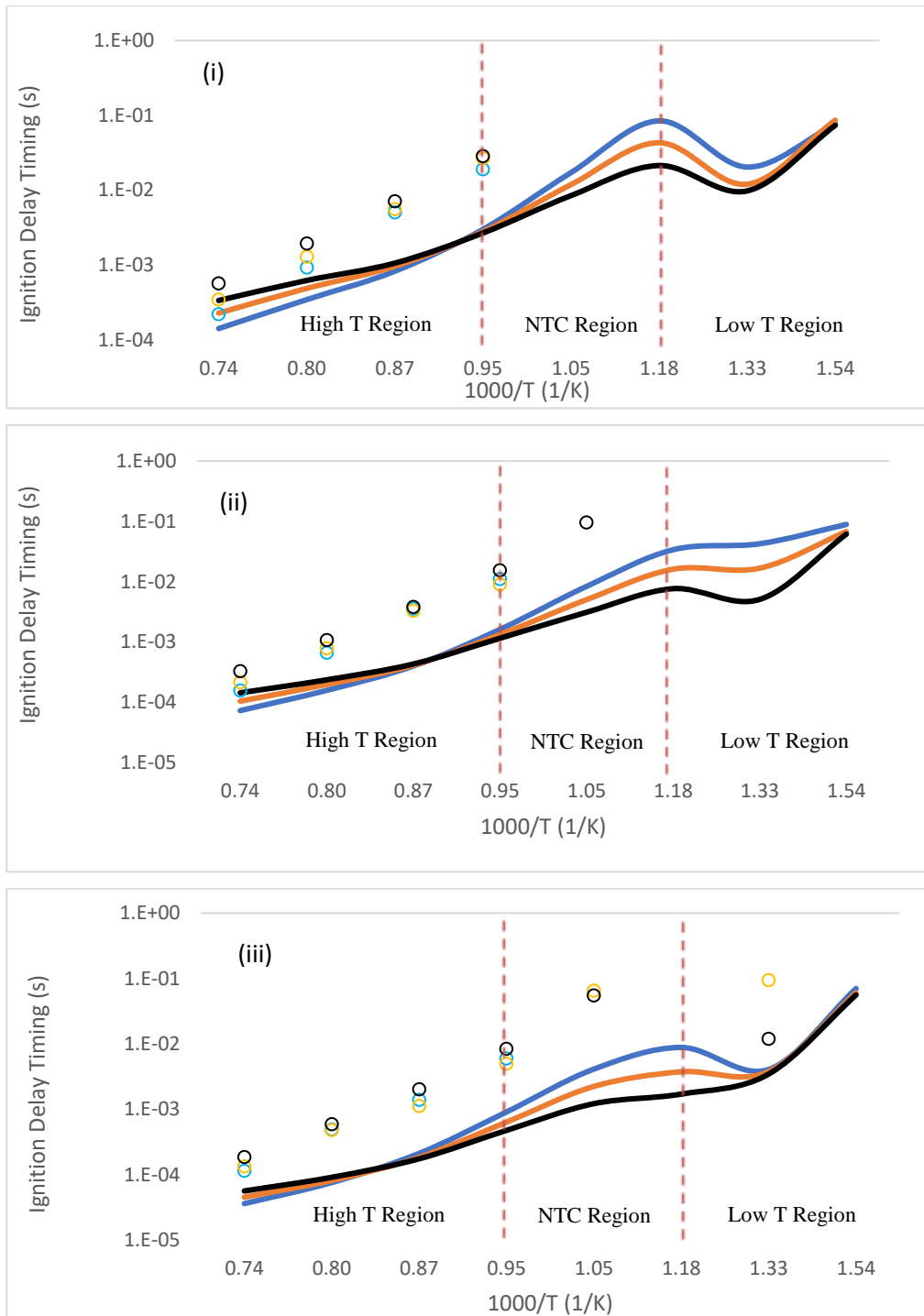
Figure 4.12: ID Timing predicted by the Detailed Model (solid lines) and the Reduced Model (symbols) of *HMN* **Before** the Adjustment of A-Factor Constant at ϕ of 0.5 (Blue), 1.0 (Orange), 2.0 (Black) and Initial Pressure of (i) 5 bar, (ii) 10 bar, (iii) 20 bar.

4.7.5 Adjustment of A-Factor Constant

Since the removal of species from the chemical kinetic model would cause deviation in the ID timing predictions, the A-factor constant of Arrhenius parameters of the elementary reactions are adjusted in this section. It is noteworthy that the isomer lumping method caused the largest difference in ID timing predictions among the five reduction methods. This is because of the isomers with similar production and consumption reaction pathways are lumped into a representative lump. Nevertheless, a single representative lump is inadequate to represent the whole isomer group and therefore the A-factor constant of Arrhenius parameters is required to be tuned. It is remarkable that only the A-factor constants of the reactions with high normalized temperature sensitivity are chosen for tuning as they have greater impact on the ID timing predictions. Figure 4.13 illustrates the comparisons of the normalised temperature A-factor sensitivity of reactions at different temperatures for reduced HXN and HMN models.
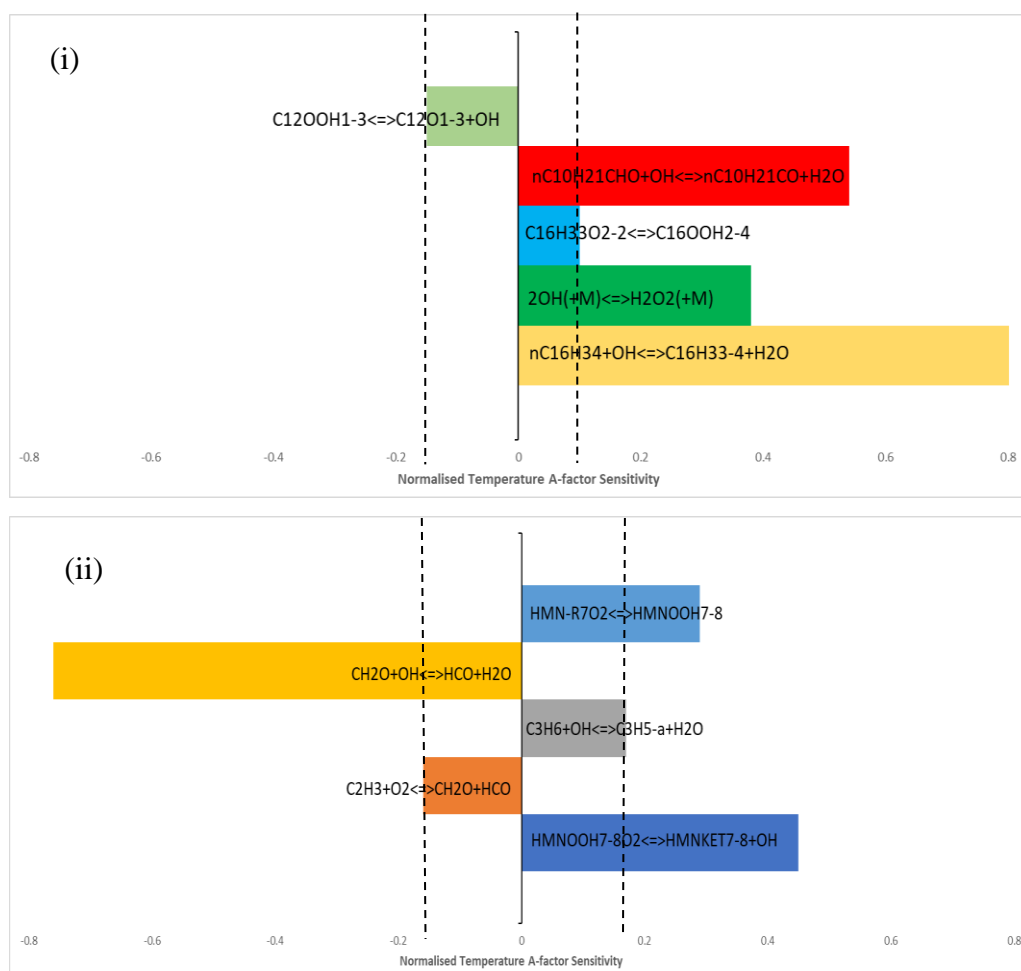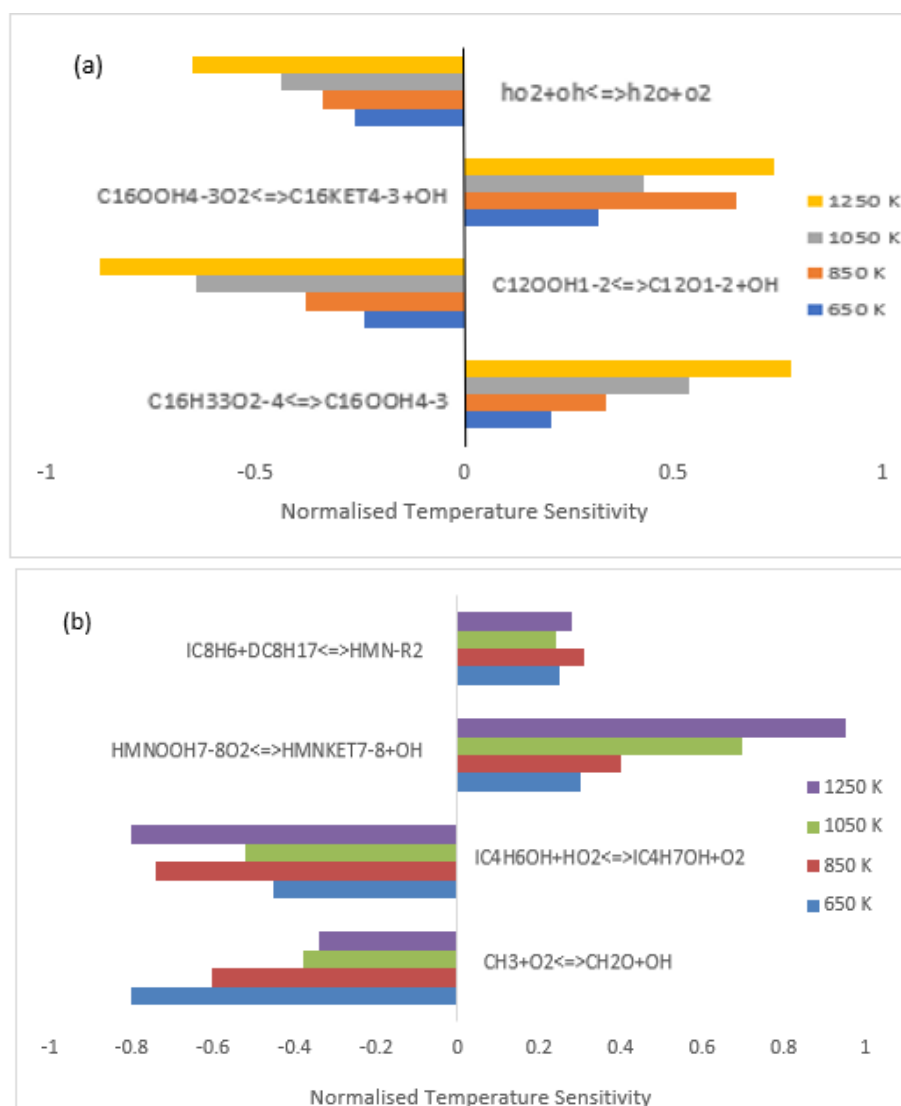
Figure 4.13: Normalised Temperature A-Factor Sensitivity of Reactions for reduced (i) *n-Hexadecane* and (ii) *HMN* models at ϕ of 1.0, Pressure of 10 bar and Temperature of 650 K, 850 K, 1050 K and 1250 K.

Once the reactions with high $Sen_{normalised}$ are confirmed, the A-factor constants of these reactions are selected for tuning. The original and modified A-factor constant of the selected reactions for HXN model and HMN model are reported in Table 4.4 and Table 4.5 respectively. In this study, the temperature region of the ID timing graph is divided into high temperature region (1050 K to 1350 K), Negative Temperature Coefficient (NTC) region (850 K to 1050 K) and low temperature region (650 K to 850 K).

Table 4.4: The Adjustment of A-Factor Constants of Reactions for *n-Hexadecane* Models.

HXN		
Reactions	A-Factor Constants	Effects
(R1) $C_{16}H_{33}O_2$-4<=>$C_{16}OOH_4$-3	2.00E+11 (Original) 6.00E+12 (Adjusted)	Improvement at low and high temperature
(R2) $C_{12}OOH_1$-2<=>$C_{12}O_1$-2+OH	6.00E+11 (Original) 8.00E+12 (Adjusted)	Improvement in overall temperature
(R3) $C_{12}OOH_1$-2<=>$C_{12}H_{24}$-1+HO_2	1.61E+20 (Original) 5.61E+21 (Adjusted)	Improvement at low temperature
(R4) $C_{16}OOH_4$-3O_2<=>$C_{16}KET_4$-3+OH	1.00E+11 (Original) 5.00E+12 (Adjusted)	Improvement at NTC and high temperature

Table 4.5: The Adjustment of A-Factor Constants of Reactions for *HMN* Models.

HMN		
Reactions	A-Factor Constants	Effects
(R5) CH_3+O_2<=>CH_2O+OH	7.47E+11 (Original) 7.47E+12 (Adjusted)	Improvement in overall temperature
(R6) IC_4H_6OH+HO_2<=>IC_4H_7OH+O_2	4.19E+12 (Original) 4.19E+13 (Adjusted)	Improvement at NTC
(R7) $HMNOOH_7$-8O_2<=>$HMNKET_7$-8+OH	1.25E+10 (Original) 5.25E+08 (Adjusted)	Improvement at low temperature

For HXN model, the A-factor constant for reaction $C_{16}H_{33}O_2$-$4 <=> C_{16}OOH4$-3 is increased to 6.00E+12 to improve the ID timing of low and high temperature regions. There is an improvement in overall temperature can be observed from the ID timing plots by adjusting the A-factor constant of $C_{12}OOH1$-$2 <=> C_{12}O1$-2+OH to 8.00E12. In order to get a more adequate prediction in the ID timing, the A-factor for the reaction $C_{12}OOH1$-$2 <=> C_{12}H_{24}$-$1+HO_2$ is increased to 5.61E21. It is observed that the A-factor for the reaction $C_{12}OOH1$-$2 <=> C_{12}H_{24}$-$1+HO_2$ has a great effect on ID timings at the region of low temperature. Next, the value of the A-factor constant of $C_{16}OOH4$-$3O_2 <=> C_{16}KET4$-3+OH is increased from 1.00E11 to 5.00E12 to improve the ID timing at NTC region and high temperature region.

Furthermore, there are only three A-factor constants are required to be adjusted for HMN model in order to reduce the maximum deviation of ID timings to below 50 % as shown in Table 4.5. The values of the A-factor for reactions $CH_3+O_2 <=> CH_2O+OH$ and $IC_4H_6OH+HO_2 <=> IC_4H_7OH+O_2$ are improved by one order of magnitude to enhance the predictions of ID timing in overall temperature and NTC region respectively. Moreover, it is noted that ID timing at low temperature region can be greatly affected by adjusting the A-factor constants of $HMNOOH7$-$8O2 <=> HMNKET7$-8+OH from 1.25E10 to 5.25E8. As a result of applying integrated reduction techniques proposed by Poon et al. (2013), an optimised reduced HXN model with only 434 reactions and 108 species and an optimised HMN model with 507 reactions and 132 species were successfully produced. The sizes of the chemical kinetic model of HXN and HMN in each stage of the reductions are summarised in Figure 4.14 and Figure 4.15 respectively.
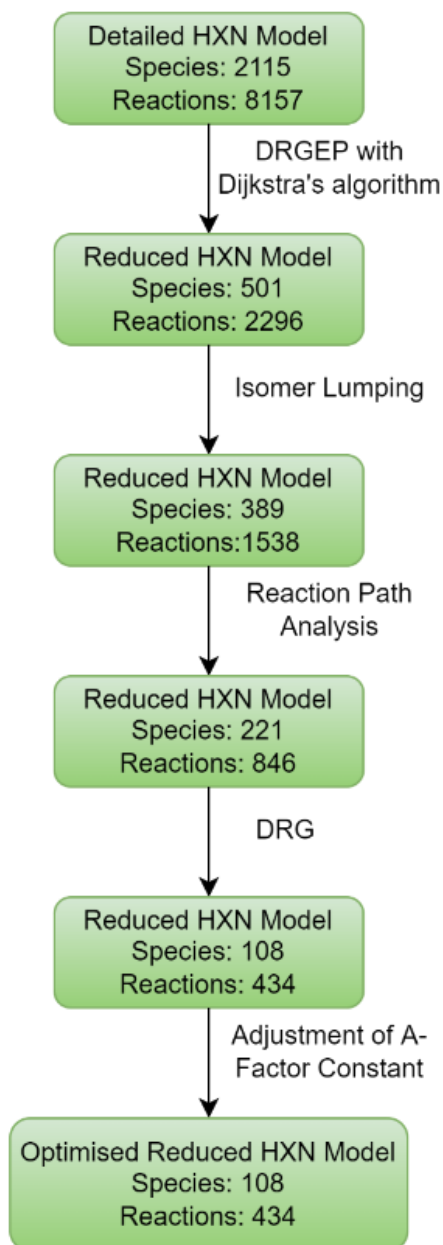
Figure 4.14: The Size of the *n-Hexadecane* Chemical Kinetic Models in Each
Reduction Stage.
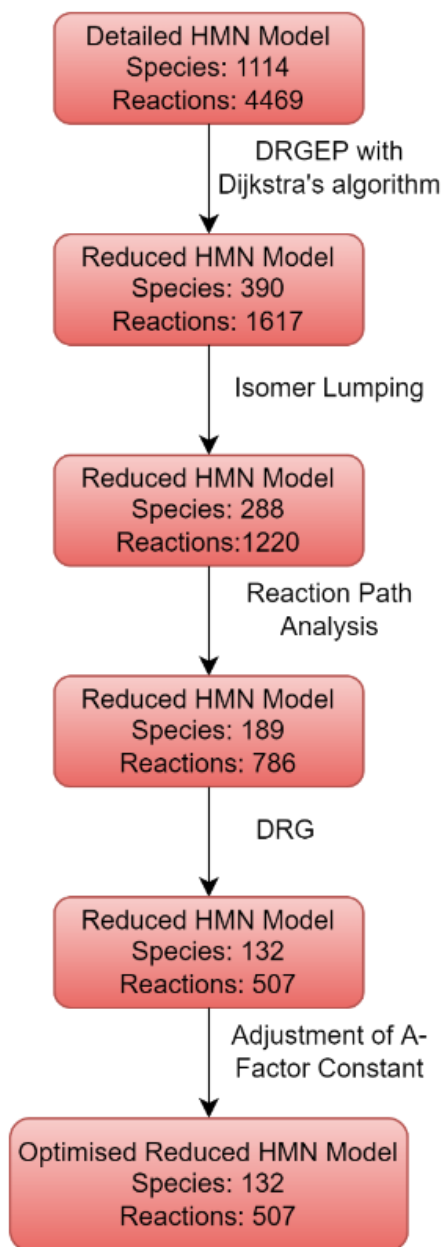
Figure 4.15: The Size of the *HMN* Chemical Kinetic Models in Each Reduction
Stage.

4.8 Reduced Model Validations against the Detailed Model Under Auto-ignition Conditions In 0-D Simulations

Upon successful development of the optimised reduced models of HXN and HMN in the previous section, the model validations of these reduced models against their detailed counterparts under auto-ignition conditions are then carried out by comparing the ID timing and species profiles predictions computed by the detailed model and the reduced model. The testing conditions

presented in Section 4.5 are applied to validate the optimized reduced models. Consequently, the results of the validations for the reduced models with respect to the detailed models are presented from Figure 4.16 to Figure 4.23. The ID timings calculated by the optimised reduced models and the detailed models of HXN and HMN are illustrated in Figure 4.16 and Figure 4.17 respectively. It can be noticed that the slopes of the ID timings calculated by both optimised reduced models are comparable with those of their corresponding detailed models even though the sizes of the detailed HXN model and the detailed HMN model are reduced by 94.89 % and 88.15 % respectively. Besides, the maximum deviations in ID timings of the optimised reduced HXN model and the optimised reduced HMN model are 37.16 % and 38.22 % respectively. These deviations are acceptable for a large-scale model reduction since the maximum deviations of both optimised reduced models are within the error tolerance of 50 %.
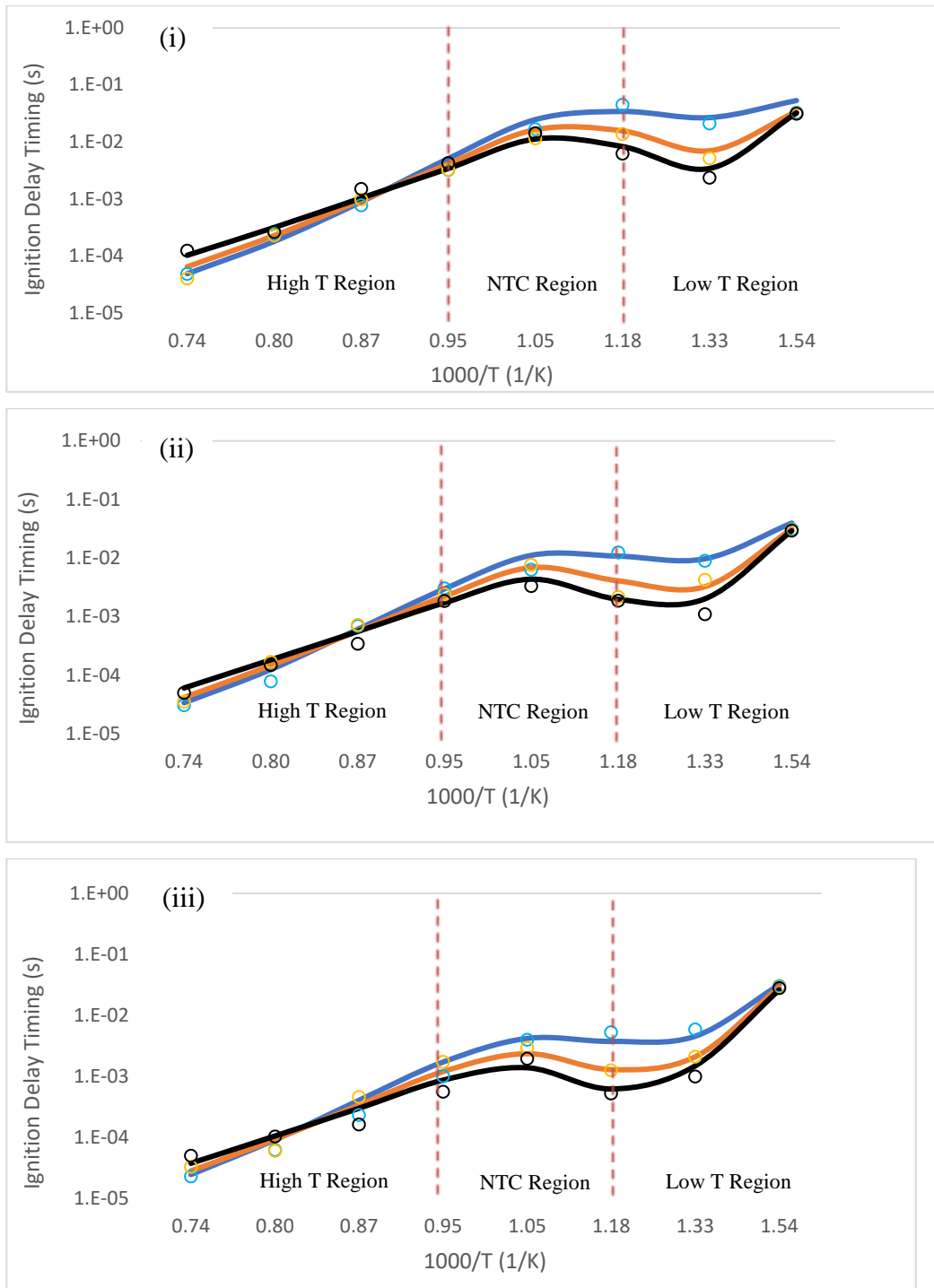
Figure 4.16: ID Timing predicted by the Detailed Model (solid lines) and the
Optimised Reduced Model (symbols) of *N-Hexadecane* **After** the
Adjustment of A-Factor Constant at ϕ of 0.5 (Blue), 1.0 (Orange),
2.0 (Black) and Initial Pressure of (i) 5 bar, (ii) 10 bar, (iii) 20 bar.
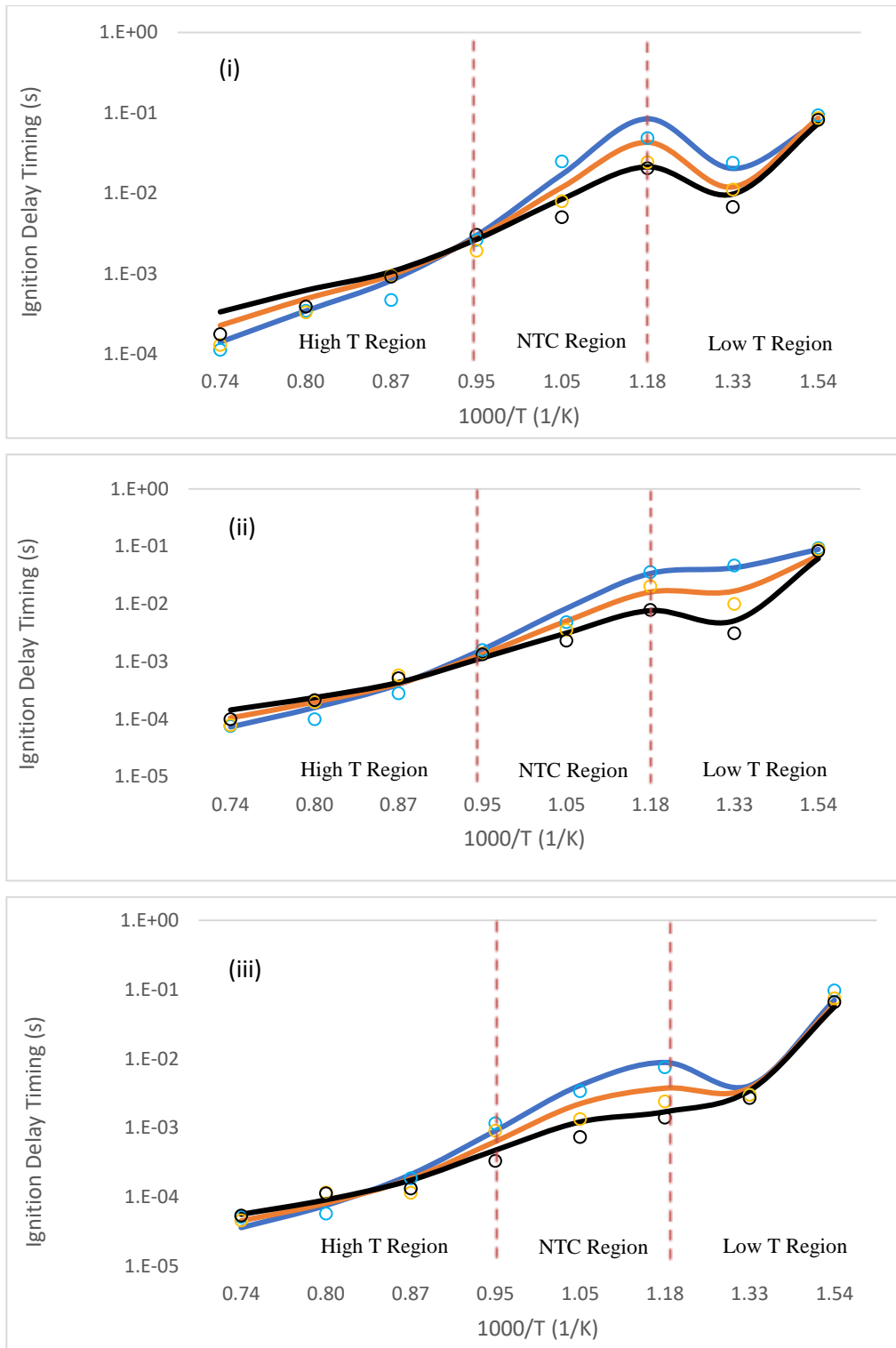
Figure 4.17: ID Timing predicted by the Detailed Model (solid lines) and the Optimised Reduced Model (symbols) of *HMN* **After** the Adjustment of A-Factor Constant at ϕ of 0.5 (Blue), 1.0 (Orange), 2.0 (Black) and Initial Pressure of (i) 5 bar, (ii) 10 bar, (iii) 20 bar.

Following that, the comparisons of the species profiles computed by the detailed mechanisms and reduced mechanisms are carried out for the model validations as well. Figure 4.18, Figure 4.19 and Figure 4.20 display the computation results of the species profiles for HXN models while Figure 4.21, Figure 4.22 and Figure 4.23 show the species profiles computed by HMN models. It is noteworthy that comparable species temporal evolution trends can be observed for all the testing conditions reported in Table 4.1. Therefore, only the simulation results for ϕ of 1, initial pressure of 1 bar and initial temperature of 950 K are reported in this paper. CO_2 is the major emission species and C_2H_2 is known as the soot precursor species. Additionally, O_2 is an important reactant species in monitoring the fuel concentrations during the process of combustion. Next, HO_2 species play an important role in the reactions of chain branching. OH radical is an important species in the process of fuel oxidation because it is a reactive chemical intermediate. Lastly, H_2 is a common species that can be found in the jet fuel. Due to these reasons, the species that mentioned earlier are selected for the evaluation of species profiles.

Referring to the computation results presented from Figure 4.18 to Figure 4.23, it is proven that the trends of the species concentration profiles computed by both reduced chemical kinetic mechanisms are in good agreement with their corresponding detailed chemical kinetic mechanisms for all evaluated species. Nevertheless, it was found that all the species concentration profiles computed by the reduced mechanism of HXN and HMN are shifted to a shorter time. This can be attributed to the discrepancy in ID timing predictions between the detailed mechanisms and reduced mechanisms. The commencements of the processes of species decomposition and formation are matched with the corresponding ID timings calculated for selected species. Furthermore, the shifting in species profiles computed using the reduced model is caused by the substitution of the isomer group into a representative lump in the isomer lumping stage. The representative species itself cannot cope with the production and consumption rate of the isomer group. Nevertheless, the overall species profiles predictions of both reduced models are adequate since the species profiles predictions of the detailed models at steady state are comparable with those of the reduced models. In short, the reduced HXN and HMN models

developed through five-stage reduction scheme are able to provide the results in acceptable range even though the chemical kinetic models have been simplified.
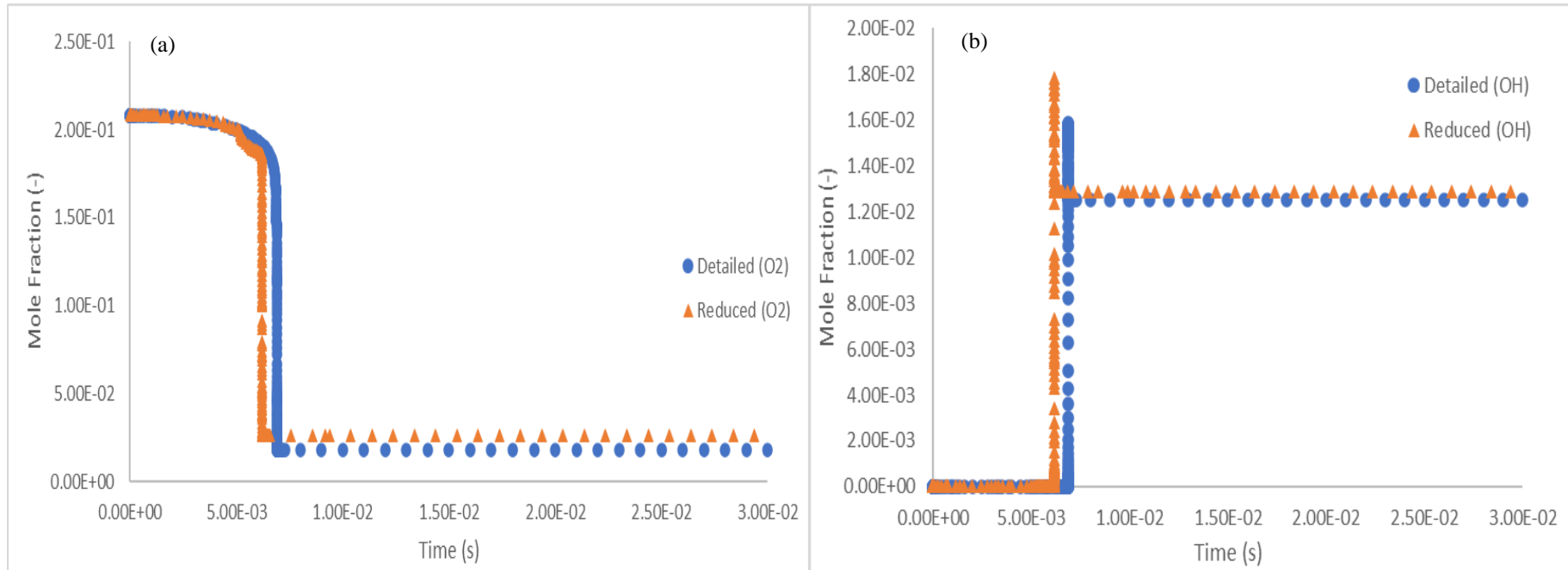
Figure 4.18: Computed Species Profiles Predictions of (a) O2 and (b) OH by Detailed Model (Circle) and Optimised Reduced Model (Triangle) of *n-Hexadecane* for ϕ of 1, Pressure of 1 bar and Temperature of 950 K.
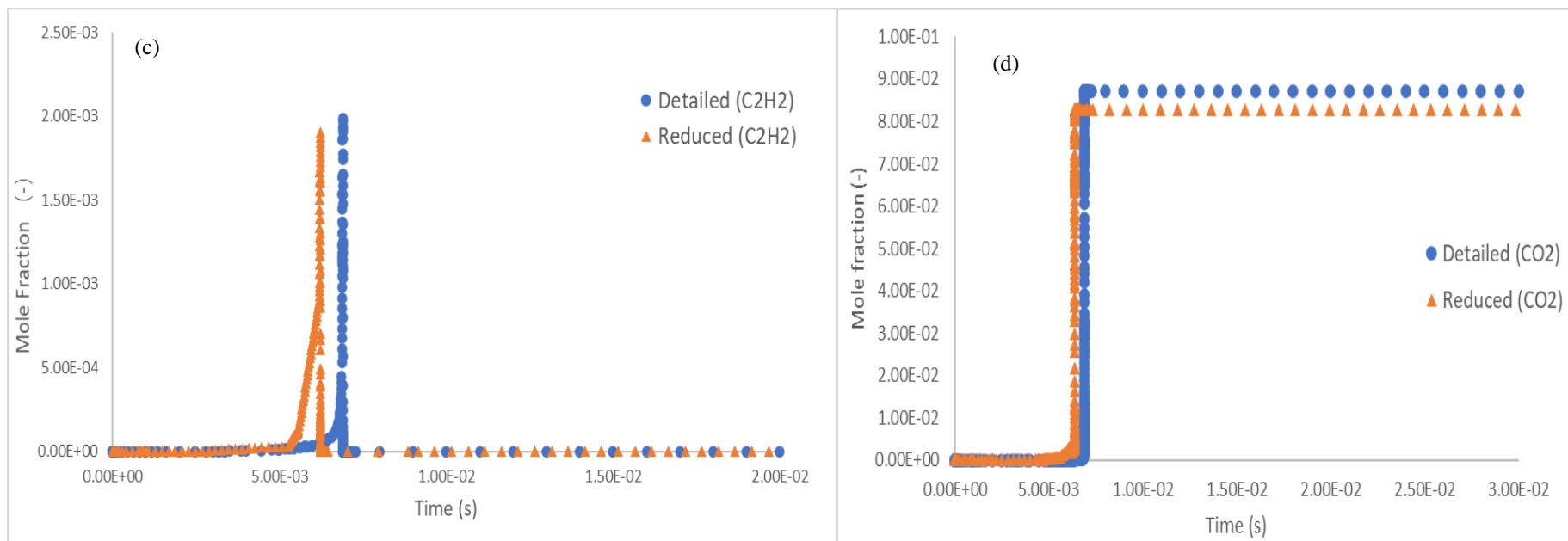
Figure 4.19: Computed Species Profiles Predictions of (c) C2H2 and (d) CO2 by Detailed Model (Circle) and Optimised Reduced Model (Triangle) of *n-Hexadecane* for ϕ of 1, Pressure of 1 bar and Temperature of 950 K.
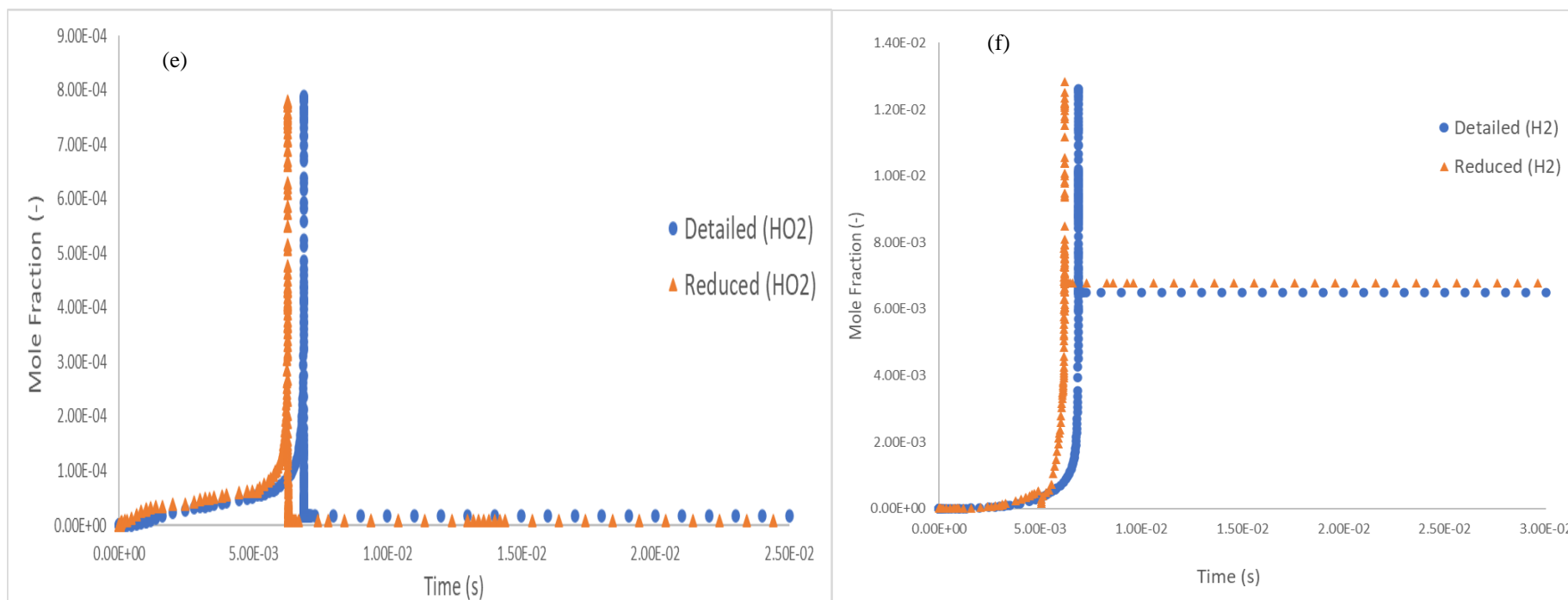
Figure 4.20: Computed Species Profiles Predictions of (e) HO2 and (f) H2 by Detailed Model (Circle) and Optimised Reduced Model (Triangle) of *n-Hexadecane* for ϕ of 1, Pressure of 1 bar and Temperature of 950 K.
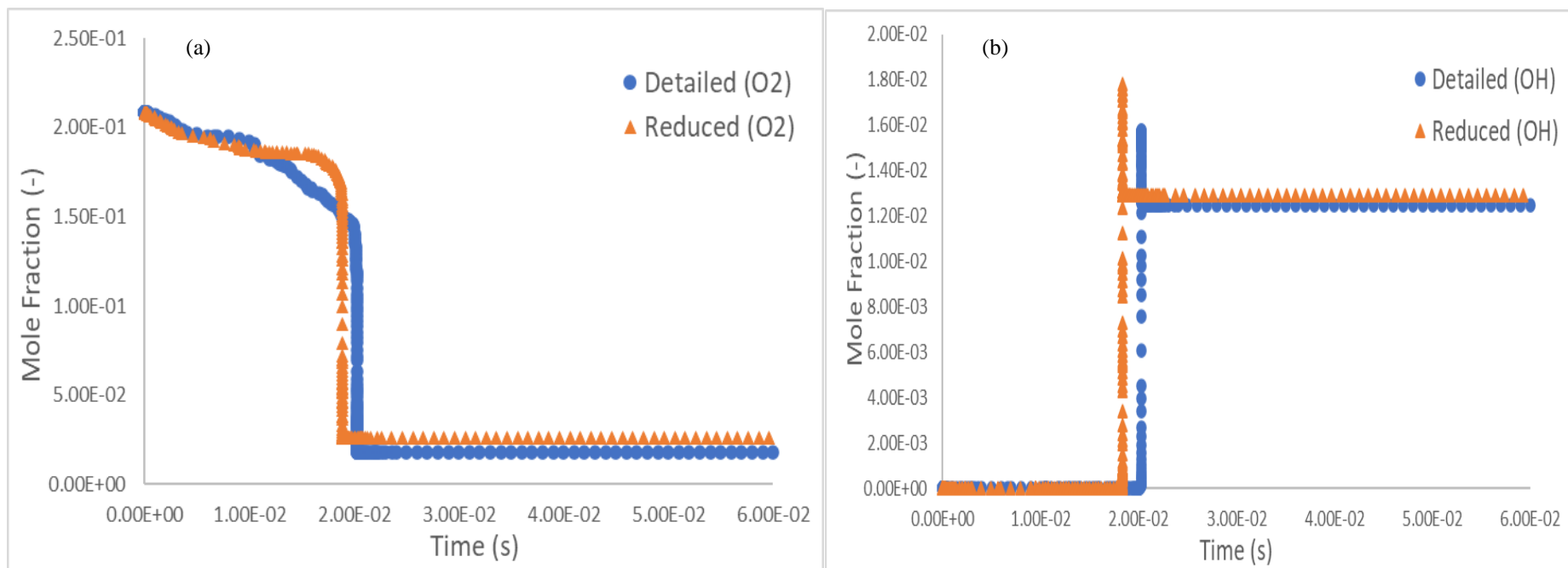
Figure 4.21: Computed Species Profiles Predictions of (a) O2 and (b) OH by Detailed Model (Circle) and Optimised Reduced Model (Triangle) of *HMN* for ϕ of 1, Pressure of 1 bar and Temperature of 950 K.
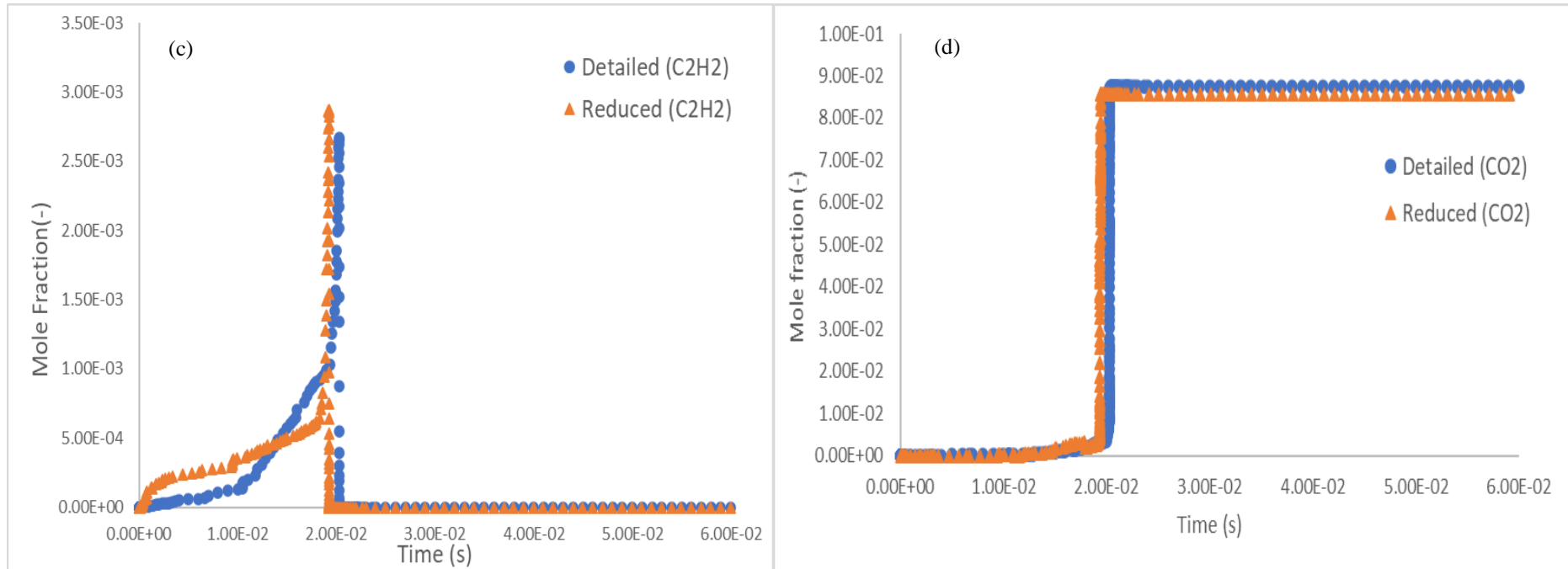
Figure 4.22: Computed Species Profiles Predictions of (c) C2H2 and (d) CO2 by Detailed Model (Circle) and Optimised Reduced Model (Triangle) of *HMN* for ϕ of 1, Pressure of 1 bar and Temperature of 950 K.
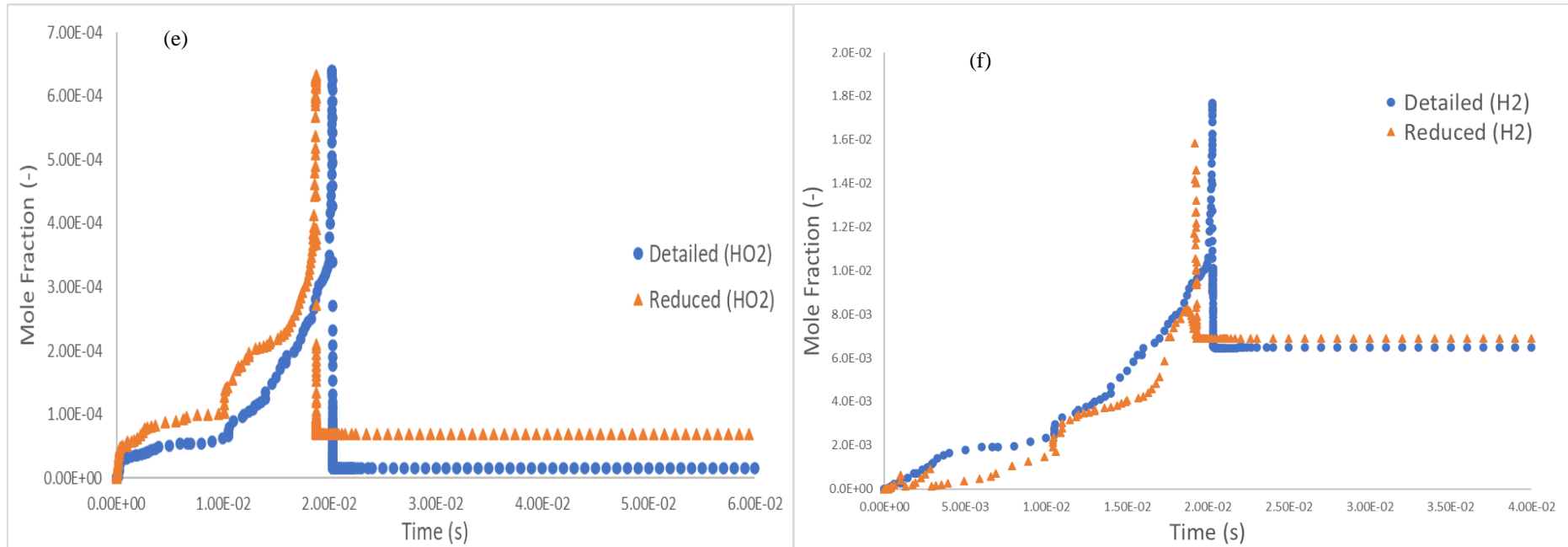
Figure 4.23: Computed Species Profiles Predictions of (e) HO2 and (f) H2 by Detailed Model (Circle) and Optimised Reduced Model (Triangle) of *HMN* for ϕ of 1, Pressure of 1 bar and Temperature of 950 K.

4.9   Development of a Reduced HRJ Surrogate Fuel Model

According to the studies by Chang et al. (2015), a single component reduced surrogates of branched-alkanes model is unable to reproduce the characteristics of combustion of the cyclo-alkanes, n-alkanes and aromatic compounds of the jet fuel. The formation of polycyclic hydrocarbons is also unable to be described well by a single component reduced surrogates model. As such, multi-component HRJ surrogate fuel models are more desirable than single component surrogate fuel model to predict the combustions characteristic of the actual HRJ fuel (Poon, et al., 2016b).

The "reduced prior to combination" method is used to combine the reduced models of each constituent of HRJ fuel into a single representative model which is also known as a multi-component reduced HRJ surrogate fuel model. On the other hand, the "combined prior to reduction method combines the detailed chemical kinetic model of each constituent of HRJ fuel before conducting the model reduction. According to the researches of Poon et al. (2013) and Tan et al. (2021), the "reduced prior to combination" method is more computationally feasible than the "combined prior to reduction" method as it simplifies the analysis process. On top of that, the complexity of the analysis process will be greatly reduced when the size of the mechanism is smaller. Therefore, the "reduced prior to combination" method is more suitable to be used in this study.

In this research, the mechanism merging consists of two stages. The first stage of the mechanism merging is to combine the reduced model for HXN and the reduced model for HMN established in this work. Subsequently, two components reduced HRJ surrogate fuel model with 738 reactions and 201 species is created. This model is represented by the abbreviation J2_201. Next, the reduced methyl-cyclohexane (MCH) mechanism derived by Tan et al. (2021) is directly utilized here to merge with J2_201. The reduced MCH model is derived from the detailed MCH model developed by Weber et al. (2014) which consists of 6498 reactions and 1540 species. MCH model is used as the cyclo-alkanes model for the formulation of the reduced HRJ surrogate fuel model. The table below summarises the information of the selected chemical kinetic mechanisms in the mechanism merging.

Table 4.6: The Information of the Selected Detailed and Reduced Mechanism in Mechanism Merging.

Mechanism	Detailed Mechanism		Reduced Mechanism		Hydrocarbon Group
	N_{sp} [a]	N_{rec} [b]	N_{sp} [a]	N_{rec} [b]	
HXN	2115	8157	108	434	n-alkanes
HMN	1114	4469	132	507	Branched-alkanes
MCH	1540	6498	86	524	Cyclo-alkanes

[a] N_{sp} represents number of species

[b] N_{rec} represents number of reactions

Upon completion of combining J2_201 model and the reduced MCH model, a multi-component of HRJ surrogate fuel model with 987 reactions and 246 species is synthesized. J3_246 is used as the abbreviation of the multi-components of HRJ surrogate fuel model. The figure below summarizes the flow of the development of the reduced HRJ surrogate fuel model.
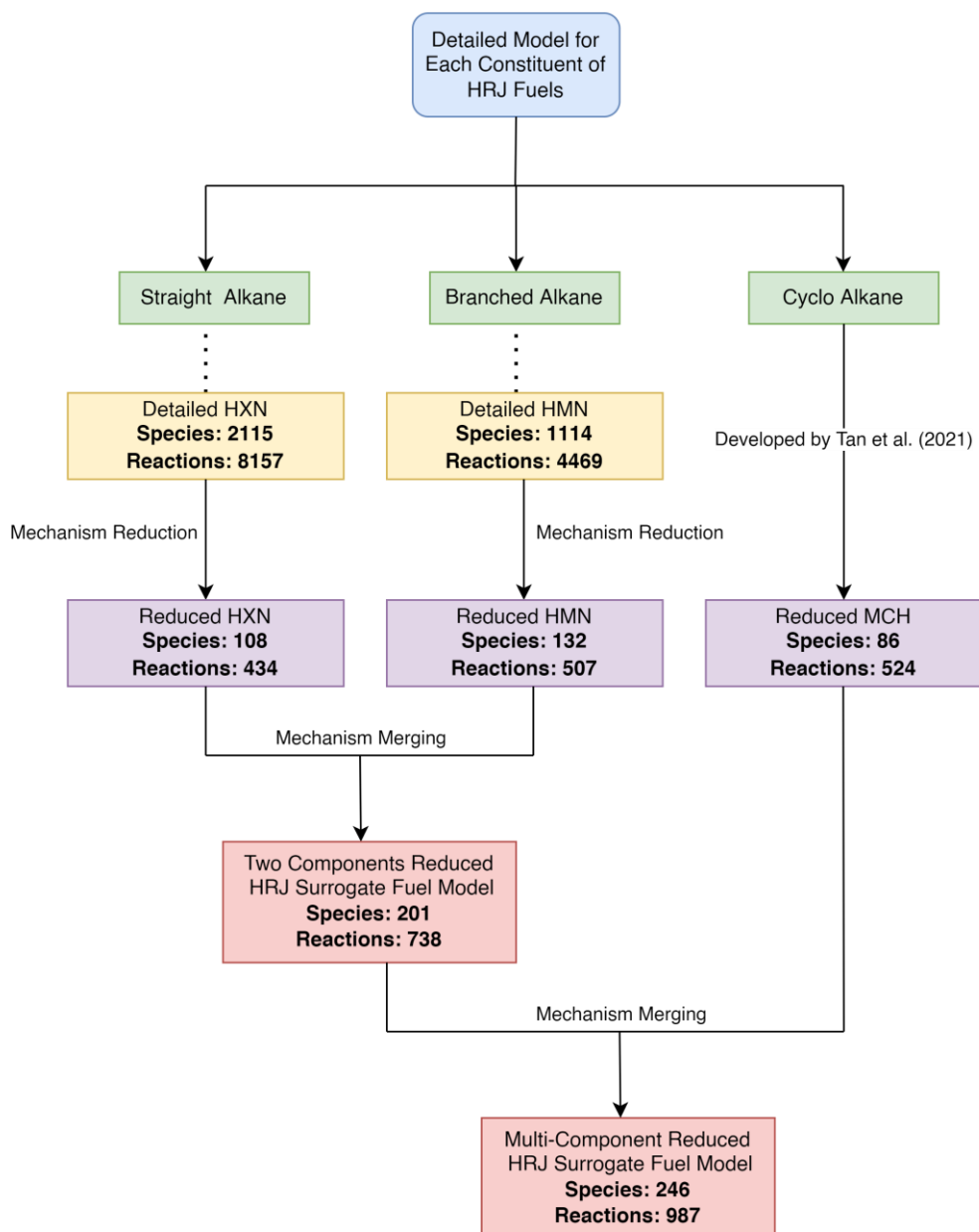
Figure 4.24: Overall Flow of the Development of Reduced HRJ Surrogate Fuel
Model.

Subsequently, the validations of J3_246 against the detailed models for
each constituent in terms of ID timings are executed in 0-D simulation under a
broad range of auto-ignition conditions. The objective of the validation process
is to ensure the performance of the HRJ surrogate fuel model in ID timing
predictions is retained after performing the mechanism merging. Referring to
the results demonstrated in Figure 4.25, a good agreement in the ID timing
predictions is attained between J3_246 and the detailed model of HXN with a

maximum deviation of 39.87 %. Besides, the ID timings computed by J3_246 also agree fairly well with those of the detailed HMN mechanism as shown in Figure 4.26. This is because of the maximum deviation for this comparison is only 40.64 %. Moreover, according to the results shown in Figure 4.27, a close agreement is achieved between the detailed MCH models and J3_246 with a maximum deviation of 30.83 % in ID timing predictions. All the maximum deviations in ID timings are within the maximum tolerable deviation. Hence, J3_246 is able to replicate the ignition behaviour of the CHRJ-6152 fuel.
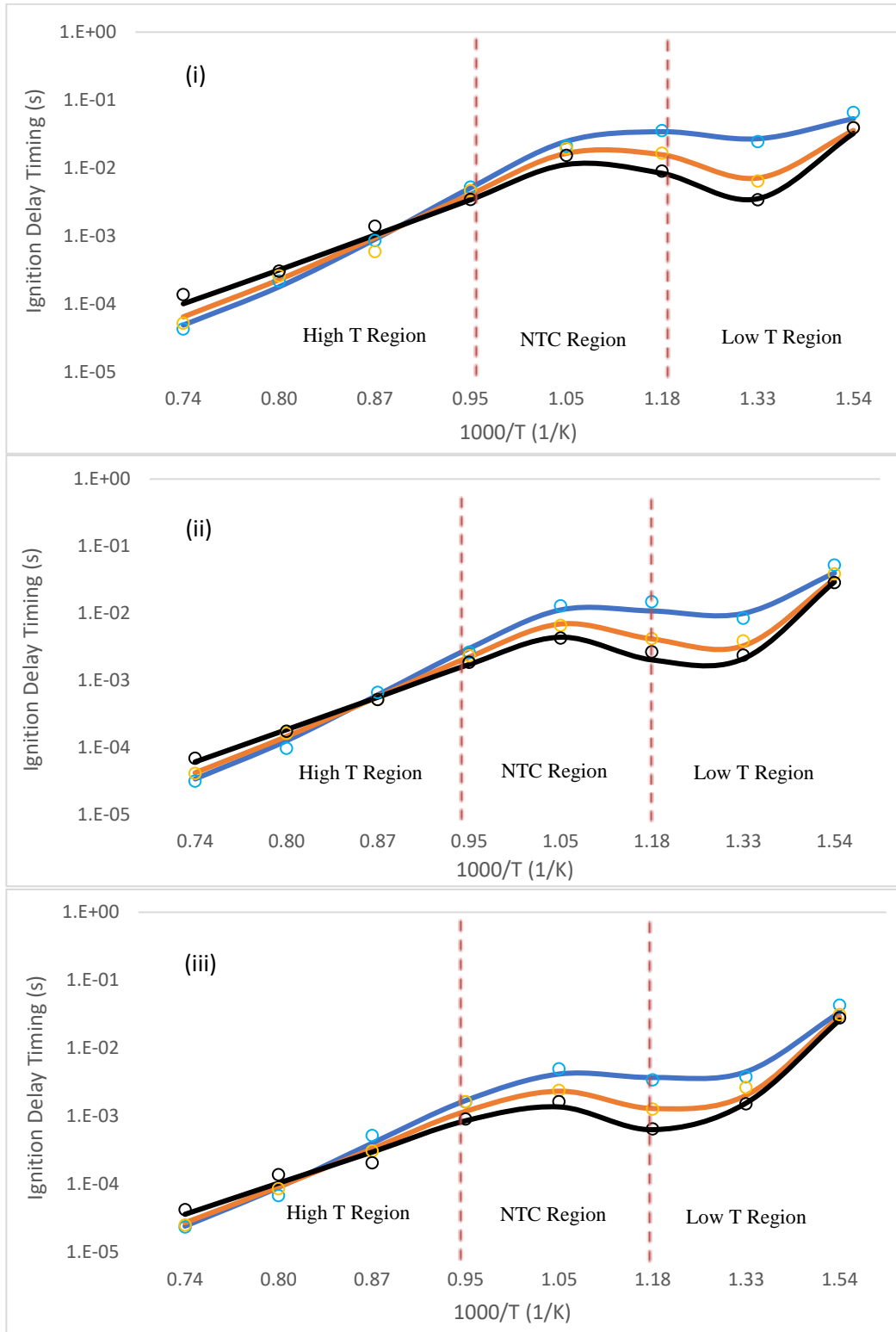
Figure 4.25: Computed ID Timing of *HXN* by J3_246 (Symbols) and Detailed Model (Solid Lines) at ϕ of 0.5 (Blue), 1.0 (Orange), 2.0 (Black) and Initial Pressure of (i) 5 bar, (ii) 10 bar, (iii) 20 bar.
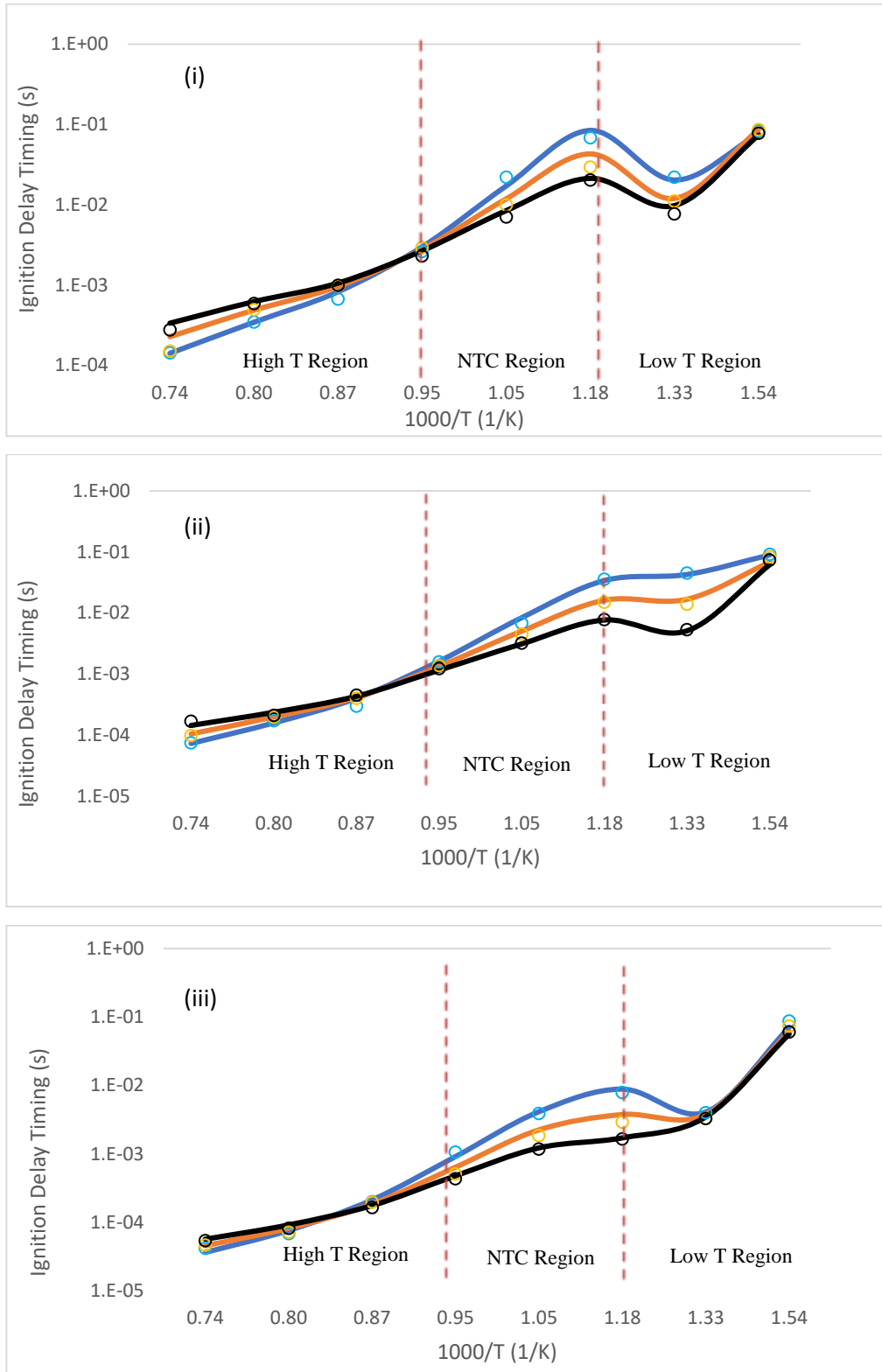
Figure 4.26: Computed ID Timing of *HMN* by J3_246 (Symbols) and Detailed Model (Solid Lines) at ϕ of 0.5 (Blue), 1.0 (Orange), 2.0 (Black) and Initial Pressure of (i) 5 bar, (ii) 10 bar, (iii) 20 bar.
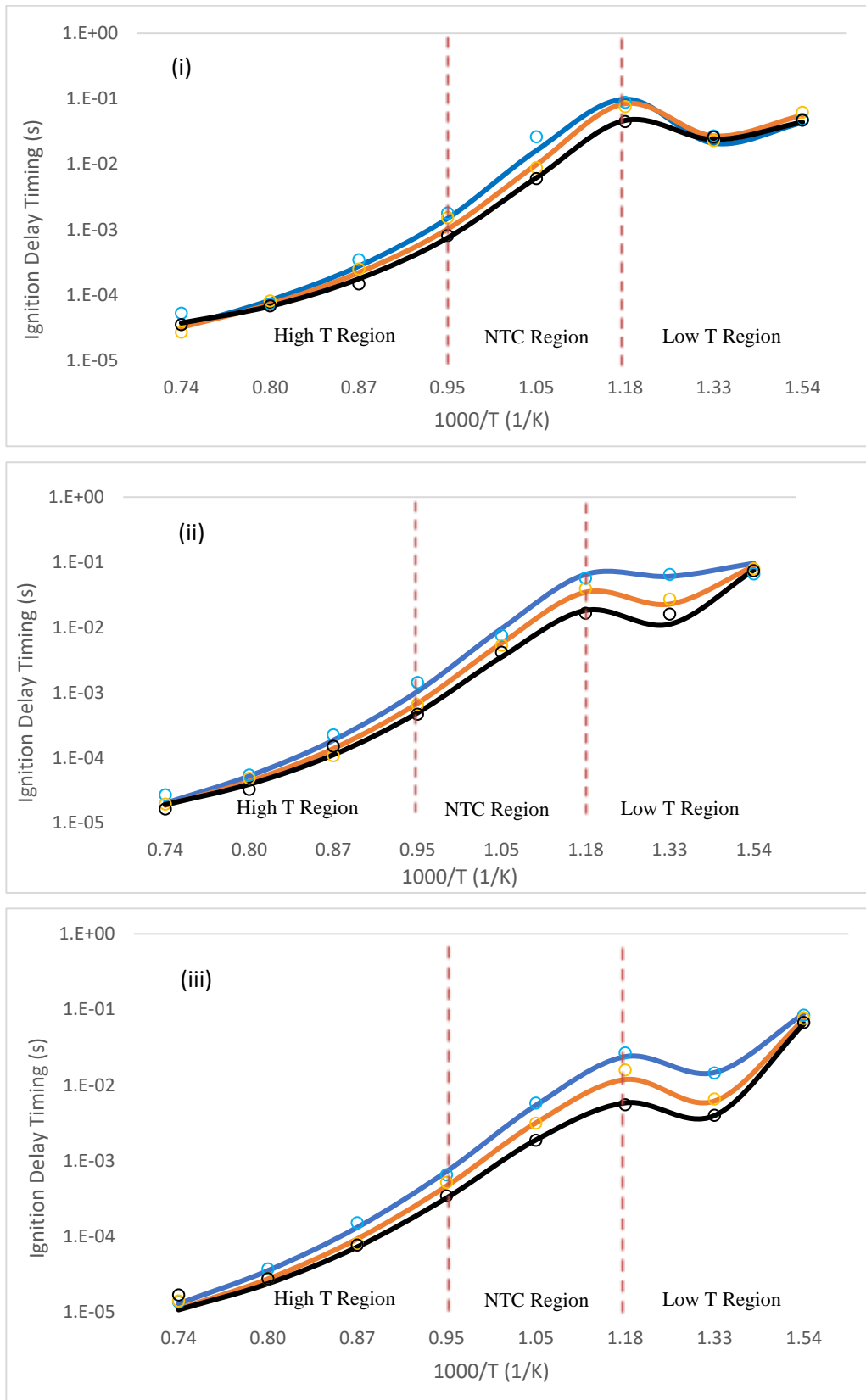
Figure 4.27: Computed ID Timing of *MCH* by J3_246 (Symbols) and Detailed Model (Solid Lines) at ϕ of 0.5 (Blue), 1.0 (Orange), 2.0 (Black) and Initial Pressure of (i) 5 bar, (ii) 10 bar, (iii) 20 bar.

4.10   Summary

In short, the optimized reduced HXN model with 108 species and the optimized reduced HMN model with 132 species were successfully derived through the integrated reduction techniques. The maximum deviations in ID timings for both reduced HXN model and reduced HMN model are within the maximum tolerable induced error of 50 %. Hence, both reduced models developed can reproduce the predictions of ID timing of those of the detailed models although 94.89 % and 88.15 % reduction in the size of the HXN and HMN models respectively. Besides, the computed species profiles by both reduced mechanisms also exhibit comparable trends with those of the detailed mechanisms but shifted to a shorter time. The reduced MCH model developed by Tan et al. (2021) was used to combine with the optimized HXN model and HMN model. After conducting the mechanism merging, a multi-components HRJ surrogate fuel model, J3_246 with 987 reactions and 246 species was synthesized successfully. The simulation results also proved that J3_246 can reproduce the predictions of ID timing of those of the detailed mechanism for each constituent of CHRJ-6152 fuel.

CHAPTER 5

CONCLUSIONS AND RECOMMENDATIONS

5.1 Conclusions

A reduced model for HXN with only 108 species and a reduced model for HMN with 132 species were derived successfully by using the Intel core i5 laptop with 8 GB RAM and 2.5 GHz processing speed. The application of the five-stage chemical kinetic reduction scheme on the detailed HXN and HMN mechanisms has attained overall species reduction of 94.89 % and 88.15 % respectively. Meanwhile, the computational time of the simulation has been reduced by approximately 99 % and 97 % for HXN and HMN models respectively. Each simulation of CHEMKIN-PRO took about 1 s to be done upon the successful development of the reduced models.

The validations of the reduced models against their corresponding detailed models were also performed by using the closed homogeneous batch reactor model for a broad range of auto-ignition conditions. Both reduced chemical kinetic mechanisms developed in this research are capable to replicate the ID timing and species concentration profiles of the corresponding detailed models with a reasonably close agreement. The maximum deviations in ID timing are 37.16 % and 38.22 % for the optimized reduced HXN model and the optimized reduced HMN model respectively. The maximum deviation in ID timing for both reduced models fall within the maximum tolerable deviation of 50 %. Hence, both reduced models are said to be valid and ready to be carried forward to the mechanism merging to develop the multi-component reduced HRJ surrogate fuel model.

A multi-component reduced HRJ fuel model was developed successfully by combining the reduced HXN model and the reduced HMN model developed in this work with the reduced MCH model developed by Tan et. al (2021). This multi-component reduced HRJ surrogate fuel model is denoted by the abbreviation J3_246. Upon successfully merging, J3_246 model with 246 species is formed. Since CHRJ-6152 fuel is chosen as the target fuel to be studied in this project, HXN, HMN and MCH are selected to be the

representatives of the straight alkanes, branched-alkanes and cyclo-alkanes components for CHRJ-6152 fuel. These selections are made attributed to CHRJ-6152 fuel contains 78.9 % of branched-alkanes, 11.1 % of cyclo-alkanes and 10.2 % of n-alkanes. It is noteworthy that CHRJ-6152 fuel is only comprised of 0.2 % of aromatics compounds and thus it is excluded from this study. J3_246 was validated against the detailed models for each constituent with respect to the predictions of ID timing in 0-D chemical kinetic simulation. In conclusion, J3_246 is ready to be used as the HRJ surrogate fuel model since it is able to replicate the actual ignition behaviour of the actual HRJ fuel.

5.2　　　Recommendations for Future Work

This project was constrained by some remarkable limitations as listed below:

1) The model validations were performed by using a closed homogeneous batch reactor model under auto-ignition conditions only.

2) The reduced mechanisms developed in this study were only validated in 0-D chemical kinetic simulations.

3) The aromatic compound of the CHRJ-6152 fuel is not included in the development of HRJ surrogate fuel model.

4) There is no experimental data that can be used to validate the reduced models.

In order to further validate the reduced models as well as to improve the performance of the reduced models, the following suggested steps can be done in the future.

1) The model validations against the detailed chemical kinetic mechanism with respect to the predictions of ID timing and species profiles under jet-stirred reactor (JSR) conditions can be carried out by using the perfectly stirred reactor (PSR). According to Cheng et al. (2015), the conditions of JSR are significant in modeling the process of combustion at steady-state. Also, higher accuracy and precision in ID timing and species profiles predictions of the reduced model can be obtained after JSR conditions data sources are added in the simulation.

2) Since the results were generated via simulation in ideal settings, the reduced models are suggested to be validated against the results of the experiment for JSR conditions and auto-ignition conditions to further verify the reduced models developed can replicate the ID timings and species profiles of the detailed models reasonably.

3) Two-dimensional (2-D) spray combustion simulations are recommended to be carried out to test the fidelity of the reduced models.

4) The simulations of three-dimensional (3-D) internal combustion engines can be carried out as well. By doing so, the performance of the reduced models can be improved.

REFERENCES

Aasberg-Petersen, K., Christensen, T.S., Dybkjær, I., Sehested, J., Østberg, M., Coertzen, R.M., Keyser, M.J. and Steynberg, A.P., 2004. Synthesis gas production for FT synthesis. *Studies in Surface Science and Catalysis*, 152, pp.258–405.

Acampora, L. and Marra, F.S., 2017. *Comparison of detailed reaction mechanisms for an alternative Jet Fuel surrogate by Parametric Continuation*.

Adewuyi, A.O., 2016. Determinants of import demand for non-renewable energy (petroleum) products: Empirical evidence from Nigeria. *Energy Policy*, 95, pp.73–93.

Agency for Toxic Substances and Disease Registry, 2017. *TOXICOLOGICAL PROFILE FOR JP-5, JP-8, AND JET A FUELS*.

Ajam, M. and Viljoen, C.L., 2011. *Synergies between renewable kerosene and Fischer-Tropsch Synthetic Paraffinic Kerosene (FT-SPK) 1 SYNERGIES BETWEEN RENEWABLE KEROSENE AND FISCHER-TROPSCH SYNTHETIC PARAFFINIC KEROSENE (FT-SPK)*. [online] Available at: <https://www.researchgate.net/publication/287632420> [Accessed 3 Jul. 2021].

Alhikami, A.F. and Wang, W.C., 2021. Experimental study of the spray ignition characteristics of hydro-processed renewable jet and petroleum jet fuels in a constant volume combustion chamber. *Fuel*, 283.

Allen, C., Toulson, E., Edwards, T. and Lee, T., 2012. Application of a novel charge preparation approach to testing the autoignition characteristics of JP-8 and camelina hydroprocessed renewable jet fuel in a rapid compression machine. *Combustion and Flame*, 159(9), pp.2780–2788.

Allen, C., Toulson, E. and Lee, T., 2011. An Experimental Investigation of the Autoignition Characteristics of Camelina-Based Hydroprocessed Renewable Jet Fuel. pp.1–8.

An, J. and Jiang, Y., 2013. Differences between Direct Relation Graph and Error-propagation-based Reduction Methods for Large Hydrocarbons. *Procedia Engineering*, 62, pp.342–349.

Chang, Y., Jia, M., Li, Y., Liu, Y., Xie, M., Wang, H. and Reitz, R.D., 2015. Development of a skeletal mechanism for diesel surrogate fuel by using a decoupling methodology. *Combustion and Flame*, 162(10), pp.3785–3802.

Chen, Y.K., Lin, C.H. and Wang, W.C., 2020a. The conversion of biomass into renewable jet fuel. *Energy*, 201.

Chen, Y.K., Lin, C.H. and Wang, W.C., 2020b. The conversion of biomass into renewable jet fuel. *Energy*, 201, pp.1–8.

Cheng, X., Ng, H.K., Gan, S., Ho, J.H. and Pang, K.M., 2015. Development and validation of a generic reduced chemical kinetic mechanism for CFD spray combustion modelling of biodiesel fuels. *Combustion and Flame*, 162(6), pp.2354–2370.

Chu, P.L., Vanderghem, C., MacLean, H.L. and Saville, B.A., 2017. Financial analysis and risk assessment of hydroprocessed renewable jet fuel production from camelina, carinata and used cooking oil. *Applied Energy*, 198, pp.401–409.

Corporan, E., Dewitt, M.J., Klingshirn, C.D., Anneken, D., Shafer, L. and Striebich, R., 2012. Comparisons of emissions characteristics of several turbine engines burning fischer-tropsch and hydroprocessed esters and fatty acids alternative jet fuels. In: *Proceedings of the ASME Turbo Expo*. pp.425–436.

Engineering and Technology History Wiki, 2019. *Jet Fuel* . [online] Available at: <https://ethw.org/Jet_Fuel> [Accessed 1 Jul. 2021].

Escobar, J., 2006. *Turbine Engine History* . [online] Available at: <https://www.aviationpros.com/engines-components/aircraft-engines/turbine-engines-parts/article/10383708/turbine-engine-history> [Accessed 22 Aug. 2021].

Farm Energy, 2019. *Camelina for Biofuel Production* . [online] Available at: <https://farm-energy.extension.org/camelina-for-biofuel-production/> [Accessed 7 Jul. 2021].

Hemighaus, G., Boval, T., Bosley, C., Organ, R., Lind, J., Brouette, R., Thompson, T., Lynch, J. and Jones, J., 2006. *Alternative Jet Fuels*.

Herbinet, O., Pitz, W.J. and Westbrook, C.K., 2008. Detailed chemical kinetic oxidation mechanism for a biodiesel surrogate. *Combustion and Flame*, 154(3), pp.507–528.

Hileman, J.I. and Stratton, R.W., 2014. Alternative jet fuel feasibility. *Transport Policy*, [online] pp.1–11. Available at: <http://dx.doi.org/10.1016/j.tranpol.2014.02.018> [Accessed 8 Aug. 2021].

Hui, X., Kumar, K., Sung, C.J., Edwards, T. and Gardner, D., 2012. Experimental studies on the combustion characteristics of alternative jet fuels. *Fuel*, 98, pp.176–182.

International Civil Aviation Organization, 2021. *Alternative Fuels: Questions and Answers*. [online] Available at: <https://www.icao.int/environmental-protection/Pages/AltFuel-SustainableAltFuels.aspx> [Accessed 30 Jun. 2021].

Johnson, D.W., 2017. The Effects of Storage on Turbine Engine Fuels. *Flight Physics - Models, Techniques and Technologies*, pp.193–206.

Karanikas, N., Foster, C., Beltran Hernandez, A., Harvey, A., Targal, O. and Horswill, N., 2021a. Conventional and Alternative Aviation Fuels: Occupational Exposure and Health Effects. *Journal of Chemical Health and Safety*, 28(3), pp.159–170.

Karanikas, N., Foster, C., Beltran Hernandez, A., Harvey, A., Targal, O. and Horswill, N., 2021b. Conventional and Alternative Aviation Fuels: Occupational Exposure and Health Effects. *Journal of Chemical Health and Safety*, pp.1–42.

Kumar, K. and Sung, C.J., 2010. A comparative experimental study of the autoignition characteristics of alternative and conventional jet fuel/oxidizer mixtures. *Fuel*, 89(10), pp.2853–2863.

Larsson, J., Kamb, A., Nässén, J. and Åkerman, J., 2018. Measuring greenhouse gas emissions from international air travel of a country's residents methodological development and application for Sweden. *Environmental Impact Assessment Review*, 72, pp.137–144.

Le, M.K. and Kook Sanghoon, 2015. Injection Pressure Effects on the Flame Development in a Light-Duty Optical Diesel Engine on JSTOR. [online] 8(2), pp.609–624. Available at: <https://www.jstor.org/stable/26277972?saml_data=eyJzYW1sVG9rZW4iOiI1YWE5MDNjYy00MDhlLTQzNzUtOWJkNC0zMjQ3YWRkYzhhN2MiLCJpbnN0aXR1dGlvbklkcyI6WyIzODJjNmYzMS05YWM4LTQwZjMtYjE5ZC1hY2M4YmYyMDMxZTMiXX0&seq=1> [Accessed 12 Apr. 2022].

Lee, C.Y., Cheng, X., Mun Poon, H., Reddy Yelugoti, S. and Wang, W.C., 2022. The spray ignition characteristics of ethanol blended with hydro-processed renewable diesel in a constant volume combustion chamber. *Fuel*, [online] 314. Available at: <https://doi.org/10.1016/j.fuel.2021.123089> [Accessed 14 Apr. 2022].

Lu, T. and Law, C.K., 2006. Linear time reduction of large kinetic mechanisms with directed relation graph: N-Heptane and iso-octane. *Combustion and Flame*, 144(1–2), pp.24–36.

Lu, T. and Law, C.K., 2009. Toward accommodating realistic fuel chemistry in large-scale computations. *Progress in Energy and Combustion Science*, 35(2), pp.192–215.

Lu, T.F. and Law, C.K., 2008. Strategies for mechanism reduction for large hydrocarbons: n-heptane. *Combustion and Flame*, 154(1–2), pp.153–163.

Luo, Z., Plomer, M., Lu, T., Som, S. and Longman, D.E., 2012. A reduced mechanism for biodiesel surrogates with low temperature chemistry for compression ignition engine applications. *Combustion Theory and Modelling*, 16(2), pp.369–385.

Mangus, M., Mattson, J. and Depcik, C., 2015. Performance and emissions characteristics of hydroprocessed renewable jet fuel blends in a single-cylinder compression ignition engine with electronically controlled fuel injection. *Combustion Science and Technology*, 187(6), pp.857–873.

Mawhood, R., Gazis, E., de Jong, S., Hoefnagels, R. and Slade, R., 2016. Production pathways for renewable jet fuel: a review of commercialization status and future prospects. *Biofuels, Bioproducts and Biorefining*, 10(4), pp.462–484.

National Academies of Sciences, E. and M., 2016. *Commercial aircraft propulsion and energy systems research: reducing global carbon emissions. Commercial Aircraft Propulsion and Energy Systems Research: Reducing Global Carbon Emissions*. Washington, DC: The National Academies Press.

National Geographic Society, 2021. *Petroleum* . [online] Available at: <https://www.nationalgeographic.org/encyclopedia/petroleum/> [Accessed 1 Jul. 2021].

Niemeyer, K.E., Sung, C.J. and Raju, M.P., 2010. Skeletal mechanism generation for surrogate fuels using directed relation graph with error propagation and sensitivity analysis. *Combustion and Flame*, 157(9), pp.1760–1770.

Oehlschlaeger, M.A., Steinberg, J., Westbrook, C.K. and Pitz, W.J., 2009. The autoignition of iso-cetane at high to moderate temperatures and elevated pressures: Shock tube experiments and kinetic modeling. *Combustion and Flame*, 156(11), pp.2165–2172.

Oldani, A., Valco, D., Min, K., Edwards, J., Kweon, C.B., Allen, C. and Lee, T., 2015. Conventional and Bio-Derived Jet Fuel Surrogate Modeling in Low Temperature and Lean Combustion. *Energy and Fuels*, 29(7), pp.4597–4607.

Pan, L., Kokjohn, S. and Huang, Z., 2015. Development and validation of a reduced chemical kinetic model for dimethyl ether combustion. [online] pp.1–13. Available at: <http://dx.doi.org/10.1016/j.fuel.2015.07.066> [Accessed 8 Aug. 2021].

Patel, A., Kong, S.-C. and Reitz, R.D., 2004. Development and Validation of a Reduced Reaction Mechanism for HCCI Engine Simulations. pp.1–16.

Pearlson, M., Wollersheim, C. and Hileman, J., 2013. A techno-economic review of hydroprocessed renewable esters and fatty acids for jet fuel production. *Biofuels, Bioproducts and Biorefining*, 7(1), pp.89–96.

Pearlson, M.N., 2011. A techno-economic and environmental assessment of hydroprocessed renewable distillate fuels. [online] pp.1–106. Available at: <https://dspace.mit.edu/handle/1721.1/65508> [Accessed 11 Jul. 2021].

Pepiot-Desjardins, P. and Pitsch, H., 2008. An efficient error-propagation-based reduction method for large chemical kinetic mechanisms. *Combustion and Flame*, 154(1–2), pp.67–81.

Poon, H.M., 2016. Development of integrated chemical kinetic mechanism reduction scheme for diesel and biodiesel fuel surrogates for multi-dimensional CFD applications. pp.1–37.

Poon, H.M., Ng, H.K., Gan, S., Pang, K.M. and Schramm, J., 2013. Evaluation and Development of Chemical Kinetic Mechanism Reduction Scheme for Biodiesel and Diesel Fuel Surrogates. *SAE International Journal of Fuels and Lubricants*, 6(3), pp.729–744.

Poon, H.M., Ng, H.K., Gan, S., Pang, K.M. and Schramm, J., 2014a. Development and Validation of Chemical Kinetic Mechanism Reduction Scheme for Large-Scale Mechanisms. *SAE International Journal of Fuels and Lubricants*, 7(3), pp.653–662.

Poon, H.M., Ng, H.K. and Gan, S.Y., 2018. APPLICATION OF INTEGRATED CHEMICALKINETIC MECHANISM REDUCTION SCHEME ON SMALL-SCALE MECHANISM - ETHYLEN. *Journal of Engineering Science and Technology*, [online] 13, pp.640–655. Available at: <http://scholar.googleusercontent.com/scholar?q=cache:T34co3D64gQJ:schol ar.google.com/&hl=zh-CN&as_sdt=0,5&as_vis=1> [Accessed 31 Jul. 2021].

Poon, H.M., Ng, H.K., Gan, S.Y., Pang, K.M. and Schramm, J., 2014b. Chemical Kinetic Mechanism Reduction Scheme for Diesel Fuel Surrogate. *Applied Mechanics and Materials*, 541–542, pp.1006–1010.

Renewable Carbon News, 2009. *Camelina-based Renewable Jet Fuel* . [online] Available at: <https://renewable-carbon.eu/news/camelina-based-renewable-jet-fuel-8232shows-84-carbon-emissions-reduction/> [Accessed 7 Jul. 2021].

Repsol, 2018. *The best product for militray use*. [online] Available at: <https://www.repsol.com/en/products-and-services/aviation/jp-8/index.cshtml> [Accessed 4 Jul. 2021].

Sarathy, S.M., Westbrook, C.K., Mehl, M., Pitz, W.J., Togbe, C., Dagaut, P., Wang, H., Oehlschlaeger, M.A., Niemann, U., Seshadri, K., Veloo, P.S., Ji, C., Egolfopoulos, F.N. and Lu, T., 2011. Comprehensive chemical kinetic modeling of the oxidation of 2-methylalkanes from C7 to C20. *Combustion and Flame*, 158(12), pp.2338–2357.

SGS Spain, 2013. *Tech Talks: Introduction to Jet Fuel*. [online] Available at: <https://www.sgs.es/en/news/2013/02/tech-talks-introduction-to-jet-fuel> [Accessed 1 Jul. 2021].

Shila, J.J.H., 2017. *TECHNO-ECONOMIC ANALYSIS OF CAMELINA-DERIVED HYDROPROCESSED RENEWABLE JET FUEL AND ITS IMPLICATIONS ON THE AVIATION INDUSTRY*.

Shonnard, D.R., Williams, L. and Kalnes, T.N., 2010a. Camelina-derived jet fuel and diesel: sustainable advanced biofuels. *Environmental Progress and Sustainable Energy*, 29(3), pp.382–392.

Shonnard, D.R., Williams, L. and Kalnes, T.N., 2010b. Camelina-derived jet fuel and diesel: Sustainable advanced biofuels. *Environmental Progress and Sustainable Energy*, 29(3), pp.382–392.

Stagni, A., Frassoldati, A., Cuoci, A., Faravelli, T. and Ranzi, E., 2016. Skeletal mechanism reduction through species-targeted sensitivity analysis. *Combustion and Flame*, 163, pp.382–393.

Stratton, R.W., Wong, H.M. and Hileman, J.I., 2010. *Life Cycle Greenhouse Gas Emissions fron Alternative Jet Fuel*. [online] Available at: <http://web.mit.edu/aeroastro/partner/reports/proj28/partner-proj28-2010-001.pdf> [Accessed 8 Aug. 2021].

Tan, J., Ng, C.J., Saw, L.H. and Poon, H.M., 2021. Formulation of a Multicomponent Kinetic Model for Diesel-Alcohol Blends. *SAE International Journal of Fuels and Lubricants*, 15(1).

Vasu, S.S., Davidson, D.F. and Hanson, R.K., 2008. Jet fuel ignition delay times: Shock tube experiments over wide conditions and surrogate model predictions. *Combustion and Flame*, 152(1–2), pp.125–143.

Walluk, M.R., Bradley, M.A., Trabold, T.A., Smith, D.F., Junaedi, C. and Roychoudhury, S., 2015. Comparison of reforming performance of JP-8 and HRJ-5 for fuel cell applications. *Fuel*, 139, pp.35–39.

Wang, H., Yao, M., Yue, Z., Jia, M. and Reitz, R.D., 2015. A reduced toluene reference fuel chemical kinetic mechanism for combustion and polycyclic-aromatic hydrocarbon predictions. [online] 162(6), pp.2390–2404. Available at: <http://dx.doi.org/10.1016/j.combustflame.2015.02.005> [Accessed 2 Aug. 2021].

Wang, W.-C., Tao, L., Markham, J., Zhang, Y., Tan, E., Batan, L., Warner, E. and Biddy, M., 2016. *Review of Biojet Fuel Conversion Technologies*. [online] Available at: <www.nrel.gov/publications.> [Accessed 8 Aug. 2021].

Wang, W.C. and Tao, L., 2016. *Bio-jet fuel conversion technologies*. *Renewable and Sustainable Energy Reviews*, .

Westbrook, C.K., Pitz, W.J., Herbinet, O., Curran, H.J. and Silke, E.J., 2008. A Detailed Chemical Kinetic Reaction Mechanism for n-Alkane Hydrocarbons From n-Octane to n-Hexadecane. [online] Available at: <https://www.researchgate.net/publication/239882784_A_Detailed_Chemical_Kinetic_Reaction_Mechanism_for_n-Alkane_Hydrocarbons_From_n-Octane_to_n-Hexadecane> [Accessed 14 Apr. 2022].

Xin, Y., Sheen, D.A., Wang, H. and Law, C.K., 2014. Skeletal reaction model generation, uncertainty quantification and minimization: Combustion of butane. *Combustion and Flame*, 161(12), pp.3031–3039.

Yang, J., Johansson, M., Naik, C., Puduppakkam, K., Golovitchev, V. and Meeks, E., 2012. 3D CFD Modeling of a Biodiesel-Fueled Diesel Engine Based on a Detailed Chemical Mechanism. *SAE Technical Papers*. [online] Available at: <https://www.sae.org/publications/technical-papers/content/2012-01-0151/> [Accessed 16 Apr. 2022].

Yang, Y. and Boehman, A.L., 2009. Experimental study of cyclohexane and methylcyclohexane oxidation at low to intermediate temperature in a motored engine. *Proceedings of the Combustion Institute*, 32(1), pp.419–426.

Zhang, C., Hui, X., Lin, Y. and Sung, C.J., 2016. Recent development in studies of alternative jet fuel combustion: Progress, challenges, and opportunities. *Renewable and Sustainable Energy Reviews*, 54, pp.120–138.

Zheng, J., Yang, W., Miller, D.L. and Cernansky, N.P., 2002. A skeletal chemical kinetic model for the HCCI combustion process. *SAE Technical Papers*, pp.1–17.

APPENDICES

Appendix A: The Gantt Chart of the Project

No.	Task Description	Task Duration (Week)	Start Date	End Date	1	2	3	4	5	6	7	8	9	10	11	12	13	14
1.1	FYP Title Registration	1	7th June 2021	13th June 2021	P													
		1	7th June 2021	13th June 2021	A													
1.2	Project Planning	2	7th June 2021	20th June 2021	P	P												
		2	7th June 2021	20th June 2021	A	A												
1.3	Data Gathering	13	14th June 2021	12th Sep 2021		P	P	P	P	P	P	P	P	P	P	P	P	P
		13	14th June 2021	12th Sep 2021		A	A	A	A	A	A	A	A	A	A	A	A	A
1.4	Literature Review	5	21st June 2021	25th July 2021			P	P	P	P	P							
		6	21st June 2021	1st Aug 2021			A	A	A	A	A	A						
1.5	Methodology Formulation	2	26th July 2021	8th Aug 2021								P	P					
		2	26th July 2021	8th Aug 2021									A	A				
1.6	Report Writing	3	9th Aug 2021	29th Aug 2021										P	P	P		
		3	9th Aug 2021	29th Aug 2021											A	A	A	
1.7	Preparation for Presentation	2	30th Aug 2021	12th Sep 2021													P	P
		2	30th Aug 2021	12th Sep 2021													A	A

Legend: P = Planned, A = Actual

Figure A-1: Gantt Chart of the Project Work Plan for Phase 1 of FYP.

No.	Task Description	Task Duration (Week)	Start Date	End Date	1	2	3	4	5	6	7	8	9	10	11	12	13	14
2.1	DRGEP Reduction	3	24th Jan 2022	13th Feb 2022	P	P	P											
		4	25th Jan 2022	19th Feb 2022	A	A	A	A										
2.2	Isomer Lumping and Reaction Path Analysis	3	20th Feb 2022	6th Mar 2022				P	P	P								
		5	20th Feb 2022	20th Mar 2022				A	A	A	A	A						
2.3	DRG Reduction	1	21st Mar 2022	3rd Apr 2022									P					
		1	21st Mar 2022	3rd Apr 2022									A	A				
2.4	Adjustment of A-Factor Constant	5	4th Apr 2022	10th Apr 2022										P				
		6	4th Apr 2022	10th Apr 2022											A			
2.5	Mechanism Merging	5	9th Apr 2022	10th Apr 2022										P				
		6	9th Apr 2022	10th Apr 2022											A			
2.6	Model Validation	8	20th Feb 2022	10th Apr 2022									P	P	P			
		8	20th Feb 2022	10th Apr 2022										A	A	A		
2.7	Report Writing	4	28th Mar 2022	24th Apr 2022										P	P	P	P	
		4	28th Mar 2022	24th Apr 2022											A	A	A	
2.8	Preparation for Presentation	2	18th Apr 2022	25th Apr 2022													P	P
		2	18th Apr 2022	25th Apr 2022													A	A

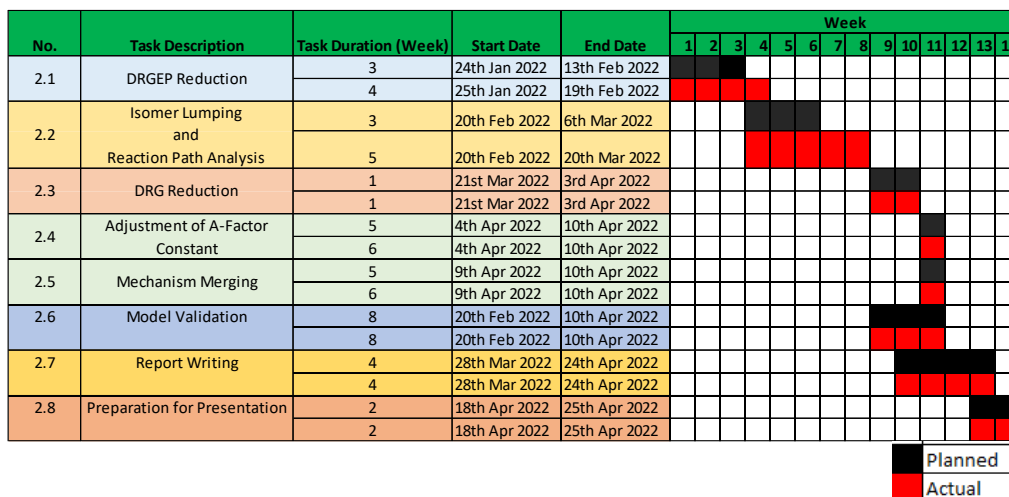Legend: P = Planned, A = Actual

Figure A-2: Gantt Chart of the Project Work Plan for Phase 2 of FYP.

Appendix B: The Remaining Species of HXN Model

```
SPECIES
h h2 o o2 oh
h2o n2 co hco co2
ch3 ch4 ho2 h2o2 ch2o
ch3o c2h6 c2h4 c2h5 ch2
ch c2h c2h2 c2h3 ch3oh
ch2oh ch2co hcco pc2h4oh ch3co
ch2cho ch3cho c3h4-a c3h4-p c3h6
nc3h7 c4h8-1 pc4h9 c2h5cho c2h5co
c2h5o ch3o2 c2h5o2 c2h3o1-2 c2h4o2h
o2c2h4oh c2h3co c2h3cho nc3h7o pc4h9o2
c3h5-a c3h3 c3h2 ch2(s) hoch2o
hocho c6h13-1 c6h12-1 c6h13o2-1 c6h12ooh1-2
c6h12ooh1-2o2 nc7h16 c7h15-1 nc16h34 c16h33-4
c15h31-1 nc14h30 c14h29-1 c13h27-1 c12h25-1
nc10h22 c10h21-1 nc9h20 c9h19-1 nc8h18
c8h17-1 c12h24-1 c10h20-1 c8h16-1 c12h25o-1
c16h33o2-4 c15h31o2-1 c14h29o2-1 c13h27o2-1 c12h25o2-1
c10h21o2-1 c8h17o2-1 c16h33o2h-4 c16ooh4-3 c12ooh1-2
c10ooh1-2 c8ooh1-2 c16ooh4-3o2 c12ooh1-2o2 c10ooh1-2o2
c8ooh1-2o2 c12o1-2 c10o1-2 c8o1-2 c16ket4-3
c12ket1-2 c10ket1-2 c8ket1-2 nc10h21cho nc8h17cho
nc6h13cho nc12h25co nc10h21co
```

Figure B-1: The List of the Species for Reduced HXN Model.

Appendix C: The Remaining Species of HMN Model

```
SPECIES
hmn hmn-r2 hmn-r4 hmn-r7 ac16h32
cc16h32 hmn-r2o hmn-r4o hmn-r7o hmn-r2o2
hmn-r4o2 hmn-r7o2 hmnooh2-1 hmnooh4-2 hmnooh7-8
hmnooh2-1o2 hmnooh4-2o2 hmnooh7-8o2 hmno1-2 hmno2-4
hmno7-8 hmnket2-1 hmnket4-2 hmnket7-8 ac15h31
cc15h31 dc15h31 ac12h25 fc12h25 ac11h23
sc11h23 cc9h19 bc15h30 cc15h30 ec15h30
hc15h30 bc11h22 cc11h22 dc7h15cho dc7h15co
ac11h23cho ac11h23co hc11h23cho hc11h23co h
h2 o o2 oh h2o
n2 co hco co2 ch3
ch4 ho2 h2o2 ch2o ch3o
c2h6 c2h4 c2h5 ch2 ch
c2h c2h2 c2h3 ch3oh ch2oh
ch2co hcco ch3co ch2cho c3h4-a
c3h4-p c3h6 nc3h7 ic3h7 ic4h7
ic4h8 tc4h9 ic4h9 ic4h10 ch3coch3
ch3coch2 ac5h10 ic5h9 neoc5h11 ic4h8o
ic4h8oh io2c4h8oh ic4h7o c3h3 c3h2
ho2cho o2cho ocho ch2(s) ic4h7-i1
tc3h6cho ic3h7cho ic4h7oh ic3h6co ic4h6oh
tc3h6oh tc4h8cho hoch2o hocho ac6h12
ic6h11 neoc6h12 neoc6h11 tc4h9cho tc4h9co
xc7h14 yc7h14 nc7h15 pc7h15 qc7h15
oc7h14 pc7h15o2 pc7h15o2h pc7h15o cc8h17
dc8h17 ic8h16 ic8h15 cc8h17o2 dc8h17o2
cc8h17o2h cc8h17o
```

Figure C-1: The List of the Species for Reduced HMN Model.

Appendix D: The Remaining Species of MCH Model

```
SPECIES
h h2 o o2 oh
h2o n2 ho2 h2o2 co
co2 ch2o hco
hcoh
hocho ocho
ch3oh
ch2oh ch3o ch3o2h ch3o2 ch4
ch3 ch2 ch2(s) c2h5 c2h4
c2h3 c2h2 c2h ch3cho ch3co
ch2cho
ch2co hcco
ch3co3h ch3co3 c2h5o
c2h5o2h c2h5o2 c2h4o1-2 c2h3cho c2h3co
c3h6 c3h5-a
c3h4-a c3h3 c3h5o
h2cc
c4h6 c4h4 c4h2
c4h5-n
c5h91-4 c6h11
c6h6 c5h6 c6h5 c6h5o c6h5oh
c5h5 c5h4o c5h3o
c6h5ch2 c6h5ch3 c6h4ch3
cychexene
mchr2
mchr3 mch kc7h13g mch2oo mch3oo
mch2qx mch3qj1 c7ene-one c7ene-onej mch2qxqj
mch2oxq mch2oxoj chxrad
chx1*o2j
c6h11-16
cyhx1n3j
cyhx13ene cyhx13n5j
```

Figure D-1: The List of the Species for Reduced MCH Model.

Appendix E: The Species of J2_201 Model

```
SPECIES
hmn hmn-r2 hmn-r4 hmn-r7 ac16h32
cc16h32 hmn-r2o hmn-r4o hmn-r7o hmn-r2o2
hmn-r4o2 hmn-r7o2 hmnooh2-1 hmnooh4-2 hmnooh7-8
hmnooh2-1o2 hmnooh4-2o2 hmnooh7-8o2 hmno1-2 hmno2-4
hmno7-8 hmnket2-1 hmnket4-2 hmnket7-8 ac15h31
cc15h31 dc15h31 ac12h25 fc12h25 ac11h23
sc11h23 cc9h19 bc15h30 cc15h30 ec15h30
hc15h30 bc11h22 cc11h22 dc7h15cho dc7h15co
ac11h23cho ac11h23co hc11h23cho hc11h23co h
h2 o o2 oh h2o
n2 co hco co2 ch3
ch4 ho2 h2o2 ch2o ch3o
c2h6 c2h4 c2h5 ch2 ch
c2h c2h2 c2h3 ch3oh ch2oh
ch2co hcco ch3co ch2cho c3h4-a
c3h4-p c3h6 nc3h7 ic3h7 ic4h7
ic4h8 tc4h9 ic4h9 ic4h10 ch3coch3
ch3coch2 ac5h10 ic5h9 neoc5h11 ic4h8o
ic4h8oh io2c4h8oh ic4h7o c3h3 c3h2
ho2cho o2cho ocho ch2(s) ic4h7-i1
tc3h6cho ic3h7cho ic4h7oh ic3h6co ic4h6oh
tc3h6oh tc4h8cho hoch2o hocho ac6h12
ic6h11 neoc6h12 neoc6h11 tc4h9cho tc4h9co
xc7h14 yc7h14 nc7h15 pc7h15 qc7h15
oc7h14 pc7h15o2 pc7h15o2h pc7h15o cc8h17
dc8h17 ic8h16 ic8h15 cc8h17o2 dc8h17o2
cc8h17o2h cc8h17o
pc2h4oh ch3cho c4h8-1 pc4h9 c2h5cho
c2h5co c2h5o ch3o2 c2h5o2 c2h3o1-2
c2h4o2h o2c2h4oh c2h3co c2h3cho nc3h7o
pc4h9o2 c3h5-a c6h13-1 c6h12-1 c6h13o2-1
c6h12ooh1-2 c6h12ooh1-2o2 nc7h16 c7h15-1 nc16h34
c16h33-4 c15h31-1 nc14h30 c14h29-1 c13h27-1
c12h25-1 nc10h22 c10h21-1 nc9h20 c9h19-1
nc8h18 c8h17-1 c12h24-1 c10h20-1 c8h16-1
c12h25o-1 c16h33o2-4 c15h31o2-1 c14h29o2-1 c13h27o2-1
c12h25o2-1 c10h21o2-1 c8h17o2-1 c16h33o2h-4 c16ooh4-3
c12ooh1-2 c10ooh1-2 c8ooh1-2 c16ooh4-3o2 c12ooh1-2o2
c10ooh1-2o2 c8ooh1-2o2 c12o1-2 c10o1-2 c8o1-2
c16ket4-3 c12ket1-2 c10ket1-2 c8ket1-2 nc10h21cho
nc8h17cho nc6h13cho nc12h25co nc10h21co
```

Figure E-1: The List of the Species for J2_201 Model.

Appendix F: The Species of J3_246 Model

```
SPECIES
hmn hmn-r2 hmn-r4 hmn-r7 ac16h32
cc16h32 hmn-r2o hmn-r4o hmn-r7o hmn-r2o2
hmn-r4o2 hmn-r7o2 hmnooh2-1 hmnooh4-2 hmnooh7-8
hmnooh2-1o2 hmnooh4-2o2 hmnooh7-8o2 hmno1-2 hmno2-4
hmno7-8 hmnket2-1 hmnket4-2 hmnket7-8 ac15h31
cc15h31 dc15h31 ac12h25 fc12h25 ac11h23
sc11h23 cc9h19 bc15h30 cc15h30 ec15h30
hc15h30 bc11h22 cc11h22 dc7h15cho dc7h15co
ac11h23cho ac11h23co hc11h23cho hc11h23co h
h2 o o2 oh h2o
n2 co hco co2 ch3
ch4 ho2 h2o2 ch2o ch3o
c2h6 c2h4 c2h5 ch2 ch
c2h c2h2 c2h3 ch3oh ch2oh
ch2co hcco ch3co ch2cho c3h4-a
c3h4-p c3h6 nc3h7 ic3h7 ic4h7
ic4h8 tc4h9 ic4h9 ic4h10 ch3coch3
ch3coch2 ac5h10 ic5h9 neoc5h11 ic4h8o
ic4h8oh io2c4h8oh ic4h7o c3h3 c3h2
ho2cho o2cho ocho ch2(s) ic4h7-i1
tc3h6cho ic3h7cho ic4h7oh ic3h6co ic4h6oh
tc3h6oh tc4h8cho hoch2o hocho ac6h12
ic6h11 neoc6h12 neoc6h11 tc4h9cho tc4h9co
xc7h14 yc7h14 nc7h15 pc7h15 qc7h15
oc7h14 pc7h15o2 pc7h15o2h pc7h15o cc8h17
dc8h17 ic8h16 ic8h15 cc8h17o2 dc8h17o2
cc8h17o2h cc8h17o
pc2h4oh ch3cho c4h8-1 pc4h9 c2h5cho
c2h5co c2h5o ch3o2 c2h5o2 c2h3o1-2
c2h4o2h o2c2h4oh c2h3co c2h3cho nc3h7o
pc4h9o2 c3h5-a c6h13-1 c6h12-1 c6h13o2-1
c6h12ooh1-2 c6h12ooh1-2o2 nc7h16 c7h15-1 nc16h34
c16h33-4 c15h31-1 nc14h30 c14h29-1 c13h27-1
c12h25-1 nc10h22 c10h21-1 nc9h20 c9h19-1
nc8h18 c8h17-1 c12h24-1 c10h20-1 c8h16-1
c12h25o-1 c16h33o2-4 c15h31o2-1 c14h29o2-1 c13h27o2-1
c12h25o2-1 c10h21o2-1 c8h17o2-1 c16h33o2h-4 c16ooh4-3
c12ooh1-2 c10ooh1-2 c8ooh1-2 c16ooh4-3o2 c12ooh1-2o2
c10ooh1-2o2 c8ooh1-2o2 c12o1-2 c10o1-2 c8o1-2
c16ket4-3 c12ket1-2 c10ket1-2 c8ket1-2 nc10h21cho
nc8h17cho nc6h13cho nc12h25co nc10h21co
hcoh ch3o2h ch3co3h ch3co3 c2h5o2h
c2h4o1-2 c3h5o h2cc c4h6 c4h4
c4h2 c4h5-n c5h91-4 c6h11 c6h11-16
c6h6 c5h6 c6h5 c6h5o c6h5oh
c6h5ch2 c6h5ch3 c5h5 c5h4o
c5h3o c6h4ch3 cychexene mchr2 mchr3
mch mch2oo mch3oo mch2qx mch3qj1
mch2qxqj kc7h13g mch2oxq mch2oxoj c7ene-one
c7ene-onej chxrad
chx1*o2j cyhx1n3j
cyhx13ene cyhx13n5j
```

Figure F-1: The List of the Species for J3_246 Model.